PREDICTION OF THE RESPONSE OF THE CANADIAN SUPER CRITICAL WATER REACTOR TO POTENTIAL LOSS OF FORCED FLOW SCENARIOS

PREDICTION OF THE RESPONSE OF THE CANADIAN SUPER CRITICAL WATER REACTOR TO POTENTIAL LOSS OF FORCED FLOW SCENARIOS

By
YANG WU, B.Eng.

A Thesis
Submitted to the School of Graduate Studies
in Partial Fulfilment of the Requirements
for the Degree

Master of Applied Science

McMaster University

Master of Applied Science (2014) McMaster University
(Engineering Physics) Hamilton, Ontario, Canada

TITLE: Prediction of the Response of the Canadian Super Critical Water Reactor to Potential Loss of Forced Flow Scenario

AUTHOR: Yang Wu
B.Eng. in Nuclear Engineering and Technology
University of Science and Technology of China

SUPERVISOR: Dr. David Novog

NUMBER OF PAGES: xv, 121

Abstract

The pressure tube type Super Critical Water Reactor (SCWR) is a Gen IV reactor concept which is currently being developed by Canada. The Canadian SCWR operates at high temperature and pressure (the coolant temperature and pressure at the reactor core outlet is 625 ^{o}C and 25MPa respectively) with a direct once-through cycle. The unique channel distributed core and passive moderator cooling systems allow the design to achieve potentially "no core melt" goal during the postulated accident scenarios. The no core melt concept is defined as a case where fuel melting is precluded for postulated events for a long period of time without human intervention. In the context of this thesis it means that fuel sheath temperatures will remain within acceptable limits even considering the loss of all forced circulation. Generation III designs typically require water makeup within a period of up to seven days, while the GEN IV design described here achieves indefinite heat removal even for prolonged station blackouts. The primary purpose of this study is to assess the Canadian pre-conceptual SCWR design for Loss of Flow Accident (LOFA) leading to degraded cooling conditions, and in particular for cases involving a failure of Isolation Cooling systems, a common safety system in many GEN III+ designs. For the SCWR additional defense-in-depth measures are included such that a complete failure of IC cooling does not result in sheath melting.

The thermal-hydraulic system code CATHENA is used for the reactor safety analysis in many CANDU reactors. A CATHENA idealization is constructed based on the current Canadian SCWR concept design. Both the coolant and the moderator systems are modeled in the idealization. All 336 fuel channels with detailed heat transfer models are included via channel grouping. Simulations for the steady state normal operation and the postulated loss-of-flow accident (LOFA) are performed. Particular focus is placed on fuel cooling for the Station Blackout scenario where all normal forms of cooling are deemed unavailable because of a loss of all main and emergency power supplies. Also for such an event the Isolation Condensers are designed to be the primary heat sink for decay heat removal. However in the event of a failure of one or both ICs (such as that experienced in

Fukushima Daiichi Unit #1), the SCWR system employs an additional passive heat sink which precludes fuel failures. The goal of this thesis is to use CATHENA to predict the fuel temperature responses of this new passive heat removal system which is specific to the Canadian SCWR. While the CATHENA code has not undergone rigorous validation for super critical water conditions, it has been benchmarked against other systems codes for similar transients. Full validation for CATHENA for SCWR applications is beyond the scope of this work.

The simulation results show that for the steady state normal operation, the highest fuel sheath temperature for the maximum power channel at beginning-of-cycle (BOC), middle-of-cycle (MOC) and end-of-cycle (EOC) are 829.2 ^{o}C, 778.0 ^{o}C and 795.6^{o}C respectively. These changes in the steady state fuel sheath temperatures are the result of the large swings in channel power that occur with fuel burnup for the pre-conceptual design assessed in this thesis. In the final conceptual design stages channel power flattening will be improved and power swings will be limited throughout the fuel cycle due to a combination of burnable absorbers and control assemblies (similar to a BWR). As such the conceptual design will experience less variation in the fuel sheath temperatures as a function of burnup.

For the LOFA transients involving failure of emergency power and failure of isolation condensers, the highest cladding temperature of 1059 ^{o}C is predicted for the pins of the Inner Ring which is lower than the melting point of the Zr-modified Stainless Steel fuel cladding. Radiation heat transfer is the dominant cooling mechanism in the early stage of the transient and during times when the peak cladding temperature is obtained. During these periods heat is rejected from the fuel pins to the inner surfaces of the pressure tube assembly, and then to the passive moderator system. The results show a high sensitivity of maximum fuel sheath temperature as a function of flow rundown and reactor SCRAM characteristics. However, as the transient progressed, convective heat transfer dominates the cooling procedure as natural circulation is developed and established in the core. This is a unique feature of the SCWR in that the high density differences between the inlet and outlet plena act as a

driving force for recirculation flows within the core. This convective cooling mode acts to greatly reduce the cladding temperatures in the intermediate phases of the accident. As the densities equalize the natural circulation is reduced but by this point the reactor decay heat is such that the system cooldown and depressurization are self-induced. The direction and intensity of the natural circulation flows is also sensitive to channel grouping assumptions used in the analysis.

Further studies should be focused on determining the orifices sizes at the fuel channel inlets, as they are important in the prediction of maximum sheath temperature in both steady state and LOFA transient, and they may play a role in the magnitude of the recirculation flows that develop in the intermediate stages of the transient. In particular orifice sizing is sensitive to the channel power variations as a function of burnup, and hence the power control system of the reactor should be such as to minimize the channel power swings over a fuel cycle. Also, enhancement and modification should be applied to the CATHENA code to improve its performance in subcritical to supercritical pressure transition (for cases that show depressurization due to overcooling) as well as the heat transfer calculation near the pseudo-critical temperature (since in many cases the induced flow was sensitive to the convective heat transfer assumptions and it is known that near the pseudo critical transition the CATHENA correlations are inaccurate). Since the natural circulation flows are sensitive to the grouping assumptions, a model with no channel grouping should be employed so the best possible picture of recirculation flows can be determined.

Acknowledgements

I would like to express my sincere gratitude to my academic supervisor Dr. D. R. Novog, for his invaluable guidance, encouragement and patience.

I would like to specifically thank Dr. Thomas Beuthe for his assistance, advice and support throughout this project.

I would also like to acknowledge the financial support of NRCAN and NSERC who funded this Generation IV project.

Also, I give my heartfelt gratitude to all my friends and colleagues at McMaster University. Thank you for the fun time in the last two years and for providing me helpful comments and valuable suggestions on my project.

The deepest appreciation is offered to my grandpa who has read this project many times over, who has inspired me to become a better person, and who has taught me more than anyone.

Table of Contents

List of Figures

List of Tables

Nomenclature

Abbreviations

AECL	Atomic Energy of Canada Limited
ATHAS	Advanced Thermal Analysis System
BOC	Beginning-of-Cycle
BWR	Boiling Water Reactor
CANDU	CANada Deuterium Uranium reactor
CATHENA	THErmal-hydraulic Network Analysis
CGNPC	China General Nuclear Power Group
CONV	Convection
D-B	Dittus-Boelter
EOC	End-of-cycle
GEOFAC	GEOmetry FACtors
GIF	Generation IV International Forum
HERC	High Efficiency Re-Entrant Channel
HPCI	High Pressure Coolant Injection
HPLWR	High Performance Light Water Reactor
IC	Isolation Condenser
IR	Inner Ring
JSCWR	Japanese Supercritical Water-Cooled Reactor
LPCI	Low Pressure Coolant Injection
MOC	Middle-of-cycle
OR	Outer Ring
PWR	Pressurized Water Reactor
S1	Section1
SCWR	Supercritical Water-Cooled Reactor

Letters

A	Area
C	Flow Profile Coefficient
C_p	Specific Heat
D	Diameter
g	Gravity Acceleration
h	Heat Transfer Coefficient
H	Flow Enthalpy
k	Thermal conductivity
l	Liquid
m	Mass
Nu	Nusselt Number ($Nu = hL/\lambda$)
P	Pressure
Pr	Prandtl Number ($Pr = \frac{C_p \mu}{\lambda} = \frac{\nu}{\alpha}$)
Q	Heat Flux
Re	Reynolds Number ($Re = UL/\nu$)
T	Temperature
v	Velocity
$V_{i \to j}$	View Factor between Surface i and j
X	Mass Fraction
x	Axial Location of Heated Length
ρ	Density
μ	Dynamic Viscosity
ε	Emissivity
τ	Shear Force
α	Void Fraction

σ	Stefan-Boltzmann Constant

Subscript

b	Bulk
i	Inner (Diameter)
in	Inlet
k	Phase k, could be liquid or gas
nc	Non-Condensable
o	Outer (Diameter)
out	Outlet
pc	Pseudo-Critical
w	Wall
z	Z direction

1 Introduction and Background

1.1 The Canadian Supercritical Water Reactor Conceptual Design

The Generation IV International Forum (GIF) is an inter-governmental treaty based organization committed to develop the next generation nuclear energy systems. The GIF goals are to coordinate and share information regarding GEN IV reactor development. The primary evaluations of the designs within GIF are based on economics, safety, sustainability and proliferation resistance.

The Supercritical Water-Cooled Reactor (SCWR) concept is the only Generation IV reactor concept utilizing water as the main coolant. It is operated at high pressure and high temperature, and with a direct thermodynamic cycle. Currently, there are two main SCWR concepts being developed worldwide with both pressure vessel and pressure tube designs being considered. Canada is developing the pressure tube type SCWR because of its extensive experience in pressure-tube type reactors.

The primary goals for the Canadian SCWR are satisfied by: enhanced safety by employing passive safety systems; lower cost of construction and operations by adopting simplified designs (i.e. direct cycle), reduced containment size; enhanced thermodynamic cycle efficiency (at approximately 48% efficiency) by using high temperature supercritical water as the working fluid; and improved proliferation resistance and minimization of waste by adopting new fuel designs.

A key metric in evaluation of the GEN IV concepts is the improvement in safety. This thesis examines the behavior of the Canadian SCWR design under certain Loss of Flow Scenarios. Of particular importance is the Station Blackout Scenario (SBO) wherein all actively-powered protective components such as pumps and valves are assumed to fail in their safety function

(similar to the Fukushima Daiichi Unit 1 accident in 2011). In this event the SCWR is designed to rely on cooling via either of the redundant Isolation Condensers (IC), which is a passive safety system that is already employed in some Boiling Water Reactors such as the GEN III+ ESBWR design. Isolation Condensers utilize natural circulation to transport heat from the core to a large reservoir of water located at a higher elevation. In the event of a SBO with a postulated failure of both redundant isolation condensers, the Canadian GEN IV concept employs an additional engineered barrier involving passive heat removal to the moderator system and heat rejection through tertiary and passive heat sinks to the environment. This thesis provides prediction of the fuel sheath temperature responses wherein all mitigation systems are assumed unavailable with the exception of the passive moderator heat removal system. While flow stagnation and fuel heat up occur for these scenarios, the combination of radiative heat transfer with additional contributions from internal convection inside the core, is capable of removing heat such that the fuel sheath safety criteria are met.

1.1.1 Reactor Core

Figure 1.1 illustrates the current Canadian pressure-tube type SCWR conceptual design. The reactor core consists of 336 individual fuel channels, each with a 5 meter long active fuel assembly with the total reactor thermal power of approximately 2540MW (The thermodynamic cycle efficiency of the plant is assumed to be 48%. Therefore, the electric power generated by the plant is approximately 1200MW). As is shown on the diagram, the high-temperature, high-pressure light water coolant is separated from the low-temperature, low-pressure heavy water moderator by the pressure tubes. The coolant at 25.8MPa and 350 ^{o}C enters the inlet plenum and is then distributed into the center flow tube of each fuel channel. The coolant then flows downwards along the center flow tubes. After exiting the center flow tubes, the coolant changes flow direction (at this time, the coolant temperature is 371 ^{o}C, which is lower than the pseudo-critical temperature of 385 ^{o}C) and starts to flow upwards along the fuel assemblies and absorbs the heat

generated as a result of fission. Outlet flows are collected in the outlet plenum (the coolant temperature and pressure are 625 ^{o}C and 25MPa respectively at the exit of the outlet plenum) and then are directly fed to the high-pressure turbines through the hot-leg piping.

The pressure tubes are surrounded by the low-pressure, low-temperature heavy water moderator contained in the calandria vessel. The proposed moderator system operates under normal conditions using a combination of active and passive systems. The active system supplements the continuously operational passive system so that boiling is precluded in the moderator during normal operation. The active system also helps to assure that two-phase natural circulation instabilities are avoided during start-up and shutdown of the reactor. The passive components of the moderator system consist of a two-phase flashing riser which provides a heat sink pathway to heat exchanges which reject heat to the environment. The passive system is in operation at all times and hence requires no power or changes in valve positions. Under emergency or accident conditions the passive moderator cooling system is designed to provide sufficient heat sink capabilities so as to preclude fuel melting. The reactivity control and emergency shutdown devices which are also located within the calandria vessel are currently under development at AECL. A fundamental difference in the Canadian system compared to other SCWR designs is that all reactivity and safety system components penetrate the low-pressure moderator system such that issues with control rod movements, sealing and potential complications with ejection are reduced. Key parameters regarding the Canadian SCWR concept are summarized in Table 1.1.

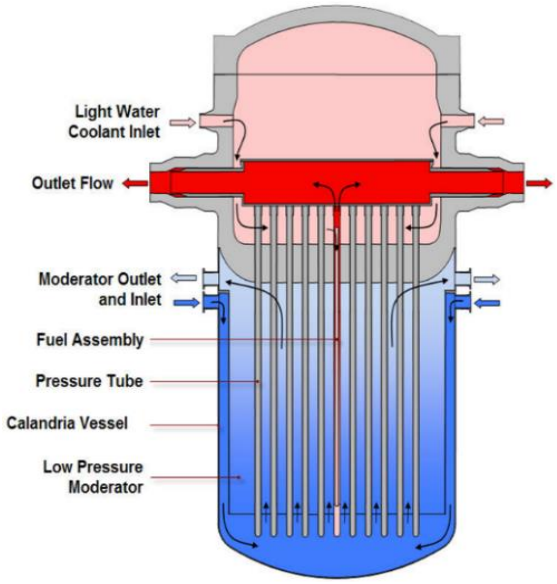

Figure 1.1 Current Design of the Canadian pressure-tube type SCWR [1]

Table 1.1Key Parameters of the Canadian SCWR Concept

Parameter	Value
Thermal Power	2540 MW
Electric Power	1200 MW
Coolant	Light water
Moderator	Heavy water
Inlet/ Outlet Temperatures	350 ^{o}C/625 ^{o}C
Inlet/ Outlet Pressures	26MPa/25MPa
Channels	336
Fuel Assembly Length	500 cm
Fuel Batches	3
Core Radius (including radial reflector region)	355 cm
Core Height (including axial D_2O reflector regions)	650 cm

1.1.2 Fuel and Fuel Channel

The fuel channel design referred as High Efficiency Re-Entrant Channel (HERC) is implemented in the Canadian SCWR concept. Figure 1.2 shows the configuration of the Canadian SCWR fuel bundle. The specifications and materials for the HERC are provided in Table 1.2. As is shown in Figure 1.2 (a), the center flow tube is a physical barrier separating the low-temperature coolant which is flowing downwards and the high-temperature coolant which is flowing upwards. The center flow tube is a solid Zirconium Hydride tube with zirconium-modified stainless steel cladding on the inner and outer surfaces. The zirconium hydride provides extra neutron moderation which helps balance the power distribution between the inner and outer rings. AECL is currently researching alternative insulators for the inner flow tube.

The outmost layer of the HERC is the Excel alloy pressure tube which is designed to withstand the high reactor operation pressure. The Zirconia isolator (Yitria-stabilized Zirconia ceramic) located between the fuel assemblies and the pressure tubes isolates the pressure tube from the high-temperature coolant and thus keeps the pressure tube temperature close to the moderator temperature. The inner and outer surfaces of the isolator are cladded with zirconium-modified stainless steel and Excel alloy which is referred as the Liner Tube and Outer Liner. The presence of the liners minimizes the potential mechanical damage to the isolators from both sides.

The proposed fuel design consists of 12%-15% reactor grade plutonium in Thorium. The ceramic fuel is fabricated and then packed into fuel sheaths made from zirconium-modified 310 stainless steel of which the melting temperature is approximately 1400℃-1450℃ [2]. The combination of the solid ceramic fuel and encapsulated fuel sheath provide barriers to fission product release in case of a postulated accident. Maintaining sheath integrity during these accidents helps to insure that regulatory limits on radioactive releases are met. Sixty-four fuel rods are assembled into two concentric fuel rings referred as to the inner ring and outer ring. Both rings consist of 32 identical fuel pins with the outer ring elements slightly larger in diameter. The specifications and materials

for the fuel assemblies are provided in Table 1.3.

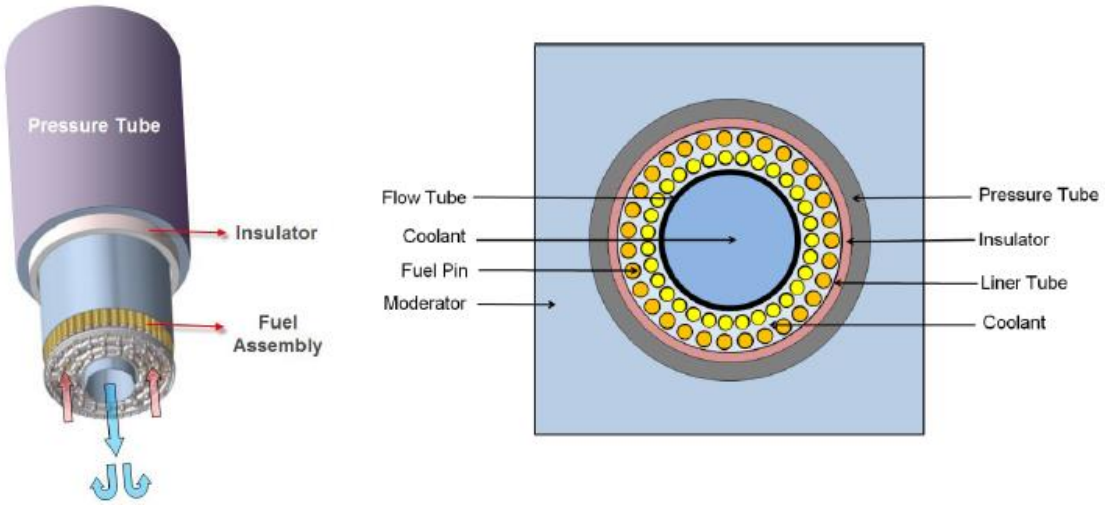

(a) Fuel Channel (b) cross-section view of fuel channel

Figure 1.2 Canadian SCWR (a) Fuel Channel and (b) cross-section view of fuel channel[3]

Table 1.2 Specifications and materials for the HERC

Component	Dimension (cm)	Material
Flow Tube Inner Cladding	3.60 radius 0.05 cm thick	Zr-modified 310 Stainless Steel (Zr-mod SS)
Center Flow Tube	3.65cm IR 1.00 cm thick	Zirconium Hydride
Flow Tube Outer Cladding	4.65 cm IR 0.05cm thick	Zr-mod SS
Liner Tube	7.20cm IR 0.05cm thick	Zr-mod SS
Insulator	7.25cm IR 0.55cm thick	Yttria Stabilized Zirconia
Outer Liner	7.80cm IR 0.05cm thick	Excel (Zirconium Alloy)

Pressure Tube	7.85cm IR 1.2cm thick	Excel (Zirconium Alloy)

Table 1.3 Specifications and Materials for the Fuel

	Inner Ring	Outer Ring
Number of Rods	32	32
Pitch Circle Radius (cm)	5.4	6.575
Radius of Fuel Pins (cm)	0.435	0.460
Thickness of Fuel Cladding (cm)	0.06	0.06
Materials of Fuel Pins	15 wt% PuO_2/ThO_2	12 wt% PuO_2/ThO_2
Materials of Fuel Cladding	Zr-mod SS	Zr-mod SS

1.1.3 "No-core-melt" for Loss-of-flow Event

The SCWR designs are intended to provide improved safety, in terms of the response to accident conditions, as well as improved resilience, in terms of flexible and alternative heat sinks in any event. Dating back to the original WASH-1400 risk assessment and continuing to modern GEN III designs a Loss of Flow Accident (LOFA) resulting from a total station blackout (SBO) represents one of the largest initiating events leading to potential core damage. As the term implies, this scenario assumes that at the beginning of the transient, the reactor loses all primary coolant flow. In addition, this scenario may be combined with the loss of emergency systems and station power supplies during a SBO. Owing to the unique features of distributed channel core and the passive moderator cooling system, the Canadian SCWR has the potential of avoiding core melting by imposing new engineered barriers and additional cooling pathway options during an SBO event. Specifically, after the event is detected and reactor trip initiated, the core power reduces to decay heat power levels of approximately 5% full power within a short period, whilst the coolant mass flow rate is reduced at a rate dictated by the inertia of the main reactor cooling pumps. The fuel sheath temperatures will rise rapidly due to the loss of convective cooling and relatively high

decay power levels. With a large temperature gradient between the fuel cladding and the surrounding ceramic liner, radiation heat transfer is significantly increased and dominates the cooling phenomena of fuel elements. The heat will be subsequently transferred from the liner tubes to the outside surface of the pressure tubes trough conduction and is eventually rejected to the moderator system. Since 2005, thermal-hydraulic and material studies have been carried out to evaluate and optimize the thermal performance of Canadian SCWR following the LOCA/ LOECC and LOFA scenarios. A detailed review of this topic is provided in Section 2.2.2. The goal of this work is to examine the transient behavior of the main heat transport system in the first several minutes of an SBO. The passive moderator cooling system and ultimate heat sink (either air coolers or isolation condenser pools) is not covered in this thesis.

1.2 The CATHENA Code

The Canadian Algorithm for THErmal-hydraulic Network Analysis (CATHENA) is a thermal-hydraulic code developed by Atomic Energy of Canada Limited (AECL) that is primarily used for analyzing the reactor upset conditions in CANDU (CANada Deuterium Uranium) reactors. It has also been used in the analysis for other facilities such as RD-14M, MAPLE-X10 and NRU. CATHENA is a one-dimensional two-fluid thermal-hydraulic package that is capable of modeling the liquid and vapor phases at different temperatures and velocities. The thermal-hydraulic system code is based on six partial differential fluid equations, three equation per phase to describe the conservation and transfer of mass, energy and momentum. An additional set of equations referred to as closure equations are included to define the interfacial relationships and the heat sources. The physical systems are modeled by a series of piping components such as pipe, reservoir, volume, tank and T-junction. The thermal-hydraulic code also includes an extensive heat transfer package (i.e. the CATHENA GENeralized Heat Transfer Package) that can accurately model heat transfer by radial and circumferential conduction, solid-solid contact, fuel channel deformation and radiation. Reference [4] provides a detailed description of the CATHENA thermal-hydraulic code. The CATHENA MOD-3.5/Rev3 and later releases are enhanced to

perform thermal-hydraulic simulations at supercritical pressure conditions. The light water properties have been extended into supercritical pressure regime, and the Dittus-Boelter correlation is automatically chosen for heat transfer at supercritical pressure.

1.3 Summary and Objectives

The pressure tube type SCWR is the Generation IV reactor concept that is currently being developed by Canada. The unique feature of the distributed channel core may allow the reactor to obtain "no-core-melt" under station blackout conditions by passive radiation heat transfer from the fuel elements to the pressure tubes and subsequently the moderator system during the Loss of Flow Accident.

The CATHENA code is a thermal-hydraulic code that is developed for analyzing the postulated upset conditions in CANDU reactors. In CATHENA MOD-3.5d/Rev 3 and later released versions, the code has been enhanced to simulate supercritical pressure conditions. To that end, the objectives of this study are to:

- Construct a model (idealization) of Canadian SCWR using CATHENA code.
- Use the CATHENA idealization to simulate steady state normal operation and the Loss of Flow Accident.
- Assess the Canadian pre-conceptual SCWR design for Loss of Flow events leading to degraded cooling conditions.
- Assess the quality of the CATHENA predictions under supercritical pressure conditions and the unique features which occur under these conditions.
- Provide information to the AECL designers on heat sink pathways and their potential to mitigate SBO events.

2 Literature Review

2.1 Other Supercritical Water-Cooled Reactor Designs

As indicated earlier, SCWR is a Gen IV reactor concept where the working fluid (i.e. light water coolant) operates at a pressure exceeding its thermodynamic critical point. Supercritical water does not exhibit a liquid to vapor phase change, instead the water density (and some other properties) decreases continuously as the temperature increases. Consequently, the boiling crisis, which plays a major role in historical water reactor safety analysis, is precluded in the SCWR designs. In addition, the coolant will experience a significant higher enthalpy rise in the core when compared to current water-cooled reactors (approximately 10 times higher depending on the reactor core design), which will minimize the coolant massflow for a given power. There are two types of SCWR concepts that are currently under development, the pressure tube type SCWR which is adopted by Canada and Russia as well as the pressure vessel type SCWR which is developed by other countries (e.g. Japan JSCWR, Europe HPLWR, China CGNPC SCWR). The general features of SCWR are listed as follows:

- Using light water as coolant; using light or heavy water as moderator
- The system is operated under supercritical pressure conditions (Pressure >22.1MPa)
- All the designs focus on a thermal neutron spectrum with optional designs for fast spectrums
- A direct thermodynamic cycle is adopted by SCWR concepts resulting in a greatly simplified and more compact plant system.
- The SCWR concepts are designed to achieve a thermal efficiency >44%
- SCWR concepts are designed for improved economics (minimized construction and operation cost and higher efficiency)
- SCWR concepts are designed for improved safety, proliferation resistance and sustainability

2.1.1 Japanese Supercritical Water Reactor (JSCWR)

The Japanese version of supercritical water reactor which is also referred as to the Super Light Water Reactor has been under development for approximately 25 years mainly by the University of Tokyo.

JSCWR is a pressure vessel type water-cooled reactor that operates over the thermodynamic critical point of water for both the moderator and coolant. The reactor core is operated at 25.0 MPa, with an inlet feedwater temperature of 290 ^{o}C and an averaged outlet coolant temperature of 560 ^{o}C. Due to high operation pressure and temperature, the thermal efficiency of JSCWR is approximately 44% which is 1.2 to 1.3 times higher than the currently operating light water reactors (LWRs)[5]. A once-through direct Rankine cycle system is adopted by the reactor concept which greatly simplifies the plant system as well as reduces the capacities of the primary system components. As is shown in Figure 2.1, the primary circuit of JSCWR mainly consists of a reactor pressure vessel, main steam lines, a turbine system, low-pressure and high-pressure condensate water pumps, feedwater heaters and feed water pumps. The reactor pressure vessel and control rods resemble PWRs, the containment and the safety systems are similar to the BWR designs [5].

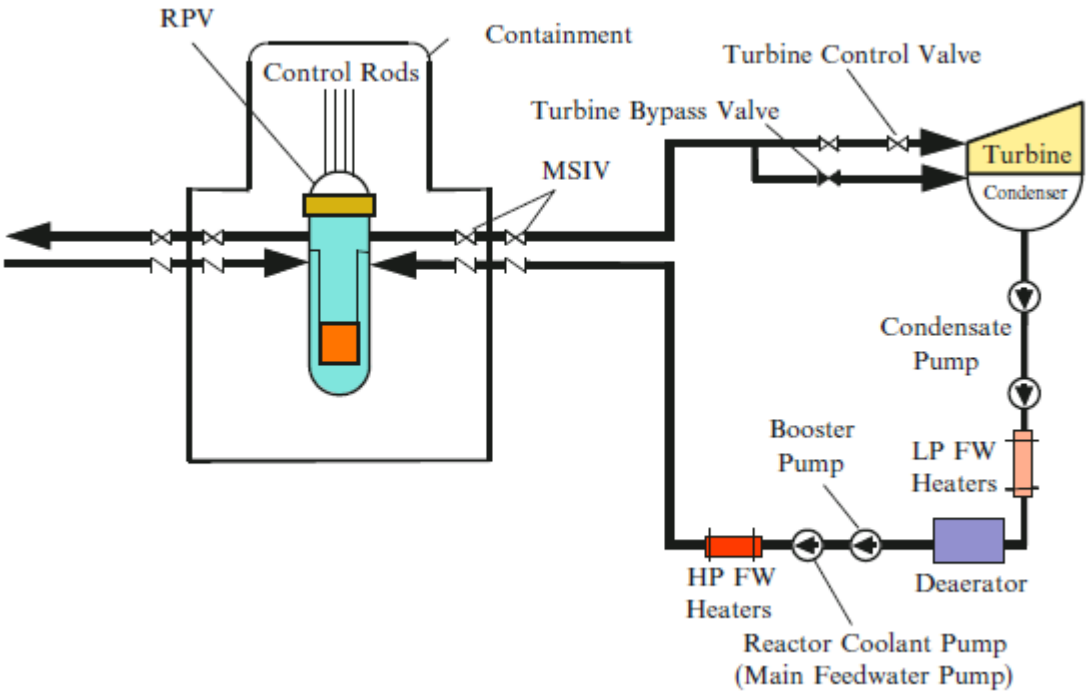

Figure 2.1 Plant Systems of the Japanese SCWR [6]

Figure 2.2 illustrates how coolant is distributed inside the reactor core. The majority of the coolant that comes out of the inlet nozzles flows downwards through the annulus regions between the reactor pressure vessel and the shroud to the lower plenum. A small portion of coolant is led to the upper dome, provides cooling to shroud head area and then flows into the bypass lines and joins the majority of coolant at the lower plenum. The fluid in the lower plenum then flows upwards along the fuel assemblies to the outlet nozzles.

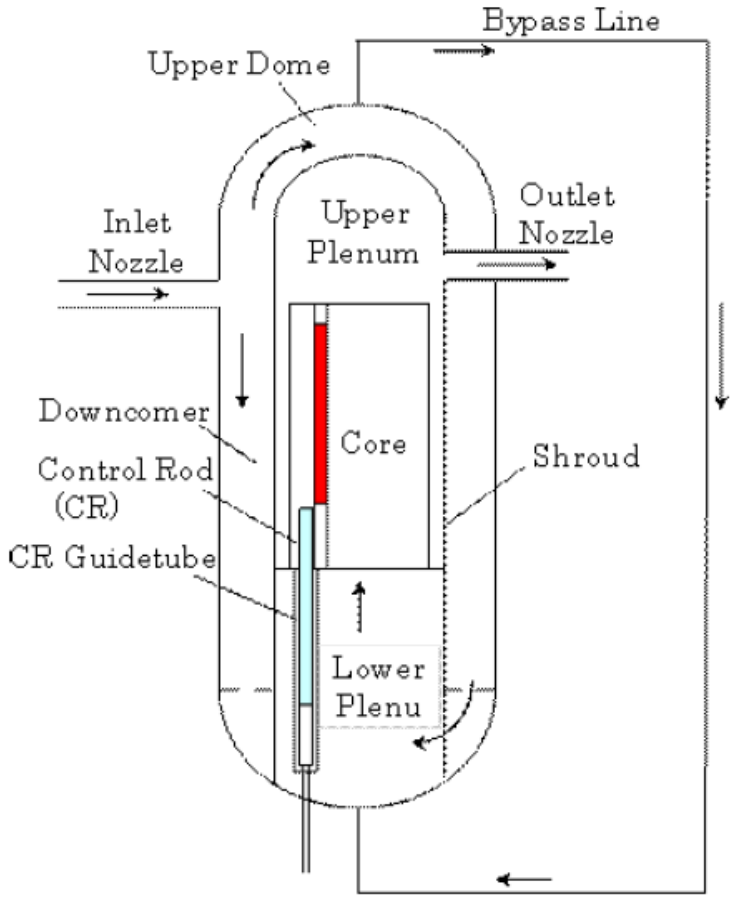

Figure 2.2 Configuration of the Reactor Pressure Vessel and Coolant Flow [6]

The cross-section view of the JSCWR fuel assembly is shown in Figure 2.3. The fuel assemble consists of a large square water rod (moderator) surrounded by 192 fuel rods. The fuel rods contain UO_2 pellets similar to LWRs with modified stainless-steel cladding. In the water rod, low temperature water flows downward to keep the reactor core moderated.

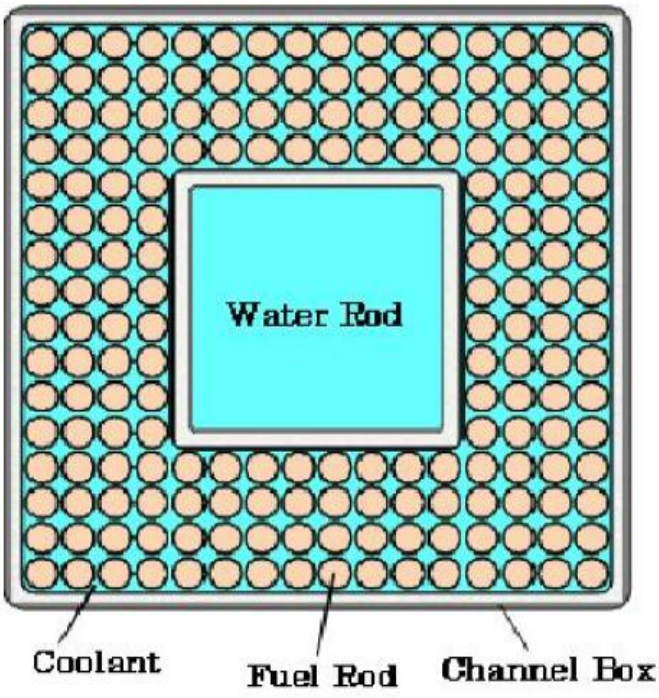

Figure 2.3 Cross-section View of the JSCWR Fuel Assembly [6]

The critical event for JSCWR is the loss of flow accident because natural circulation cannot be used for the decay heat removal in this design [5]. However, the "water source" effect observed during the transient eases the situation by provide extra flow to the channels where fuel rods located. Specifically, the temperature of the fuel rods increases significantly at the early stage of LOFA transient. This leads to an increasing amount of heat conducted to the water rod via the water rod channel box. As a result, the coolant in the water rod expands which increases the downstream massflow rate regardless of the water rod flow directions and thus maintain channel flows in the loss-of-flow events. In Canadian SCWR conceptual design, the center flow tube resembles the water rod here, and therefore, a similar "water source" effect is observed during LOFA transients. For Canadian SCWR, the "water source" effect is caused by several phenomena and a detailed discussion of this topic is provided in Section 5.2.1.3.

2.1.2 High Performance Light Water Reactor (HPLWR)

A pre-conceptual design of a pressure vessel type SCWR called HPLWR has been developed in Europe. HPLWR is a thermal reactor that uses light water as both moderator and coolant. The HPLWR has a direct Rankine cycle system, with a thermal output of 2300MWth and net power plant efficiency of 43.5%. The reactor is operated at 25MPa with a coolant inlet temperature of 310 ^{o}C and an outlet temperature of 500 ^{o}C. To avoid peak sheath temperature exceeding the safety limits of cladding material, a 3-step coolant heat up scheme is adopted [7]. Specifically, coolant firstly flows upwards in the evaporator where it undergoes the transition from liquid-like to steam-like conditions (i.e., it passes the pseudo-critical temperature). And then, the flow direction is reversed and coolant flows downwards along the first superheater. At the bottom of the reactor core, the flow direction is reversed again and the coolant flows upwards in the second superheater and reaches its envisaged outlet temperature upon exiting the second superheater region. The fission power of the superheater sections is lower compared to the evaporators due to the fuel arrangement and the neutron leakage which is why the anticipated maximum sheath temperature could be eliminated. The arrangement of the evaporator and superheaters is illustrated in Figure 2.4.

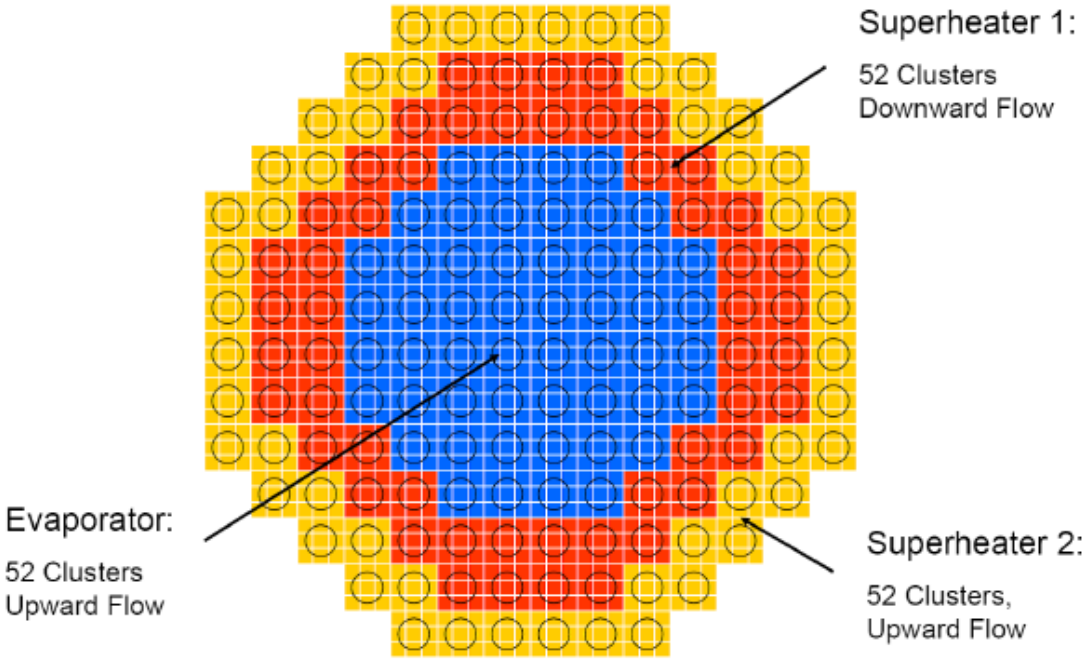

Figure 2.4 Arrangement of Evaporator and Assembly Cluster in the Core [7]

The fuel assembly design is illustrated in Figure 2.5. The fuel assembly consists of 40 fuel pins and a single moderator box. Colder feedwater run inside moderator box and the gaps between assembly boxes to provide moderation for the core. The fuel pellets are made of UO_2 with stainless-steel cladding. Wire wraps are proposed as spacers to improve coolant mixing in the assembly box.

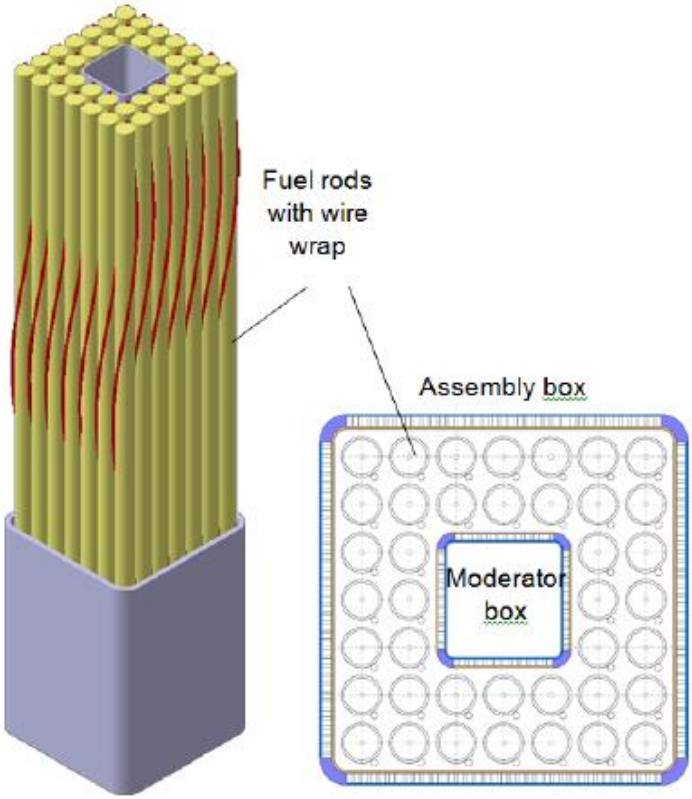

Figure 2.5 Assembly Design with Wire Wrapped Fuel Rods (left) and Cross-section View of the Fuel Assembly (right) [7]

The Safety systems of HPLWR resemble the existing BWRs. Both active (e.g. low pressure coolant injection system) and passive components (e.g. containment condenser) are adopted to perform safety-related functions in the event of transients or accidents. Studies indicate that the non-intended decrease of core coolant flow rate is one of the most important abnormal events for HPLWR. Due to the lack of recirculation in the core, HPLWR cannot be successfully cooled down by simply maintaining the coolant inventory as in a GEN III PWR or BWR. Coolant mass flow must be also maintained at all times in the case of accidents. To ensure a sufficient core coolant flow rate after reactor trip or shut down, a passive high pressure coolant injection (HPCI) system and an active low pressure coolant injection (LPCI) system are proposed to secure coolant massflow at both high pressure and low pressure conditions. The low pressure coolant injection (LPCI) system is similar to the active LPCI of BWRs while the high pressure coolant injection (HPCI) is a newly proposed idea that has not been applied to any BWRs or PWRs [8].

2.2 Related Safety Analysis for Canadian SCWR

2.2.1 No-core Melt Assessments for the High Efficiency Channel Design

The Canadian SCWR fuel design has been modified significantly since its inception more than 10 years ago. The fuel assembly evolved from the early CANFLEX designs, to subsequent 54-element design, 78-element design, 62-element design to the most resent 64-element design. Several preliminary simulations have been performed to evaluate and optimize the thermal performance of the Canadian high efficiency re-entrant channel (HERC) in a postulated loss of coolant accident with loss of emergency core cooling.

Vasic and Khartabil (2005) [9] performed simulations to optimize the thermal performance of the insulated fuel channel of the CANFLEX design by using the CATHENA code. A hypothetical decay heat curve is adopted for these simulations. The thermal-physical properties of the insulating layer were altered whilst the insulation thickness and fuel channel dimensions remain constant. The moderator passive cooling loop is assumed to be available for the decay heat removal. The study shows that the CANFLEX design has the potential of avoiding core melting by rejecting heat to the passive moderator system during the very severe LOCA/LOECC scenarios.

To obtain a better understanding of the thermal-hydraulic performance of the 54-elements fuel design, subchannel analysis under steady state normal operation conditions was performed by Shan et al. (2011) [10] using the ATHAS code. The simulation results showed that the maximum fuel cladding temperature at beginning-of-cycle (BOC) and end-of-cycle (EOC) power were 761 ^{o}C and 808 ^{o}C respectively, both of which met the thermal-hydraulic criteria of the Canadian SCWR. Again, because no control system was considered, the power swing between beginning and end-of-cycle was larger than that foreseen in the final design, and hence the analysis was conservative. In addition, the efficiency of radiation heat transfer for this fuel design was

assessed by using CATHENA code. Decay level of 1%, 2% and 3% of full power were adopted by the study. Simulation results showed that radiation heat transfer can remove 2% of the day power while the fuel sheath temperature stays below the safety limit.

The most resent literature on the assessment of SCWR high efficiency channel design is based on the 78-element design. Licht and Xu (2012) [11] performed simulations to investigate the impact of the insulator porosity on the heat transfer behaviors of the 78-element fuel channel by using the CATHENA code. The study shows that by adopting a non-porous zirconia ceramic fuel channel insulator, the sheath temperature could be maintained below the melting point when the decay heat is less than 3% of full power. Transient calculations were performed for both non-porous and 76% porous zirconia ceramic fuel channel insulator. The same decay heat curve is assumed for all the transient simulations. It is found out that the thermal resistance of the 78-element fuel assembly design considered in that work was too large for achieving the "no core melt" objective. They concluded that to obtain a better overall core thermal performance, the calculation of fuel channel design, thermal-hydraulic and reactor physics need to be coupled together. In this thesis, the latest fuel assembly design and reactor physics simulations are performed to demonstrate that the most recent proposed fuel design is capable of meeting the no core melt criteria.

2.2.2 LOCA/LOECC and LOFA Transients for Canadian SCWR

Several LOFA and LOCA/LOECC simulations for Canadian SCWR have been performed by Xi'an Jiao tong University, among which the most recent studies were performed for the 62-element design and the current Canadian SCWR design, i.e. the fuel design with high efficiency re-entrant channel (HERC) and 64-element fuel bundle.

Jia et al. (2013) performed a LOFA transient simulation in the absence of safety system for the 62-element design. A primary coolant system model and a moderator heat sink had been constructed for the SCTRAN code. However, at the time the simulations in Jia et al. were

performed, the radiation heat transfer model had not been included in the SCTRAN code and therefore radiation heat exchange between surfaces was not modeled. The sequence of events for the LOFA transient include: main feedwater flow rate linearly reduced to zero during the first 10-15s, the reactor shut down signal was triggered at 10.5s and shut down rods inserted into the core with 0.5s delay. The turbine stop valve on the main steam line closed at 11s. The simulation results showed that for this specific LOFA transient in the absence of safety system, natural circulation initiated and established at the early stage of transient. As a result, the fuel elements (the maximum fuel sheath temperature is 1211.3 ^{o}C) could remain below the safety limitation without radiation heat transfer.

A LOCA with LOECC simulation for the most resent 64-bundel design is performed by Wu et al. (2014). A SCTRAN model was created to evaluate the passive safety characteristics of the 64-element fuel bundle in the presence of radiation heat transfer. A conservative decay heat curve for the burnup of 55MWd/kg was employed in the study. A postulated double-ended break event at the cold leg had been simulated. The results showed that radiation heat transfer and natural convection were sufficient to remove the decay heat and concluded that the Canadian SCWR could achieve the “no core melt” objective in this severe LOCA event. In addition, sensitivity analysis showed that the outlet plenum size and moderator cooling affected , to some degree, the prediction of maximum fuel sheath temperature. Furthermore, the emissivity of the wall surfaces had a significant impact on the fuel sheath temperate. For cases with emissivity above 0.4, the no-core melt objective was met.

3 Theory

3.1 The Governing Equations for the CATHENA Thermal-hydraulic System Code

The thermal-hydraulic code CATHENA is a one-dimensional, non-equilibrium two fluid model [4]. Similar to other thermal-hydraulic analysis codes such as RELAP5, TRACE and etc., six differential equations are implemented to describe the liquid and gas flow fields. For each phase, the flow field is described through three equations, i.e. the conservation equation of mass, energy and momentum. The conservation equations for liquid and gas phase can be written as follows:

Mass conservation (for phase k);

$$\frac{\partial}{\partial \mathrm{t}}\langle \alpha_k \rho_k \rangle + \frac{1}{A}\frac{\partial}{\partial \mathrm{z}}\left(A\langle \alpha_k \rho_k v_k \rangle\right) = m_{ki} - \Gamma_k \tag{3-1}$$

For the single phase model described in this study, the above equation can be simplified as:

$$\frac{\partial}{\partial \mathrm{t}}\langle \rho_l \rangle + \frac{1}{A}\frac{\partial}{\partial \mathrm{z}}\left(A\langle \rho_l v_l \rangle\right) = 0 \tag{3-2}$$

Energy conservation (for phase k);

$$\frac{\partial}{\partial t}\langle \alpha_k \rho_k \left(h_k + \frac{v^2}{2}\right)\rangle + \frac{1}{A}\frac{\partial}{\partial z}\left[A\langle \alpha_k \rho_k v_k \left(h_k + \frac{v^2}{2}\right)\rangle\right] - \frac{\partial}{\partial t}\langle \alpha_k P_k \rangle$$

$$= -\left\langle P_i \frac{\partial \alpha_k}{\partial t}\right\rangle + q_{kw} + q_{ki} + \tau_{ki} v_{ki} + v_{ki} P'_{ki} + \langle m_{ki}\left(h_k + \frac{v^2}{2}\right)\rangle - \langle \alpha_k \rho_k v_k \rangle g_z \tag{3-4}$$

Where

$$P'_{ki} = (-1)^k \rho_{\mathrm{AP}} [\frac{\partial}{\partial \mathrm{t}}(v_g - v_f) + v^* \frac{\partial}{\partial z}\left(v_g - v_f\right) \tag{3-5}$$

In the above equation $(-1)^{\mathrm{k}}$ is $+1$ for liquid and -1 for gas

For the single phase model described in this study, (3-4) can be simplified as:

$$\frac{\partial}{\partial t}\langle\rho_l\left(h_l+\frac{v^2}{2}\right)\rangle+\frac{1}{A}\frac{\partial}{\partial z}\left[A\langle\rho_l v_l\left(h_l+\frac{v^2}{2}\right)\rangle\right]-\frac{\partial}{\partial t}\langle P_l\rangle=q_w-\langle\rho_l v_l\rangle g_z \quad (3\text{-}6)$$

Momentum conservation (for phase k);

$$\frac{\partial}{\partial \mathrm{t}}\langle\alpha_k\rho_k v_k\rangle+\frac{1}{A}\frac{\partial}{\partial z}(A\langle\alpha_k\rho_k v_k^2\rangle+\frac{1}{A}\frac{\partial}{\partial z}(A\langle\alpha_k P_k\rangle=\left\langle P_i\frac{1}{A}\frac{\partial}{\partial z}(A\alpha_k)\right\rangle+\tau_{kw}+\tau_{ki}+m_{ki}v_{ki}+P'_{ki}-\langle\alpha_k\rho_k\rangle g_z \quad (3\text{-}7)$$

The single phase model implemented in this study used a simplified equation as:

$$\frac{\partial}{\partial \mathrm{t}}\langle\rho_l v_l\rangle+\frac{1}{A}\frac{\partial}{\partial z}(A\langle\rho_l v_l^2\rangle+\frac{1}{A}\frac{\partial}{\partial z}(A\langle P_l\rangle)=\tau_w-\langle\rho_l\rangle g_z \quad (3\text{-}8)$$

In these equations, the A is the cross-sectional area of the conduit; m_{ki} is the interface mass transfer rate for the kth phase; Γ_k represents a source of non-condensables; v_k is the velocity of phase k, α_k is the fraction of the cross-section occupied by phase k; τ_{kw} is the wall shear component for phase k; τ_{ki} is the interface shear component for phase k; P'_{ki} is the apparent mass term; v_{ki} is the intrinsic interface velocity; q_{kw} is the wall heat transfer to phase k; q_{ki} is the heat transfer from phase k; h_{ki} is the enthalpy of phase k at the interface; and g_z is the acceleration due to gravity in the z direction [4].

The liquid and gas flow fields are coupled together with a set of interfacial closure equations also referred as the jump conditions, which define the transport of mass, energy, and momentum between the phases as well as relationships for energy and shear stresses with the wall. The other transfer mechanisms are modelled using various empirically derived constitutive relationships.

In addition, four non-condensable gases may be included in the gas phases. An additional set of mass conservation equations are defined for them.

$$\frac{\partial}{\partial \mathrm{t}} A\alpha_g \rho_g X_{nc}^i + \frac{\partial}{\partial z} A\alpha_g \rho_g C_{0g} v_g X_{nc}^i = A\Gamma_{nc}^i \tag{3-9}$$

where X_{nc}^i is the mass fraction of the i^{th} non-condensable gas components and the Γ_{nc}^i represents the source term for the i^{th} non-condensable gas components.

For fluids above the critical pressure the fluid exists as a single-phase media, albeit with steep property gradients, in particular around temperatures near the pseudo-critical temperature. In CATHENA this is simulated by solving one set of conservation equations and fixing the void fraction at a single value. This allows the solution algorithms in CATHENA to perform adequately without any modifications provided that the fluid remains above the critical pressure at all times. For case involving trans-critical pressure transient, such as those associated with depressurization transients, CATHENA cannot be used reliably at this time, since the transition may be from a single-phase media to either superheated steam, sub-cooled liquid, or into a two-phase mixture. During such transitions within CATHENA the use of a single void fraction prior to the critical pressure transition will lead to a discontinuity in void and potential code errors.

3.2 Heat Transfer under Supercritical Pressure Conditions

During normal operation, the system pressure is above the supercritical pressure. Therefore, the coolant remains in a single phase and the boiling crisis does not occur. In the supercritical pressure region, at a given pressure (denoted as pseudo-critical pressure P_{pc}), the heat capacity of water undergoes drastic variations at a certain temperature. The temperature corresponding to the maximum heat capacity is defined as the pseudo-critical temperature (T_{pc}). The pseudo-critical point is characterized with P_{pc} and T_{pc} and the combination of pseudo-critical points is referred to pseudo-critical line [12]. As shown in Figure 3.2, as the pressure increases the pseudo-critical temperature increases.

The thermal physical properties of water go through significant changes near the pseudo-critical

temperature. As shown in Figure 3.3, when approaching the pseudo-critical point, the density and thermal conductivity decrease dramatically. Similar to the specific heat variations, a local maximum value is observed in the thermal conductivity near the pseudo critical point.

Due to the strong variations of the thermal physical properties, heat transfer under super critical pressure is significantly different from single phase heat transfer at subcritical conditions. According to Jackson et al. (1979) [13], three heat transfer modes have been observed experientially, which are referred to as the Normal Heat Transfer, the Heat Transfer Enhancement and the Heat Transfer Deterioration.

The Dittus-Boelter equation is a widely used empirical correlation to calculate forced convective heat transfer for circular tubes in turbulent flow at subcritical pressure. According to the Japanese SLWR book [5], it also gives good predictions on heat transfer coefficient for supercritical fluids so long as the temperature is not near the pseudo-critical point. However, this correlation is unrealistic near the pseudo-critical point because of its high sensitivity to changes of the fluid properties (See Figure 3.1). The sharp peak in the Prandtl number at the pseudo critical point leads to an artificially high predicted heat transfer coefficient compared with the experimental data. Nevertheless, the classical Dittus-Boelter correlation is extensively used as the base of the heat transfer correlation for supercritical fluid. The Dittus-Boelter correlation can be presented generally as:

$$Nu = 0.023 \cdot Re^{0.8} \cdot Pr^{0.4} \tag{3-10}$$

where N_u is the Nusselt number, R_e is the Reynolds number, P_r is the Prandtl number.

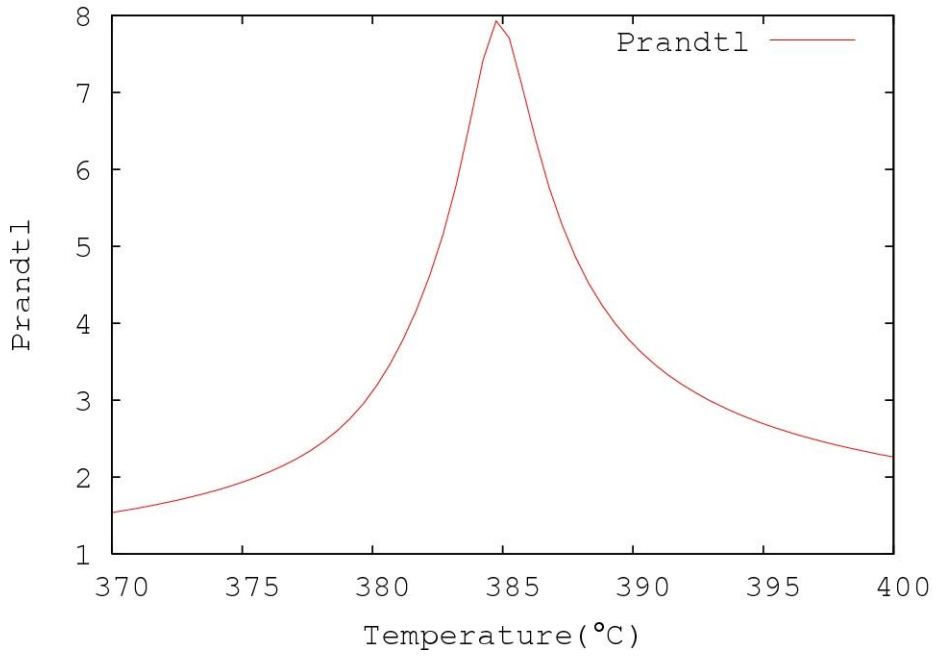

Figure 3.1 Prandtl Number at 25MPa

During the pseudo-critical transition, the thermal physical properties of fluid undergo large variations. Therefore, the bulk fluid temperature may not be representative of the near-wall fluid conditions in super critical flows [14]. Thus, for some later developed supercritical heat transfer correlations, the cross-sectional averaged Prandtl number is adopted to account for the overall thermal properties variations that take place. Two supercritical heat transfer correlations, both applicable within in the range of the operating pressures of the Canadian SCWR, are introduced below.

Bishop et al. (1964) [15] proposed a supercritical heat transfer correlation which could be written in the following form:

$$\mathrm{N}u_b = 0.0069 Re_b^{0.9} \overline{Pr_b}^{0.66} \left(\frac{\rho_w}{\rho_b}\right)^{0.43} \left(1 + 2.4\frac{D}{x}\right) \tag{3-11}$$

where $\overline{Pr_b}$ is the averaged Prandtl number, ρ_w is the fluid density near the wall; ρ_b is the bulk-fluid density; D is the inner diameter of the tube, x is the axial location along the heated

length.

The Average Prandtl number is defined as:

$$\overline{\mathrm{P}_r} = \mu\overline{c_p}/k \tag{3-12}$$

where the average specific heat capacity is defined as:

$$\overline{c_p} = (H_w - H_b)/(T_w - T_b) \tag{3-13}$$

where μ is the dynamic viscosity, k is the thermal conductivity, H_w is the fluid enthalpy near the wall, H_b is the bulk-fluid enthalpy T_w is the wall surface temperature, T_b is the bulk-fluid temperature. Since that time many authors have adopted similar approaches for the Prandtl number near the pseudo-critical point. The data was obtained under the following conditions: pressure = 22.8-27.6MPa, bulk-fluid temperature = 282-527 ^{o}C, mass flux = 651-3662 kg/m^{2}s, heat flux = 0.31-3.46 MW/m^2, bare tube and annuli with upward flow. The correlation is obtained within a fit of ±15%.

Swenson et al. (1965) [16] recommend the following correlation of which majorities of thermo physical properties are evaluated on a wall temperature.

$$\mathrm{N}u_w = 0.00459 Re_w^{0.923} \overline{P_{r_w}}^{0.613} \left(\frac{\rho_w}{\rho_b}\right)^{0.231} \tag{3-14}$$

The above equation was obtained within the following conditions: pressure = 22.8-41.4 MPa, bulk-fluid temperature = 75-576 ^{o}C and mass flux = 542-2150kg/m^{2}s. The correlation is obtained within a fit of ±15%.

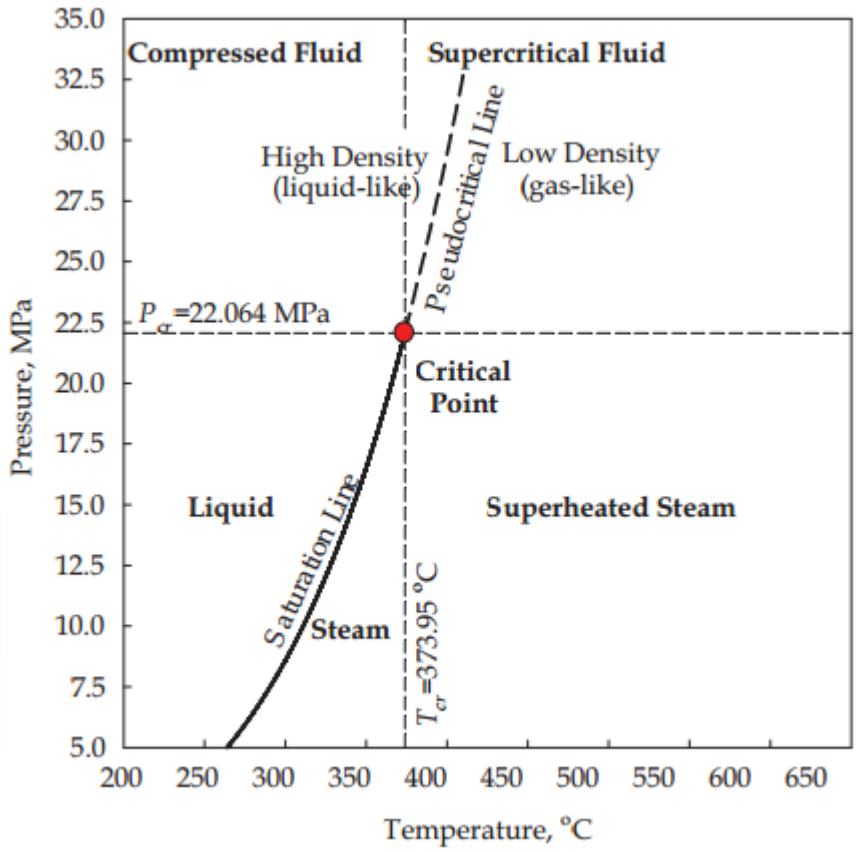

Figure 3.2 Pressure-Temperature diagrams for water (Pioro 2011) [12]

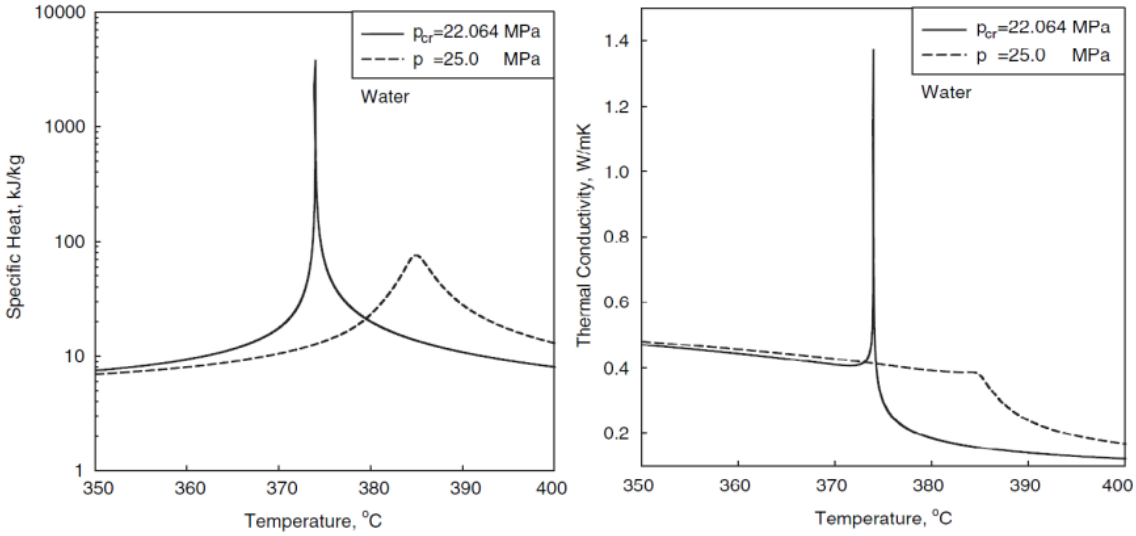

Figure 3.3 Thermo-physical Property Variation of Water (Pioro 2007) [17]

As indicated earlier, under supercritical pressure, the Dittus-Boelter equation provides relatively

accurate prediction of the heat transfer coefficient for convective heat transfer away from the pseudo-critical line. This is referred to as the Normal Heat Transfer mode. When the bulk-fluid temperature is close to the pseudo-critical temperature, either enhanced or impaired heat transfer could take place depending on the heat flux and flow conditions. At low-heat-flux conditions, improved heat transfer may occur owing to increased specific heat and decreased viscosity. This is referred to as the Heat Transfer Enhancement mode. As the heat flux increases, more heat is transferred to the near wall fluid such that the coolant temperature rises beyond the pseudo-critical temperature. As a result, fluid with higher specific heat is pushed away from the heated surface and is replaced by the low density fluid. Furthermore, the turbulent boundary layer is altered such that the transfer of heat from the laminar sub-layer to the core of the flow may be impeded. This leads to impairment of the enhanced heat transfer. This is referred to as the Heat Transfer Deterioration mode. There are two main mechanisms, i.e., buoyancy and flow acceleration that cause the heat transfer deterioration. A detailed explanation of these mechanisms is beyond the scope of this study, however deterioration tends to happen near the upstream of heated channels and is not expected to impact the maximum sheath temperature in the downstream locations of a channel.

3.3 Radiation Heat Transfer

The Stefan-Boltzmann law gives the radiation intensity from an object in terms of its temperatures:

$$P = A\varepsilon\sigma T^4 \tag{3-15}$$

where P is the total power radiated from an object; A represents the surface area of the object; σ called the Stefan-Boltzmann constant that equals to 5.6704400×10^{-8} $Js^{-1}m^{-2}K^{-4}$ and T is the absolute temperature of the object. The emissivity, ε, is the ratio of the emission intensity of the body at a certain temperatures to that of the black body at the same temperature [18]. For a grey

body, the absorptivity for all wavelengths is the same.

For radiation exchange in an enclosure, a view factor $V_{1\to2}$ is defined as the fraction of energy exiting an isothermal, opaque, and diffuse surface denoted as surface #1 (by emission or reflection), that directly impinges on surface 2 (and is absorbed or reflected) [18].The net radiation transfer from surface *i* due to exchange with all(N) surfaces of an enclosure can be written as：

$$q_i = \sum_{j=1}^{N} V_{j\to i}\, A_i \varepsilon\sigma(T_i^4 - T_j^4) \tag{3-16}$$

The radiation heat transfer model used by CATHENA (i.e. the GEOFAC package which is described in details in later chapters) is based on the following four assumptions:

- Radiation heat transfer between surfaces at different elevations is neglected (i.e., radiation is modeled in 2-dimensions in the lateral direction);
- All surfaces in the system are opaque, diffusive and grey;
- The coolant in the fuel channel neither emits nor absorbs radiant thermal energy;
- Reflectance from a surface is independent of the reflected direction and the radiation frequency.

Generally, radiation heat exchange between two specific surfaces is not easily predicable as it is varied as of a function of the surface temperatures, the wavelengths, the directions, the surface areas and the relative locations of the involved surfaces. The above four assumptions are commonly made in order to simplify the calculation of radiation heat transfer.

The first assumption indicates that in the CATHENA code, radiation heat transfer is carried out among wall surfaces of same altitudes. This is in consistence with the wall heat transfer

models (i.e. the GENHTP heat transfer package which is described in Section4.4) where the convective heat transfer between the wall surfaces and the thermal-hydraulic nodes are only calculated in lateral directions only. Since at the point of maximum sheath temperature any radiation exchange to other elevations would cause a reduction in temperature, this provides some level of conservatism to the results.

The second assumption indicates that all the radiation energy reaching the wall surfaces is either reflected or absorbed. In addition, the wall surfaces involved are characterized by having radiation properties independent of wavelengths and directions. Constant emissivity is applied to all wall surfaces regardless of the surfaces temperatures and locations.

The third assumption implies that the radiation model only calculates the radiation heat transfer among the wall surfaces. The media in between (i.e. the light water coolant) neither emits, absorbs or scatters radiation and hence has no effect on the radiation heat exchange between the surfaces. Due to the lack of experimental data on the radiation properties of light water under the supercritical pressure conditions, the reflection, absorption and transmission spectroscopies of the coolant are hard to determine and therefore those properties were not included in the CATHENA radiation heat transfer model. In theory, the present of media would impair the efficiency or radiation cooling, and thus resulting in a higher fuel sheath temperature.

The fourth assumption implies that the wall surfaces reflect the incident radiation in a diffused manner. Specifically, the wall surfaces are treated as rough surfaces and thus the radiation is reflected/ emitted equally in all directions.

4 SCWR Model Description

A CATHENA idealization (i.e., input model) was developed based on the conceptual design of the Canadian SCWR. All 336 fuel channels, the inlet and outlet plenums, main feed-water line, main steam-line, isolation valves, safety relief valve (SRV) and the heavy water moderator are included in this model. The method used for simulating the 336 fuel channels is first described, with a focus on channel grouping for the steady state simulations. Channel grouping of the parallel flow paths in the core is often used to simplify analyses relative to simulating each individual channel, and in some cases may be the only option. For example CATHENA's current nodal size and memory limits precluded simultaneous simulation of all flow paths in the core, hence some averaging of the flow paths is required. The model of the rest of the piping components is described afterwards.

4.1 Channel Grouping

In this section, the channel grouping scheme for steady state normal operation simulations is discussed. The grouping schemes for transient simulation will be described together with the transient simulation results in Section 5.2. Essentially channel grouping involves simulating of parallel flow paths with similar characteristics as a single channel, with appropriately scaled input characteristics.

The refueling scheme of the Canadian SCWR is quarter-symmetric. As an initial averaging scheme one might consider grouping the mirror image channels in each quarter of the core (i.e., 4 parallel paths are simulated as a single core pass) thus reducing the number of parallel paths from 336 to 84. However, even with this reduction the complete simulation of all 84 flow paths is not possible in CATHENA. Thus the focus of the grouping scheme in this section will examine only the 84 channels in the first-quarter of the core and how these can be reduced further. The remaining of the 336 channels will have identical behavior to the quarter core simulated below.

For steady state simulations, fuel channels in the first quarter of the core are divided into 7 groups based on their power. In addition, as channel power evolves over the batch cycles, the power at the beginning-of-cycle (i.e. 0 days), the middle-of-cycle (i.e. 210 days) and the end-of-cycle (1.e. 420 days) are all considered in the grouping. For instance, the channel power of K010 is 5.67MW at the beginning-of-cycle and 7.91MW at the end-of-cycle. If K010 were grouped into the low power group according to its beginning-of-cycle power, by the end-of-cycle, the channel power would be too high for the low power group and vice versa. So for channels like K010, it is not possible to classify which power groups they belong to as this would change over time.

This problem is overcome by classifying fuel channels using the following procedure. The first step is to locate the maximum power channels as their simulations results would potentially reveal the upper limits of the most relevant parameters such as maximum fuel sheath temperature, maximum fuel centerline temperature, orifice size, maximum mass flow rate per channel, etc. In this case, the maximum channel power is always found at channel E006 and F005 (as is shown in Figure 4.1, E006 and F005 located symmetrically in the one-quarter core) throughout the fuel cycle. A single channel group is used to model these “hot” channels since averaging them with any other lower power channel would cause a reduction in the computed channel power, and hence we would not determine the maximum channel power accurately.

						A007	A008	A009	A010
				B005	B006	B007	B008	B009	B010
		C003	C004	C005	C006	C007	C008	C009	C010
		D003	D004	D005	D006	D007	D008	D009	D010
	E002	E003	E004	E005	E006	E007	E008	E009	E010
	F002	F003	F004	F005	F006	F007	F008	F009	F010
G001	G002	G003	G004	G005	G006	G007	G008	G009	G010
H001	H002	H003	H004	H005	H006	H007	H008	H009	H010
J001	J002	J003	J004	J005	J006	J007	J008	J009	J010
K001	K002	K003	K004	K005	K006	K007	K008	K009	K010

Figure 4.1 Fuel Channel Index and Location

The second step is to divide the remaining 82 channels according to the channel power and the power history. The channels are placed into 3 groups based on the beginning-of-cycle power, namely, the low power group, the medium power group and the high power group, denoted as BL, BM and BH (nomenclature is “B” for beginning-of-cycle, and L, M, H denote the Low Medium or High channel powers). The same procedure is then repeated for the middle-of-cycle (ML, MM, MH) and end-of-cycle (EL, EM, EH) channel power distributions. After this step, each channel is assigned to one of the 3 BOC groups, one of the 3 MOC groups and one of the 3 EOC groups. For example, the channel power of H1 is 9.15MW at BOC (denoted as BH), the power then decreased to 7.90MW (denoted as MM) at MOC and slightly increased to 8.07MW at EOC (EM). Then for each channel the nomenclature is simplified to designate “xyz” where x is the beginning-of-cycle channel power (L,M,H), y is the middle-of-cycle power (L,M, H) and z is the end-of-cycle (L, M, H). Hence, channel H1 is labeled as HMM meaning it belongs to high power group at BOC and medium power groups at MOC and EOC. As there are totally three batches in a batch cycle (i.e.

420 days), and during each batch, the fuel channel belongs to one of the 3 power groups, there can be a maximum of 27 labels that describe how channel power changes over a batch cycle. Fortunately, our model did not end up with 27 groups. All the fuel channels fall into the following seven groups.

Table 4.1 Steady State Grouping Scheme

Group Label	Channel Label	Number of Channels (1/4 core)	Total Number of Parallel Pipes
LLL (Group1)	D003, C004, E003, C005, J001, A009, E010, K005, F009, J006, H006, F008, G010, K007, G007, D008, H004,J009	18	72
LMM (Group2)	G008, H007, H010, K008, H009, J008, K009, J010, K010, H008	10	40
MLL (Group3)	B010, K002, B008, H002, C009, J003 C007, G003, E005, A007, G001	11	44
MMM (Group4)	F006, B006, F002, J004 D009, J005, E009, E004, D005, D010, K004, D007, G004, C003	14	56
HMM (Group5)	D006, F004, B005, E002, A008, H001	6	24
HHH (Group6)	A010, K001, B009, J002, B007, G002, F010, K006, C008, H003, C006, F003, E008, H005, F007, G006, C010, K003, G009, J007, D004, E007, G005	23	92
HHH’ (Group7)	E006, F005	2	8

Table 4.1 shows that approximately 70% of the fuels channels consistently belong to the same power group (i.e. LLL, MMM or HHH) throughout the fuel cycle, in other words, the power variation for these channels is relatively small and hence grouping is straightforward. For the rest 30% of fuel channel, the average power swing is approximately 15% and the maximum power swing is 41% which takes place in K010.

Also note that for those 30% of channels that go through relatively large power variations, the channel power changes occur in the first 50 days, after which the power tends to remain stable. (See Figure 4.2)

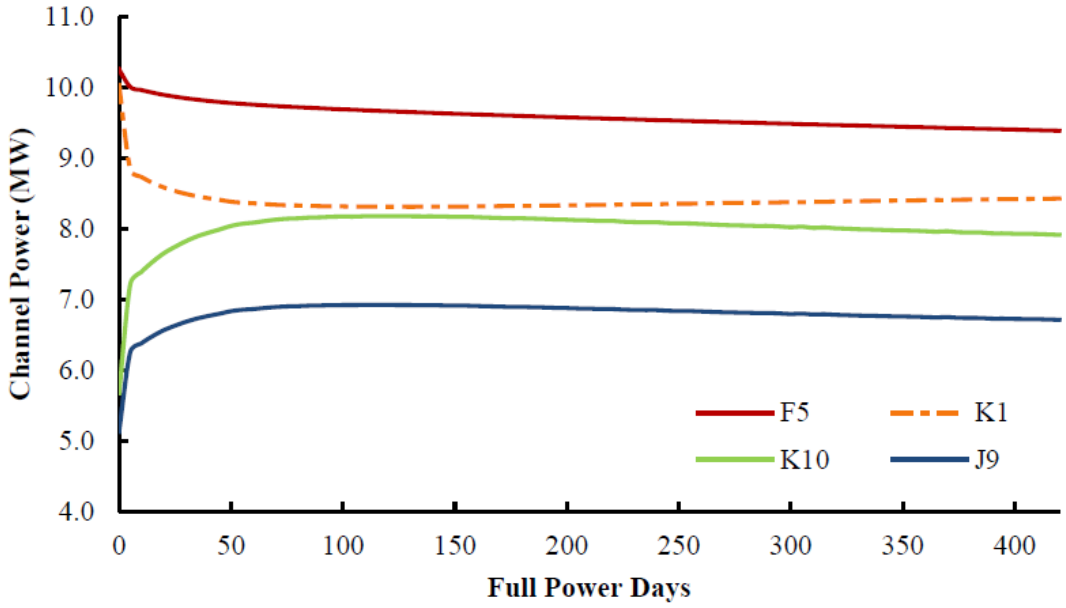

Figure 4.2 Channel Power Histories during the Equilibrium Cycle (Hummel 2014) [19]

The steady state channel power utilized in the current CATHENA models for BOC, MOC and EOC are summarized in Table 4.2

Table 4.2 Channel Power for BOC, MOC and EOC

Group Index	BOC		MOC		EOC	
	Channel	Relative to	Channel	Relative to	Channel	Relative to

	Power	Average Channel Power	Power	Average Channel Power	Power	Average Channel Power
Group1	5.95	79%	6.23	82%	6.23	82%
Group2	6.18	82%	7.90	104%	7.74	102%
Group3	7.07	94%	6.61	87%	6.65	88%
Group4	7.37	98%	7.37	98%	7.42	98%
Group5	8.68	115%	7.93	105%	8.05	106%
Group6	9.24	122%	8.75	116%	8.76	116%
Group7	10.25	136%	9.56	126%	9.38	124%
The Total Power for All 336 Channels: 2540MW The Average Channel Power:7.56MW						

The entire piping network (i.e. the thermal-hydraulic system) is described in this section. Generally, the idealization includes two thermal-hydraulics systems, one for the light water coolant and the other for the heavy water moderator which may act as the heat sink during the LOFA transients simulated later in this thesis. In the axial direction, pipes components are divided into 0.5-meter-long subsections. The junction resistances coefficients (K factor) applied at inlet plenum exit, the 180-degree bend at the bottom of the fuel channels and the plenum outlet are determined according to Crane handbook [20]. Since the hydraulic losses are dominated by these components, other loss factors such as those for the fuel element spacers or wire wrap, nozzles, etc. are not included since the details of their design were not established at the time of this thesis. Simulations demonstrated that over 95% of the pressure drop resulted from the orifice and minor bend losses, hence the impact of other smaller pressure drop components should be negligible. The safety relief valve and two isolation valves located at the main feed-water line and the main steam line are also included in the model. The components dimensions are identical to those described in the ISSCWR-6 conference paper by D.F.Wang and S.Wang [21]. The layout of the CATHENA

idealization is shown in Figure 4.3.

As shown in Figure 4.3, the model starts from Cold Leg Boundary Condition (CLEGBC) which is a reservoir component simulated as the inlet pressure boundary. Coolant from CLEGBC flows through the main feed water line (i.e., the cold leg, CLEG1 and CLEG2) and enters the inlet plenum. From the inlet plenum (IPLENUM), the coolant is distributed into the 7 fuel channel groups. In order to obtain the correct total massflow rate, each fuel channel is represented as a number of parallel pipes (the number of parallel pipes in each group is listed in Table 4.1, column 4). All fuel channels consist of a center flow tube entrance section (CCH11 and CCH12), the 5-meter-long center flow tube (CCH2), the 180 degree bending section (CCH3 and CH3), the 5 meter-long fuel region (CH2), the fuel channel exit section (CH11 and CH12, with the numbering selected so that it matches the center flow tube entrance section) and the outlet end fitting assembly (EF1 and EF2). Coolant from the fuel channels is collected in the outlet plenum (OPLENUM) and fed to the high pressure turbine through the main steam line (HLEG1, HLEG2 and HLEG3). The high pressure turbine is presented as the outlet pressure boundary (denoted as the Hot Leg Boundary Condition, i.e. HLEGBC) in the CATHENA idealization.

Since the moderator is a large volume of water with flows driven by either active or passive systems and since its primary role in this analysis is as a heat sink, its modelling is simplified as compared to a full 3-dimensional calandria vessel. Instead the moderator is modeled as a pipe with a fixed convective heat transfer coefficient and mass flow, for the scenario simulated in this thesis the moderator flow and heat transfer would be a function of the power-to-moderator at each point in time since the buoyancy driven flow will be proportional to the power-to-moderator. Again to simplify the analysis we assume a constant and low value for the moderator flow. The sensitivity to these assumptions are not specifically addressed in this work, however since the maximum clad temperatures typically occur in the first 10s of seconds, the moderator bulk flow is not expected to change significantly during this period.

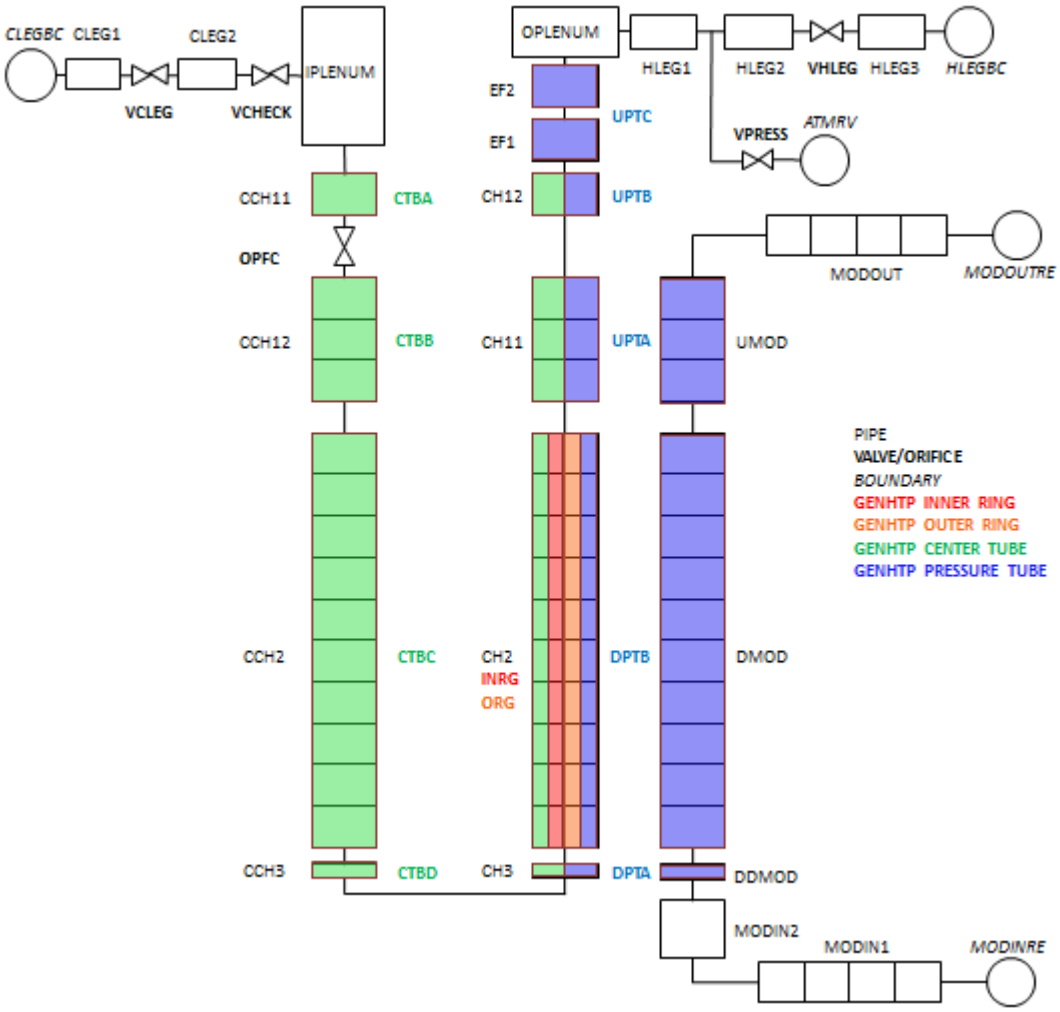

Figure 4.3 CATHENA Idealization for Canadian SCWR

4.2 System Models

Two types of CATHENA system models are included in this idealization, the junction resistance model and the valve models.

Junction resistance models are applied at three locations. The first location is between the inlet plenum (IPLENUM) and the center flow tube entrance section (CCH11). Both the IPLENUM and CCH11 are modeled as pipe components. In order to correctly simulate the pressure drop between these two components, the junction resistance coefficients (the K factors) for sharp-edged pipe

entrance are adopted. The second location is at the bottom of the fuel channel where the flow direction is reversed. The K factors at this location are calculated as the combination of the 180-degree bending and the abrupt area change. The third location is between the fuel region exit section (CH12) and the outlet plenum (OPLENUM). Similar to the first junction resistance model, the K factors for sharp-edged pipe exit are applied at this location. All the junction resistance models are listed in Table 4.3.

Table 4.3 List of Junction Resistance Models

Model Name	Location Between		Resistance (Forward, Reversed)	Remark
JINP	IPLENUM(5)	CCH11_X(1)	0.5,1.0	Flow from inlet plenum "X"=1,2,3,4,5,6,7
JTURN	CCH3_X(1)	CH3_X(1)	1.16,1.36	Flow through 180-degree bend "X"=1,2,3,4,5,6,7
JEF	CH12_X(3)	OPLENUM(1)	1.0,0.5	Flow into outlet plenum "X"=1,2,3,4,5,6,7

Four valve/orifice models are used in the CATHENA idealization.

- Valves Type 1 and 2: The two primary heat transport system isolation valves (denoted as VCLEG and VHLEG) located at main feed-water line and main steam-line are modeled as normal valves. These values remained fully open for the steady state simulations and are closed within a one-second period to initiate LOFA transient.
- Valves Type 3: a check valve (denoted as VCHECK) is located between the main feedwater line and the inlet plenum to prevent coolant flow reversal from the reactor core to the feedwater line.
- Valve Type 4: The main steam line is connected to the atmosphere pressure through the

safety relieve valve (VHLEG) of which the opening and closing pressure are 26.0MPa and 25.25MPa respectively. No SRV actions take place during the steady state simulations. However, for the transient simulations, SRV actuates frequently, especially for the first 200s.

- Valve Type 5: In order to achieve uniform coolant outlet temperatures in channels with varying powers, orifices are set up between CCH11 and CCH12 (i.e. the center flow tube entrance area) to regulate the coolant massflow rate. The open fractions of the orifice are varied by the Proportional-Integral controllers within CATHENA which will be explained in the control model section.

For all the valve/orifice models described above, the flow area equals to the cross-section area of the respective connecting pipes. Table 4.4 summarizes the valve/orifice models used in the CATHENA idealization.

Table 4.4 List of Valve/Orifice Models for Steady State Simulation

Model Name	Location Between	Flow Area (m^2)	Open Fraction	Remark
VCLEG	CLEG1,CLEG2	2.761E-01	1.0	
VCHECK	HLEG3,IPLENUM	2.761E-01	1.0	
VHLEG	HLEG2,HLEG3	5.027E-01	1.0	
VPRESS	HLEG1,ATMRV	5.027E-01	1.0	
OPFC_1	CCH11_1(1),CCH12_1(1)	4.072E-03	0.03957	Orifices at fuel channel inlets
OPFC_2	CCH11_2(1),CCH12_2(1)	4.072E-03	0.05198	
OPFC_3	CCH11_3(1),CCH12_3(1)	4.072E-03	0.04222	
OPFC_4	CCH11_4(1),CCH12_4(1)	4.072E-03	0.04795	
OPFC_5	CCH11_5(1),CCH12_5(1)	4.072E-03	0.05223	
OPFC_6	CCH11_6(1),CCH12_6(1)	4.072E-03	0.05888	
OPFC_7	CCH11_7(1),CCH12_7(1)	4.072E-03	0.06578	

4.3 System Control Models

Six types of system control models are used in the CATHENA idealization. The main controller used to establish the steady state is the Proportional-Integral (PI) controller, which is used to regulate the massflow rate at the entry of all 84 fuel channel such that a uniformed temperature field of 625 ^{o}C at the exit of the outlet plenum could be achieved. It's is found out that the orifice size is linear to the channel power. Hence, the orifice sizes of the seven channel groups are determined according to their averaged channel power. This controller is artificial and is only used in the orifice sizing calculations, once established the orifice sizes remained fixed for the duration of the analysis. It is assumed that the heat transfer between the outlet plenum and the inlet plenum will reduce the coolant temperature by 5 ^{o}C. Therefore, the coolant temperature should be approximately 630 ^{o}C upon reaching the fuel channel outlets. The temperature difference between the fuel channel outlets and the set-point (i.e. 630^{o}C) is sent back to the PI controller so that the open fraction of the orifice can be recalculated. This procedure is continually repeated until the temperature is stabilized to the set point value. As noted that the PI controllers are solely used for calculating the orifice sizes. Once the orifice size data has been collected, the PI controllers are removed from the CATHENA input file. According to the BOC, MOC and EOC power, three sets of orifice size data have been calculated. The MOC orifice sizes are selected for the steady state and transient simulations since they represent the channel powers for a large fraction of time during the batch cycle. The reactor power regulating system is still under design, but it is assumed that the reactivity devices will balance power within a small amount centered about the MOC channel powers.

The "Output" system control model is included in the CATHENA idealization to output the key parameters at various locations. For the steady state simulations, the output parameters include: fuel center-line temperatures, fuel sheath temperatures, inside and outside surface temperatures of

pressure tube, inside and outside surface temperatures of center flow tube, coolant temperatures, coolant density at fuel regions and moderator temperatures. For transient simulations, in addition to the parameters above, the pressure and coolant density in inlet and outlet plenum, the heat transfer coefficients as well as the heat fluxes at the fuel cladding, center flow tube and pressure tube are also recorded.

Coolant density variation in the fuel regions plays a crucial role in reactor physics. In order to quantitatively represent how the coolant density changed along the fuel assemblies, two additional parameters regarding coolant density are calculated in CATHENA through the "Calculate" model. These two parameters are the average coolant density and the density ratio of the top 2.5-meter coolant to the bottom 2.5-meter coolant in the fuel region. These quantities are used to study the effect of channel grouping on top-to-bottom density differences which could lead to axial power tilts in the core.

"Input Table", "Application Point" and "Table Variable" are three control models that are used together throughout the simulations to calculate and apply functional information as follows. For transient simulations, the decay heat level as well as the valve action positions are included in CATHENA via the "Input Table" model. The term "Application Point" is self-explanatory. It addresses the parameter that CATHENA is going to calculate with. As for the "Table Variable" model, it acts as a link between the "Input table" and the "Application Point". For instance, after the reactor trips, the fuel power decreases from 100% full power to approximately 5% of full power (i.e. the decay heat level) in a short period and then gradually decreases according the decay curve. The power changes are documented in the "Input Table". The inner ring and outer ring power are specified as the Application Point. Both the Application Point and the label of the power Input Table are listed in the "Table Variable" model so that when it is invoked by CATHENA, the power variation is applied to the inner ring fuel rods and outer ring fuel rods as a function of time. Table 4.5 summarizes the system control models used in the CATHENA

idealization. Since a large number of "Output" models are involved in the CATHENA idealization, they are not listed in the table.

The transient channel power is imported via an input table specifying the decay power factions as a function of time. The decay heat powers for fuel burnup of 18.3 MWd/kg, 36.7 MWd/kg and 55.0 MWd/kg are provided by AECL [22]. The decay heat power for the fuel-burnup of 36.7MWd/kg is selected for this study as it is in consistent with the orifice sizes used for the transient simulation and it provides the highest maximum fuel sheath temperature during the LOFA transients.

Table 4.5 List of System Control Table

Model Name	Controls	Set-point	Control Action	Remark
TCVA_X	Fuel channel outlet temperatures	630 ^{o}C	Change the open fraction of orifice OPFC_X	"X"=1,2,……,84
GRPAVEX	-	-	-	The average coolant density at fuel region. "X"=1,2,3,4,5,6,7
GRPRATX	-	-	-	The ratio of top half coolant density to the bottom half coolant density in fuel region "X"=1,2,3,4,5,6,7
TIMOPFCC	Isolation valve positon	-	Change the open fraction of the isolation valve on the main	The valve position is given by the input table "OPFC"

			feed-water line	
TIMOPFCH	Isolation valve positon	-	Change the open fraction of the isolation valve on the main steam line	The valve position is given by the input table “OPFC”
TIMPWR	Channel power	-	Impose decay heat power to fuel rods	The power data is given by the input table “TBPWR”

4.4 Heat Transfer

4.4.1 Solid Components

Heat transfer between wall models and thermal-hydraulic nodes are calculated by employing the GENeralized Heat-Transfer Package (GENHTP). Four wall models, namely the center flow tube (CTTB), the Inner Ring fuel rods (INRG), the Outer Ring fuel rods (ORG) and the pressure tube (DPT and UPT) are included in the CATHENA idealization (see Figure 4.3).

For the fuel elements, the 64 fuel pins are modeled by two independent GENHTP models denoted as INRG_X and ORG_X (where X is the channel group index. For steady state simulation, it could be any numbers from 1 to 7). The INRG models the 32 identical cylinders located at the inner concentric ring and the ORG models the rest 32 cylindrical fuel pins located at the outer concentric ring. The dimensions of the fuel pins are consistent with those provided in [23]. The power distribution between inner ring fuel pins and outer ring fuel pins is 48.6% and 51.4% respectively. In the axial direction, the 5-meter long fuel models are divided into 10 sections of equal length. As is shown on Figure 4.4, each axial segment is further divided into 3 circumferential sector groups with 2 sectors in each group. This section method takes advantage of

lateral symmetry to reduce the computation time. In CATHENA, the temperatures of each sector group are calculated separately, nevertheless, the different sectors in a sector group share the same temperature. For instance, sector 3 and sector 3' of the INRG (see Figure 4.4) are symmetrically located on either side of an Inner Ring fuel rod. The temperatures of these two locations are the same. By assigning them to the same sector group, the fuel temperature is only calculated once and hence reducing the computation time for heat transfer from the pin.

Note that heat conduction solution scheme for the fuel models (i.e. INRG and ORG) is selected as "radial and circumferential conduction", the heat generated in the fuel pins is not only conducted from the fuel centerline to the fuel cladding, but also from one sector group to another sector group at a specific elevation. The axial conduction and radiation heat transfer mechanisms are not modelled in CATHENA. The axial power distribution of BOC, MOC and EOC are plotted in Figure 4.5. The material properties, heat conductivity and volumetric heat capacity of the fuel pins are provided by AECL [24] and summarized in Table 4.6. The CATHENA built-in temperature-dependent thermal properties of stainless steel are used for the fuel cladding.

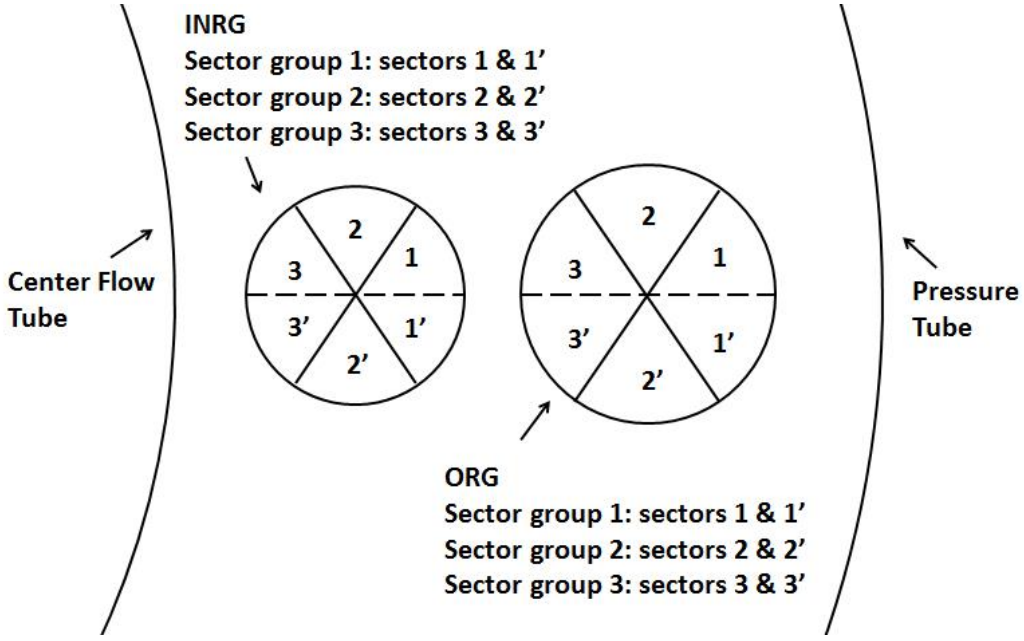

Figure 4.4 Sector Geometry and Nodalization

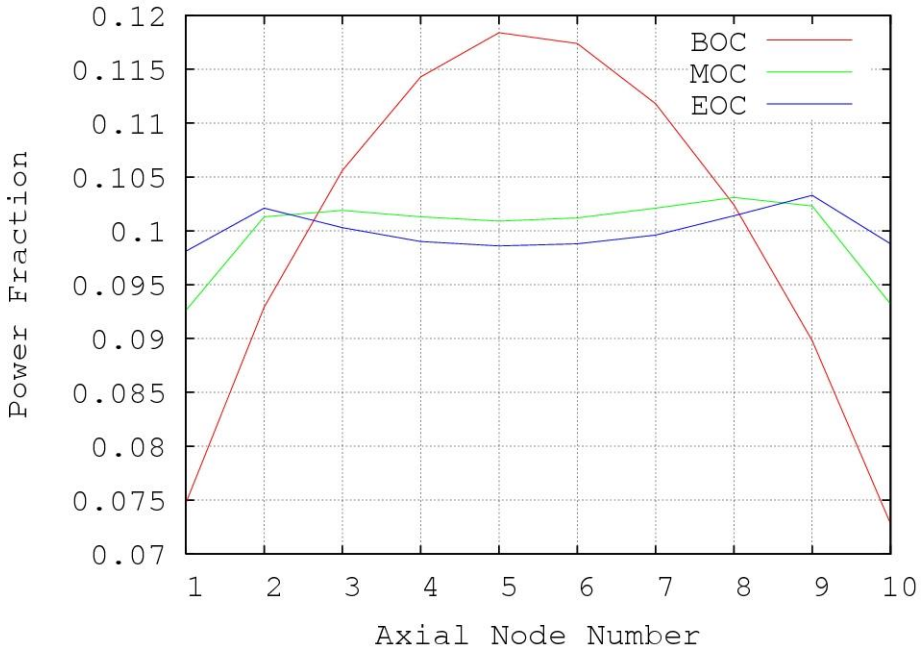

Figure 4.5 Axial Power Distributions of BOC, MOC and EOC (Power for Given Node Divided by Total Power for all 10 Axial Nodes)

Table 4.6 Thermal Heat Conductivity and Volumetric Heat Capacity of the Fuel

Temperature (℃)	Inner Ring		Outer Ring	
	Thermal Conductivity (W/m/℃)	Volumetric Heat Capacity (J/m^3/℃).	Thermal Conductivity (W/m/℃)	Volumetric Capacity (J/m^3/℃).
27	3.8	2.18E+06	4.77	2.17E+06
127	3.42	2.39E+06	4.2	2.38E+06
227	3.11	2.51E+06	3.75	2.50E+06
327	2.86	2.60E+06	3.39	2.59E+06
427	2.64	2.66E+06	3.1	2.64E+06
527	2.45	2.70E+06	2.85	2.69E+06

627	2.29	2.72E+06	2.63	2.71E+06
727	2.15	2.74E+06	2.45	2.73E+06
827	2.02	2.75E+06	2.29	2.74E+06
927	1.91	2.75E+06	2.15	2.74E+06
1027	1.81	2.75E+06	2.03	2.74E+06
1127	1.72	2.75E+06	1.92	2.74E+06
1227	1.64	2.75E+06	1.82	2.74E+06
1327	1.57	2.76E+06	1.73	2.75E+06
1427	1.5	2.76E+06	1.65	2.75E+06
1527	1.44	2.78E+06	1.58	2.77E+06
1627	1.38	2.79E+06	1.51	2.79E+06
1727	1.33	2.82E+06	1.45	2.82E+06
1827	1.28	2.86E+06	1.39	2.86E+06
1927	1.23	2.91E+06	1.34	2.91E+06
2027	1.19	2.98E+06	1.29	2.98E+06
2127	1.15	3.06E+06	1.24	3.06E+06

2227	1.11	3.15E+06	1.2	3.16E+06
2327	1.08	3.26E+06	1.16	3.27E+06
2427	1.05	3.40E+06	1.12	3.41E+06
2527	1.01	3.55E+06	1.09	3.57E+06
2627	0.99	3.73E+06	1.06	3.75E+06
2727	0.96	3.93E+06	1.03	3.96E+06

In order to improve computational efficiency, the center flow tube and pressure tube are divided into a series of wall models to match the corresponding thermal-hydraulic components. For instance, the center flow tube is divided into four individual wall models, namely, CTBA, CTBB, CTBC and CTBD corresponding to the pipe components of CCH11, CCH12, CCH2 and CCH3. These wall models are further divided into segments of equal length such that the wall heat transfer segmentation coincides with the thermal-hydraulic segmentation. The dimensions of the center flow tube and the pressure tube are based on those given in [23]. The material properties of the center flow tube and the pressure tube are determined in accordance with the plots given in Reference [25] and Reference [26]. Also note that in the fuel exit section, which is the area between the top of the active fuel and the outlet plenum, there is a thin insulation coating at the outer surface of the center flow tube to prevent heat transfer from the high temperature outlet coolant to the center flow tube (CTBA and CTBB). Since no material properties of the insulation coating have been provided, it is modeled by reducing the thermal conductivities of the CTBA and CTBB by 90%.

4.4.2 Auxiliary Model/ Radiation Heat Transfer

Radiation heat transfer plays a crucial role during transient simulations especially when fuel

sheath temperatures exceed approximately 650 ^{o}C. Therefore, radiation models are included in the CATHENA idealization to simulate the heat exchange among the fuel rods, the center flow tube outer cladding and the liner tubes.

To calculate the radiation heat transfer rates at the fuel cladding, the following parameters are required: the fuel cladding temperatures, the temperatures of other wall surfaces in the enclosure, the emissivity, the areas of the wall surfaces involved and the view factor matrix. Among these parameters, the temperatures of the wall models are calculated by the code. The emissivity is given by the user, and in this case, an emissivity equals to 0.8 is applied to all the wall models (but is varied in the sensitivity studies). The surface areas are determined according to the user-defined dimensions. And the view factor matrix is generated by a separated program named GEOFAC.

GEOFAC, an abbreviation for GEOmetry FACtors, is a utility for calculating view factor matrix for use by the CATHENA Radiation Model. The GEOFAC version 1.0.2 is used in the analysis. In GEOFAC, the view factor matrix consists of all the view factors in an enclosure. The view factor $V_{i\to j}$ between each pair of surfaces *i* and *j* at any given location in GENHTP model is calculated by using Hottel's 'crossed-string' method.

There are three factors need to be specified in the GEOFAC input file. The first is the configuration. In this case, the dimensions and relative locations of the four wall models (i.e. CTBC, INRG, ORG and DPTB) are presented according to the GEOFAC user manual. The second is the number of sectors in each wall model. In the CATHENA idealization, the center flow tube (i.e. CTBC) and pressure tube (i.e. DPTB) are both divided into 6 sectors. For fuel pins, the dividing scheme in GEOFAC is consistent with the previous definitions in the GENHTP, which means there are 6 sectors for each fuel pins and a total number of 384 sectors for 64 fuel pins. In total, 396 sectors are defined in GEOFAC, and therefore, the size of the view factor matrix is 396×396. The last factor is the number of segments in each sector. The more segments per sector,

the more accurate the matrix calculation is. In this case, 100 segments per sector are chosen for all the sectors. Figure 4.6 illustrates the layout of the view factor matrix.

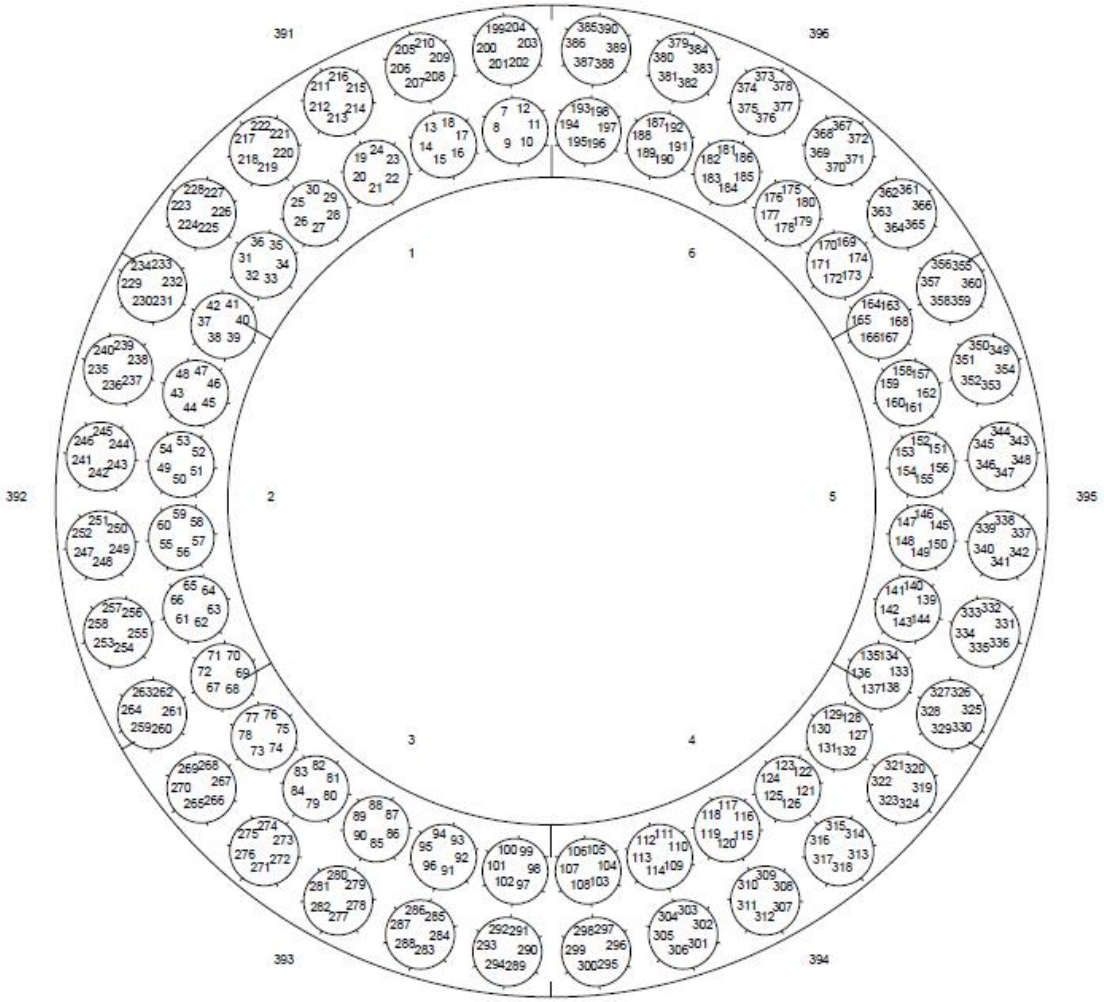

Figure 4.6 Layout of the View Factor Matrix

4.5 Boundary Conditions

All boundary conditions involved in the CATHENA idealization are listed in Table 4.7. For the coolant, boundary conditions are applied at the inlet of the main feed-water line and the outlet of the main steam line. In addition, a boundary condition of standard atmospheric pressure is specified and connected to the main steam line through the safety relief valve (which is normally closed but actuates at the relief set-point pressure).

The inlet and outlet boundary conditions for the moderator are also specified in the CATHENA input file. A mass flow boundary condition of 1650kg/s is applied to the moderator via flow boundary condition. In addition to the heat transferred from the pressure tube, a constant power of 133MW is deposited in the moderator via heat input boundary condition to model the nuclear heating during steady state operation. During the transient simulations, this net energy deposit is removed from the model and only heat conducted via the pressure tube is deposited in the moderator.

Table 4.7 List of Boundary Conditions

Model Name	BCIN	BCOUT	BCMDIN	BCMDOUT	MDRTORE	MDHEATD	ATM
Applies to	CLEGBC	HLEGBC	MODINRE	MODOUTRE	MODINRE,L-MODIN1	DMOD	ATMRV
Pressure (MPa)	25.813	24.972	0.336	0.234	-	-	0.101
Liquid Temperature (^{o}C)	350	625	55	85	-	-	-
Vapor Temperature (^{o}C)	Tsat	Tsat	Tsat	Tsat	-	-	-
Void Fraction	0.0	0.0	0.0	0.0	-	-	-
Flow Rate (kg/s) Flow B.C. only	-	-	-	-	1650	-	-
Heat Input (MW) Heat input B.C.	-	-	-	-	-	133	-

only							
Remark	Main feed water line inlet	Main steam line outlet	Moderator inlet	Moderator outlet	Moderator flow	Moderator Nuclear heating	SRV Atmosphere pressure a

4.6 Control Parameters

Table 4.8 summarizes the numeric options used in the idealization. All of the numeric options used here are in consistence with Reference [21]

Table 4.8 List of Numeric Options

Numeric Option	Justification
'HLWP-VERSION(1)'	Light water properties are extended into super critical pressure conditions
'#-PRESS-HIGH(-3)'	A warning message will be printed for the first three times when the parameters go out of range. After that, the simulation will continue with no warning message printed.
'#-PRESS-LOW(-3)'	
'#-HF-HIGH(-3)'	
'#-HF-LOW(-3)'	
'#-HG-HIGH(-3)'	
'#-HG-LOW(-3)'	
'#-VEL-HIGH(-3)'	

The steady state simulation lasts for 16000s, accomplished in two steps. From 0s to 11000s, the conductive heat transfer in the fuel models (i.e. INRG and ORG) is simulated in radial direction only. From 11000s to 16000s, the conduction solution scheme is switched to "radial and circumferential conduction" and thus the conductive heat transfer in both radial and circumferential direction are included in the simulation. The maximum and minimum time steps

implemented in the CATHENA idealization are 0.25s and 0.0005s respectively, which is consistent with Reference [21]. A restart file is generated during the steady state simulation, which contains the values for the thermal-hydraulic conditions, GENHTP conditions and the system control models. This file is used to initialize the LOFA transient. A minimum and maximum time-step of 1E-8 and 1E-2 second were adopted by transient simulations.

5 Results and discussion

5.1 Simulation Results for Steady-State Normal Operations

Steady-state simulation results for BOC, MOC and EOC are summarized in Table 5.1, Table 5.2 and Table 5.3. As shown in the tables, since MOC orifice sizes are used for all the steady simulations, the mass flow rates for the BOC, MOC and EOC are very similar, which are 1253.0kg/s, 1256.3kg/s and 1256.6kg/s respectively. The channel flow ranges from approximately 3.07kg/s for the channels in the low power group to 4.78kg/s for the channels in the maximum power group.

As indicated earlier, 30% of the fuel channels go through relatively large power swings at the beginning-of-cycle. For these channels, the BOC channel power does not match with the MOC orifices size, which leads to large temperature variations from the 630 ^{o}C- set-point at fuel channel outlet (see Table 5.1, column 3). The lowest channel outlet temperature for BOC is 489.3 ^{o}C which is found in Group2, while the highest channel outlet temperature is 704.1 ^{o}C which is found in Group5. In addition, the channel power distribution flattens with fuel depletion. For the steady state normal simulation, the highest fuel sheath temperature for the maximum power channel at beginning-of-cycle (BOC), middle-of-cycle (MOC) and end-of-cycle (EOC) are 829.2 ^{o}C, 778.0 ^{o}C and 795.6^{o}C respectively.

Except for the orifice sizes optimization algorithm discussed by Hummel et al. (2014) [19], no studies concerning channel orifice size have been found. However, as a primary design parameter, orifice size has great influence on both the fuel assembly and coolant temperatures during steady state and transient simulations. While the channel power grouping here and subsequent orifice sizes are self-consistent, the actual orifice sizing would be much more difficult and subjected to

much larger swings in channel powers if all 336 channels were simulated (since the individual channel power swings are much larger than an averaged value for a group of channel). Such detailed sizing has been presented by Hummel and Novog [19].

Table 5.1 Steady State Simulation Results for BOC

Group Index	BOC								
	Flow	Channel Flow	Coolant Temperature at Channel Outlet	Channel Power	Relative to Average Channel Power	Maximum Fuel Centerline Temperature Inner Ring	Maximum Fuel Centerline Temperature Outer Ring	Maximum Fuel Sheath Temperature Inner Ring	Maximum Fuel Sheath Temperature Outer Ring
Unit	kg/s	kg/s	^{o}C	MW	-	^{o}C	^{o}C	^{o}C	^{o}C
Group1	221.0	3.07	597.3	79%	5.95	699.1	697.4	1534.8	1468.8
Group2	158.9	3.97	489.3	82%	6.18	563.3	562.9	1414.0	1342.2
Group3	142.3	3.23	682.9	94%	7.07	801.2	798.5	1924.2	1848.5
Group4	203.7	3.64	630.3	98%	7.37	741.5	739.7	1902.7	1820.4
Group5	93.2	3.88	704.1	115%	8.68	829.2	826.5	2376.6	2279.9
Group6	396.3	4.31	675.1	122%	9.24	797.5	795.4	2476.0	2371.1
Group7	37.6	4.70	689.8	136%	10.25	816.4	814.3	2809.6	2695.1
The Total Massflow For All 336 Channels: 1253.0 kg/s									

Table 5.2 Steady State Simulation Results for MOC

Group Index	MOC								
	Flow	Channel Flow	Coolant Temperature At Channel	Channel Power	Relative to Average Channel	Maximum Fuel Centerline	Maximum Fuel Centerline	Maximum Fuel Sheath Temperature	Maximum Fuel Sheath Temperature

			Outlet		Power	Temperature Inner Ring	Temperature Outer Ring	Inner Ring	Outer Ring
Unit	kg/s	kg/s	^{o}C	MW	-	^{o}C	^{o}C	^{o}C	^{o}C
Group1	220.7	3.07	629.2	6.23	82%	767.1	764.5	1693.0	1633.8
Group2	156.4	3.91	629.9	7.90	104%	773.2	771.0	2050.4	1973.9
Group3	143.0	3.25	629.8	6.61	87%	769.1	766.5	1769.4	1707.1
Group4	204.0	3.64	629.7	7.37	98%	771.4	769.0	1932.3	1862.9
Group5	94.3	3.93	629.9	7.93	105%	773.4	771.2	2058.3	1981.3
Group6	399.8	4.35	629.4	8.75	116%	775.2	773.4	2252.3	2165.3
Group7	38.1	4.76	629.9	9.38	126%	778.0	776.3	2459.0	2362.8
The Total Massflow For All 336 Channels: 1256.3 kg/s									

Table 5.3 Steady State Simulation Results for EOC

Group Index	EOC								
	Flow	Channel Flow	Coolant Temperature at Channel Outlet	Channel Power	Relative to Average Channel Power	Maximum Fuel Sheath Temperature Inner Ring	Maximum Fuel Sheath Temperature Outer Ring	Maximum Fuel Centerline Temperature Inner Ring	Maximum Fuel Centerline Temperature Outer Ring
Unit	kg/s	kg/s	^{o}C	MW	-	^{o}C	^{o}C	^{o}C	^{o}C
Group1	220.7	3.07	628.5	6.23	82%	774.2	771.4	1727.1	1672.1
Group2	156.7	3.92	614.6	7.74	102%	762.5	760.5	2013.4	1942.3
Group3	143.0	3.25	634.8	6.65	88%	783.4	780.6	1823.8	1764.6
Group4	204.0	3.64	634.0	7.42	98%	785.1	782.5	1984.0	1916.5
Group5	94.1	3.92	640.8	8.05	106%	795.6	793.3	2137.9	2065.0
Group6	399.9	4.35	630.2	8.76	116%	784.8	782.8	2281.6	2199.6

Group7	38.2	4.78	615.2	9.38	124%	768.2	766.5	2398.9	2309.4
		The Total Massflow For All 336 Channels: 1256.6 kg/s							

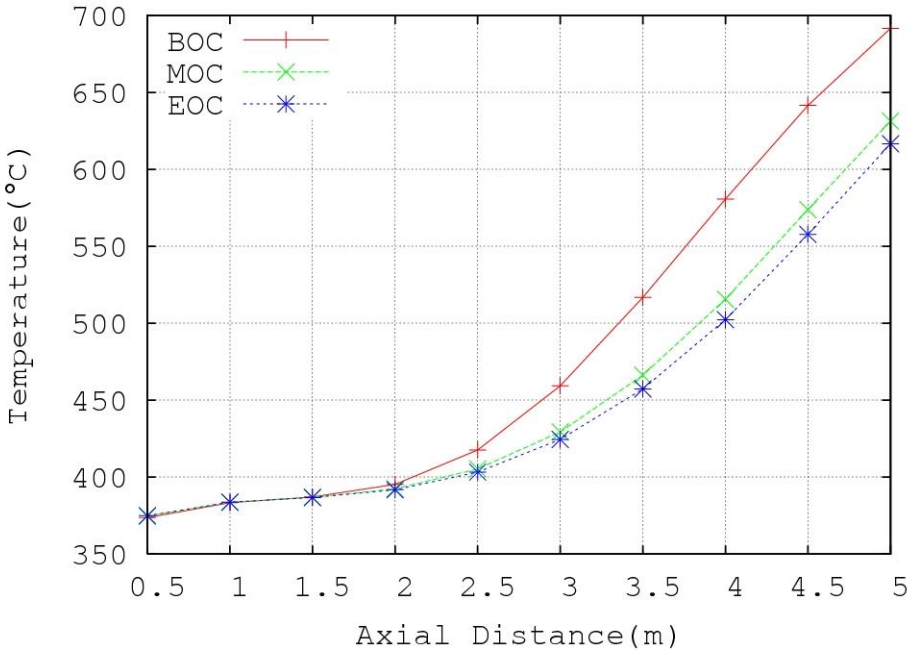

Figure 5.1 Axial Coolant Temperature Profile for the Maximum Power Channel

The calculated axial temperature profiles for the coolant, fuel center line and fuel sheath of the maximum power channel (i.e. group7) are plotted in Figure 5.1, Figure 5.2 and Figure 5.3 respectively. For the maximum channel power group, the maximum sheath temperatures for BOC, MOC and EOC are 816.4^{o}C, 778.0 ^{o}C and 768.2 ^{o}C respectively. The maximum center line temperatures for BOC, MOC and EOC are 2809.6 ^{o}C, 2459.0^{o}C and 2398.9^{o}C respectively. As is shown in Figure 30 and Figure 31, the sheath temperature of the Inner Ring and Outer Ring are approximately the same meanwhile the center line temperatures of the Inner Rings are consistently higher than that of the Outer Rings.

For the light water coolant, as it flows down along the inside surface of the center flow tube, small amount of heat is transferred to the coolant from the center flow tube. Upon reaching the bottom of the center flow tube, the flow direction reverses and the coolant starts to travel upwards along the fuel bundles. As is shown in Figure 29, upon entering the fuel region, the coolant temperature

is approximately 370 ^{o}C. A moderate increase in the coolant temperature is observed as the coolant goes through pseudo critical transitions (at 25MPa, the pseudo-critical temperature is approximately 384 ^{o}C) at the bottom of the fuel region. As indicated earlier, in CATHENA, the pseudo critical transition always accompanied by an artificially high heat transfer coefficient. This explains why there is a pronounced sheath temperature reduction at 1.5m from the bottom of the active fuel as indicated in Figure 30. The coolant reaches the maximum temperature of 691.6 ^{o}C, 631.4 ^{o}C and 615.6 ^{o}C for BOC, MOC and EOC at the top of fuel region. After passing through the outlet plenum, the coolant temperatures decrease by 5 ^{o}C due to the heat transfer between the outlet plenum and inlet plenum.

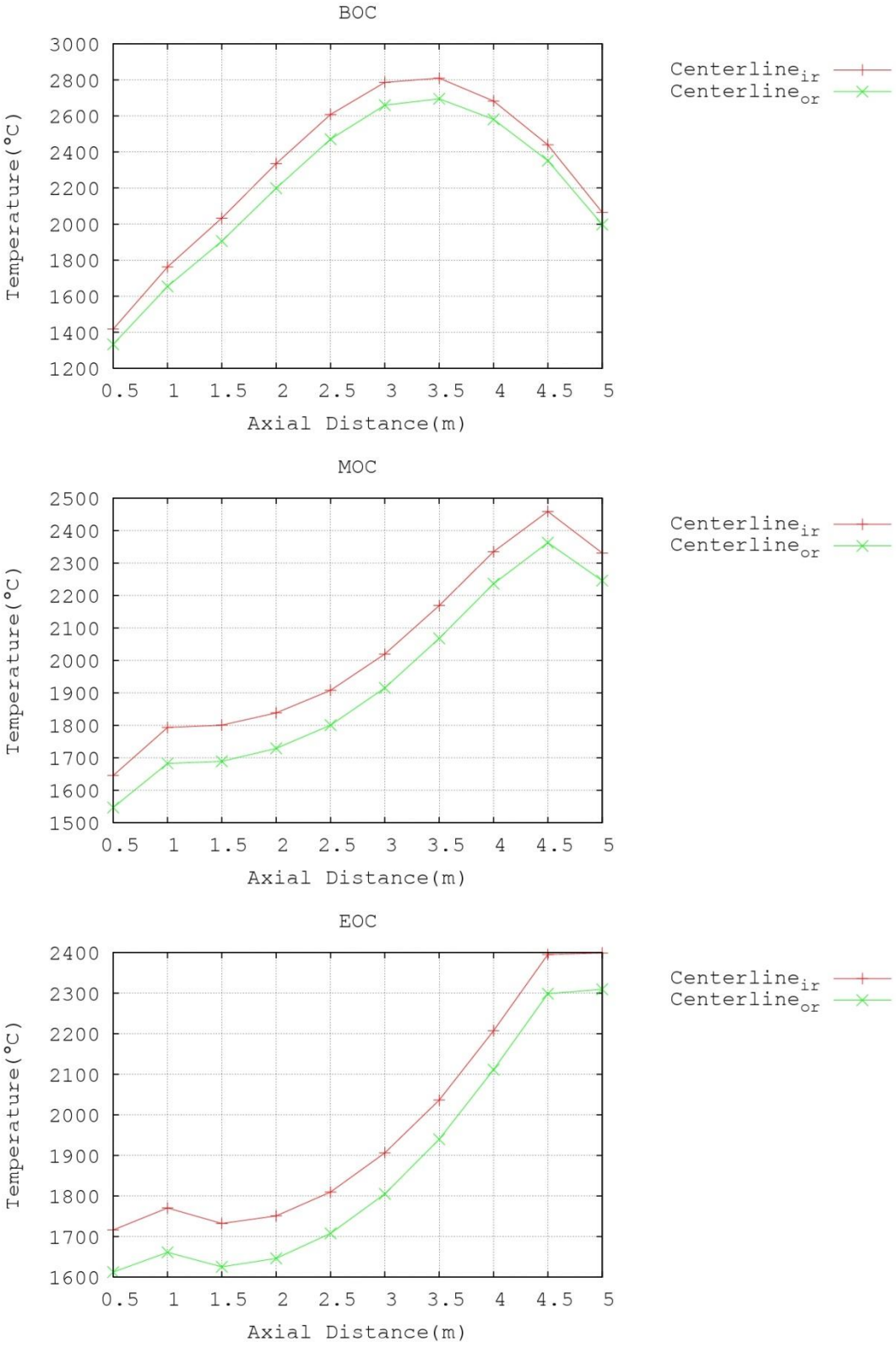

Figure 5.2 Axial Fuel Centerline Temperature Profile for the Maximum Power Channel

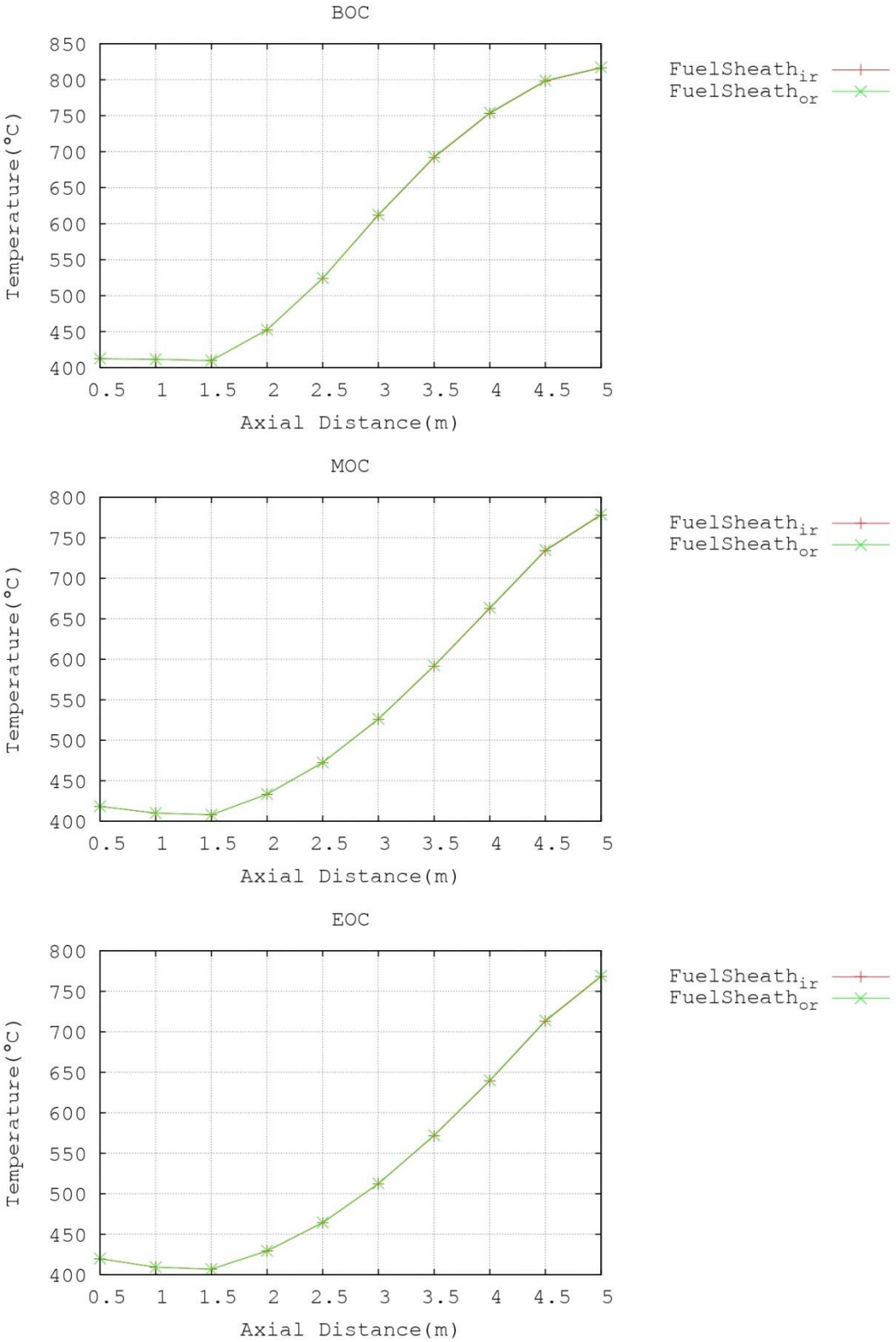

Figure 5.3 Axial Fuel Sheath Temperature Profile for the Maximum Power Channel

5.2 LOFA Transient Results

In these simulations, the LOFA transient started at 0s. A sufficiently long zero-change transient was performed prior to the LOFA such that CATHENA had reached a steady-state. Two isolation valves located at the main feed-water line and main steam line are closed from 0s to 1s simultaneously, effectively causing a complete loss of driving flow within 1s. In reality station transients would involve a flow rundown on the order of 5 to 10s depending on pump inertia, thereby making the simulated transient more severe than those anticipated in practice. Reactor shut down is credited at 0.29s due to the low flow trip (with an actuation set-point of 90% of steady state flow), and power reduction from rapid insertion of the shutdown system is credited. As a result of safety system action, the power in the simulations is ramped to decay heat in approximately 0.1s. In order to assess the sensitivity of the MCT to trip time and shutdown characteristics additional simulations are performed in Section 5.3. The sequences of events are summarized in Table 5.4.

Table 5.4 Sequences of Events for LOFA Transients

Time (s)	Events
0.0	Isolation Valves started to close leading to loss of main feedwater
0.29	Reactor shutdown signal triggered (90% of the steady state flow), control rods inserted into reactor core in 0.1s
1.0	Isolation Valves were completely closed

5.2.1 LOFA Simulation Results Using 2 Channel Groups

As shown in Table 5.5, the 336 channels are divided into two channel groups. The first group

consists of 335 channels, with an average channel power of 7.55MW. The simulation results for Group1 represent the averaged channel behaviors and thus provide the system characteristics for the entire idealization (i.e., the behavior of the flows in these 335 channels will dictate the response of the plena, SRV timing, etc…). The maximum power channel is selected and denoted as Group2. The simulation results of Group2 reveal the upper limits of the critical parameters such as maximum fuel cladding and fuel temperatures upon which the safety margin can be estimated.

The initial conditions for the simulations in both groups are the same with the exception of the channel power and the orifice size used (since the channel flow and power are matched and correspond to the more middle-of-cycle channels power distribution). Similar to the steady state simulations, as well as those performed elsewhere [19], the BOC channel power distribution may be more limiting, and that the flow-power matching using orifice sizes selected at MOC does not provide acceptable behavior during a fueling cycle. However, in this thesis it is assumed that there is a control system which is able to manage the initial channel power peaks during the BOC and hence MOC powers are selected. Since the conditions are similar the powers are matched to flow, the initial sheath temperatures prior to the transient are similar.

Table 5.5 2-Channel Groups Grouping Scheme

	Type of Channel	Number of Channels	Single Channel Power (MW)	Normalized Power Distribution (MW)[1]	Initial Massflow per Channel (kg/s)	Initial Total Massflow per Group (kg/s)
Group1	Average Power	335	7.55	0.99624	3.524	1250.929
Group2	Maximum	1	9.56	0.00376	4.758	4.758

[1] Fraction of the total core power over all channels in a channel power group.

	Power					
The Total Power of All 336 Channels is 2540MW						

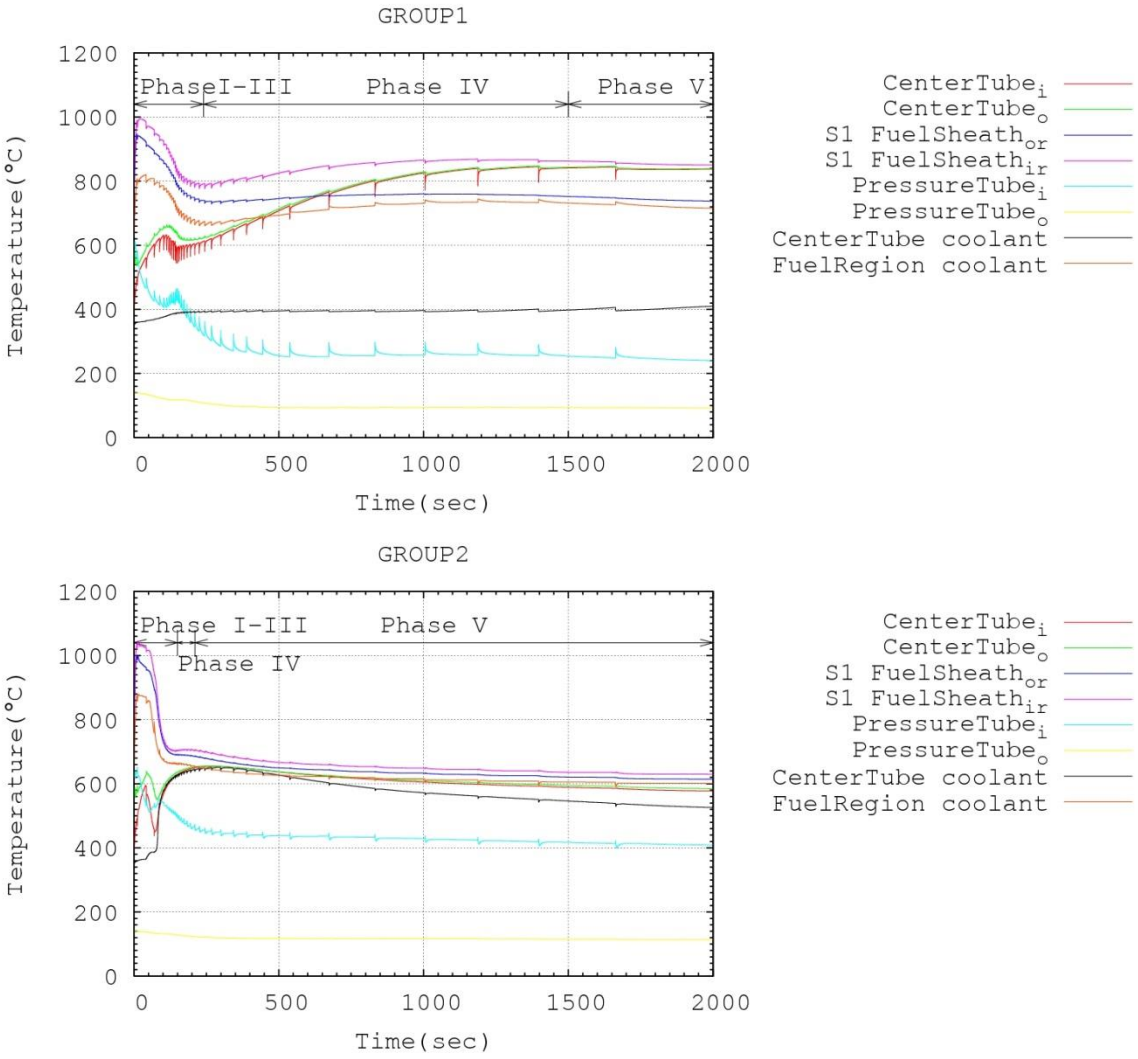

Figure 5.4 Temperature of Various Components at CH2(10)

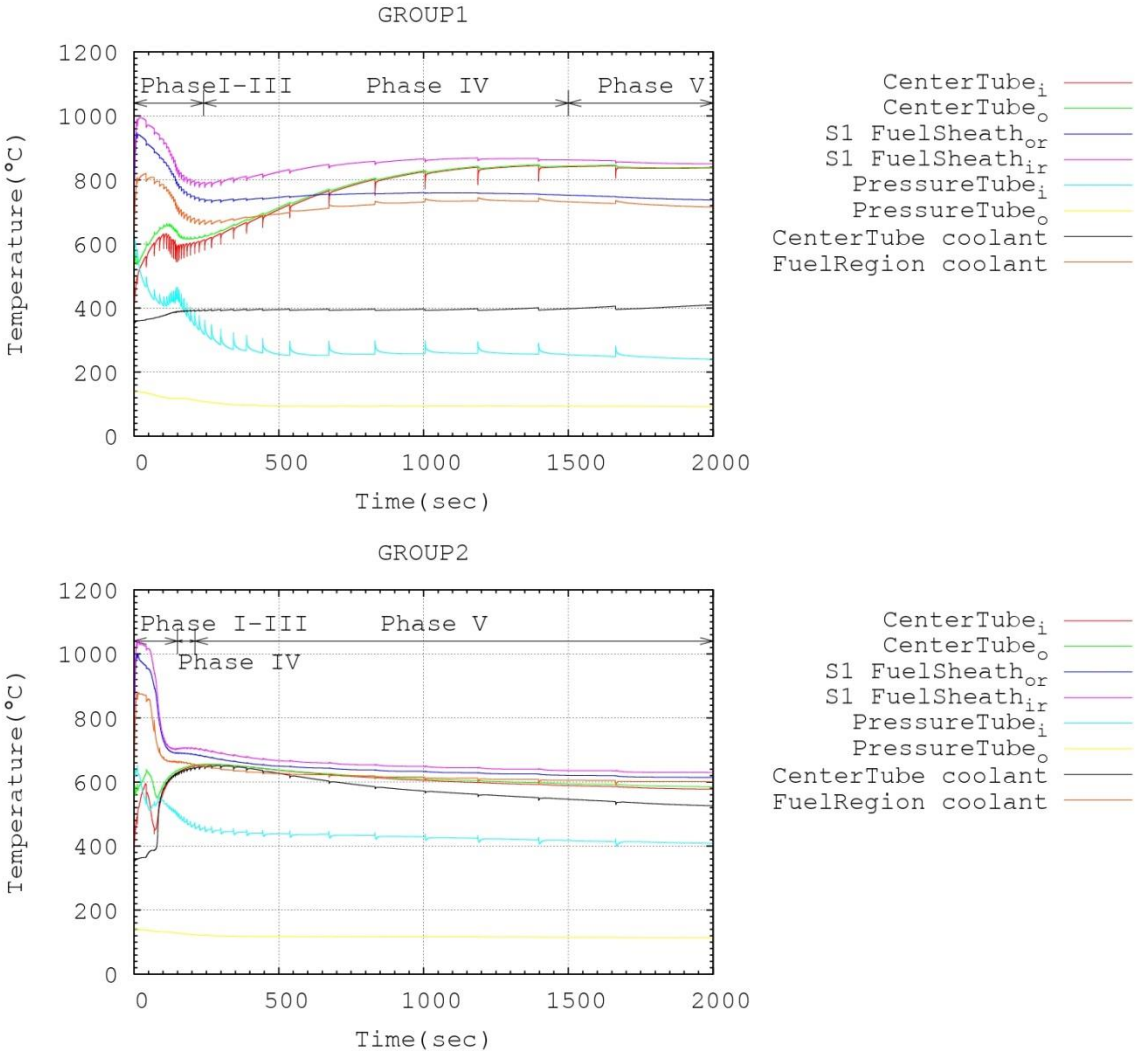

Figure 5.4 shows the fuel cladding temperature of both groups during a LOFA transient. A high level description of the transient behavior is presented in the following paragraphs and detailed analysis of the transient is provided in the following sections.

For Group1 which was the average power channel group, the transient can be divided into five phases. In Phase I, the fuel cladding temperature increases rapidly because of the rapid reduction of convective heat transfer (due to fast flow run-down) while simultaneously undergoing relative high levels of decay heat generation. At 21.6s, the fuel cladding temperature in sector 3 of the Inner Ring (denoted as IR S3, which is the sector facing the Outer Ring) at an elevation of 0.25m from the top of active fuel approaches 995 ^{o}C which is the maximum fuel cladding temperature for

the average channel. In Phase II, which takes place after the peak fuel temperature is reached, the fuel cladding temperature starts to decrease, gradually reflecting the decline of the decay heat generated within the fuel and the contributions of radiative heat transfer to fuel cooling. Phase III starts from 125s and ends at approximately 240s. In Phase III the fuel cladding temperature decreases at a greater rate than in Phase II and the potential causes of the improved cooling in Phase III are discussed later. In Phase IV, the fuel cladding temperature increases slightly until radiation heat transfer balances with the decay heat at approximately 1500s. In Phase V, fuel temperature decreases are directly linked to reduction of the decay heat and effective radiation heat transfer. While detailed flow predictions are discussed in the following sections, the flow remains near zero throughout these phases in the average channel, albeit with small changes due to relief valve action as well as some pseudo-critical coolant transitions in some pipe components. A key finding in this 2-group simulation is that in Phase V the system cooldown rate is gradual and the critical pressure is not reached within the simulation times simulated here.

For Group2, which is the highest power channel group, the transient can also be divided into five phases. Phase I, which is similar to that of Group1, starts from 0s and ends at 14s. By the end of Phase I, the fuel cladding temperature reaches 1045 ^{o}C, which is the maximum fuel cladding temperature reached of the entire simulated transient. Phase II starts from 14s and ends at 55s. During this time, fuel cladding temperatures starts to decrease due to the decline of decay heat generated in the fuel and effective radiation and some convective heat transfer among fuel rod and the surrounding components. Phase III starts at 55s which is earlier than Group1 and shows that coolant is flowing backwards inside the highest power channel from outlet plenum to inlet plenum. The causes for the reversed flow predictions are discussed in detail below. The reversed flow improves the convective heat transfer between fuel rod and surrounding coolant relative to stagnation conditions, thereby making the fuel cladding temperature lower than for totally stagnant flow. In addition, the coolant temperature inside the outlet plenum is lower than the coolant temperature in the fuel region during this phase. This inflow of colder coolant leads to larger

temperature difference between coolant and fuel cladding which contributes to higher convective heat transfer rate. Last by not least, most of the thermal-hydraulic nodes in the fuel channel network undergo pseudo-critical transition in Phase III, thereby making the convective heat transfer even stronger. By the end of Phase III, density and temperature gradients of the coolant along the channel have largely decreased, coolant and fuel cladding temperature are lower compared to Group1 (as a result of the contribution of convection in this phase). Phase IV starts from approximately 150s. During Phase IV, the fuel cladding temperature gradually decreases as the amount of heat removed from the fuel rods through radiation and natural circulation exceeds the decay heat generated within the fuel. Starting at 210s, Phase V of Group2 closely resembles Group1, the fuel sheathe temperature decreases as decay heat level declines.

There are several instances where significant flows develop during this event although the isolation valves prevent bulk flow for exiting through the cold and hot legs. These flows can be classified as short intense pulses related to relief valve action and longer duration surges with lower flow caused by pseudo-critical transitions in the pipe network which lead to fluid expansion. During all phases there is some relief valve action caused by high over-pressure in the system. The relief valve is responsible for short bursts of flow from the reactor through the hot leg and leads to small discontinuities in the temperature behavior. As the transient progresses, the frequency of relief valve action decreases and eventually stops. By the end of Phase IV the net heat removed exceeds the decay power and hence the system begins to naturally depressurize without further SRV action. The longer duration pseudo critical flow surges result from high density fluid in some nodes gradually transitioning to their low density states through the pseudo critical temperature and this leads to some redistribution of mass in the closed system. Since various nodes in the loop will undergo the transition at different times, there is a resultant net flow through some channels in either the forward or backward direction (depending on the channels power and orifice configuration). The detailed discussion of the phenomena is provided in the following sections. The time ranges of different phases for the LOFA simulation results by using 2

channel groups are summarized in Table 5.6.

Table 5.6 Time Ranges of Different Phases for 2-Channel-Group Simulation Results

	Time Range for Group1 (s)	Time Range for Group2 (s)
Phase I	0-22	0-14
Phase II	22-125	14-55
Phase III	125-240	55-150
Phase IV	240-1500	150-210
Phase V	1500-2000	210-2000

5.2.1.1 Phase I

Group1 (0-22s):

During this phase, the fuel cladding temperature, center flow tube inside surface temperature and coolant temperature in the fuel region (fuel region is the area between the center flow tube outside surface and pressure tube inside surface) are increasing rapidly. Along with the maximum clad temperature location, the temperatures of a variety of components in CH2(node 10) are plotted, corresponding to an axial location of 0.25m below the top of active fuel. As shown in Figure 5.5, within 22 second of the transient initiation, the fuel cladding temperature increased from approximately 770 ^{o}C to 995 ^{o}C. This is caused mainly by the significant reduction in convective heat transfer coefficient due to flow reduction. During this phase there is a large sensitivity to the flow rundown assumptions and the timing for reactor shutdown, the sensitivities are assessed in Section 5.3. During the steady state, convective heat transfer plays an important role in removing the heat generated in the fuel. However, during the transient the convective heat transfer is largely inhibits due to the coolant massflow rate reduction. Specifically, as shown in Figure 5.6, the coolant massflow rate drops to zero in the first one second and then only small pulses are observed following the SRV actions. Since in Phase I, the decay heat is still approximately 5.2%-3.8% of

the full power, the temperature of the fuel cladding and the surrounding coolant rises very quickly.

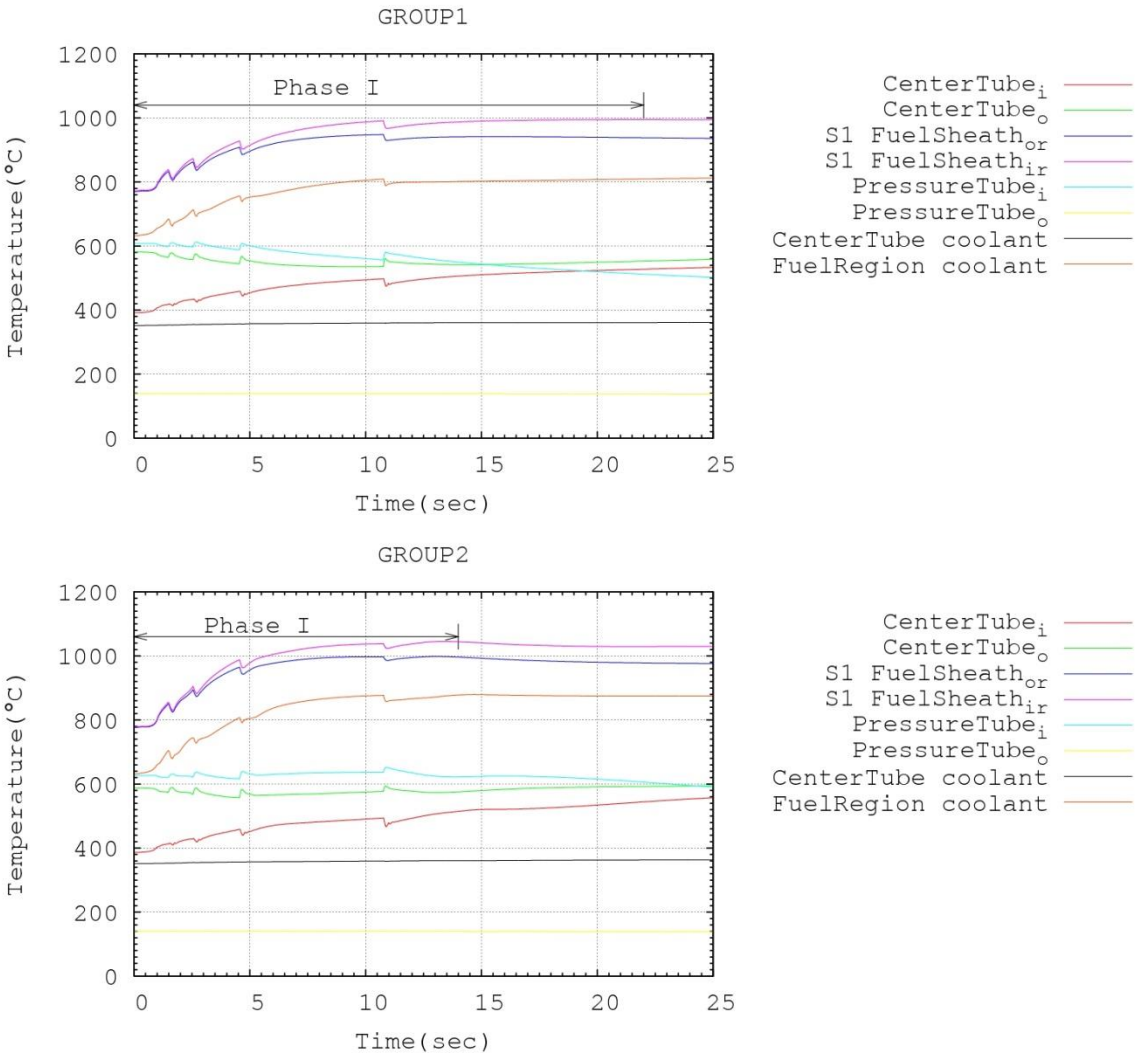

Figure 5.5 Temperature of Various Components in Phase I

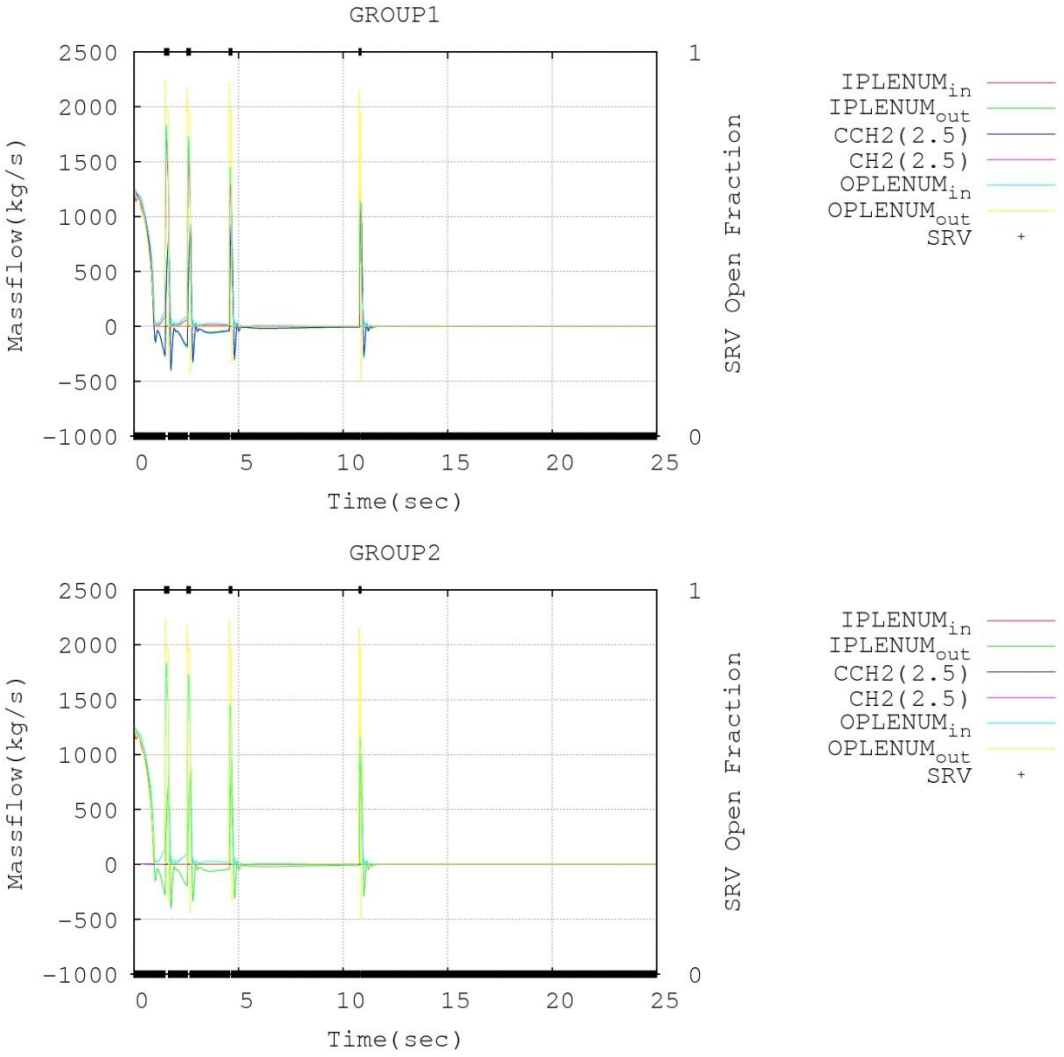

Figure 5.6 Massflow Rate at Various Locations and SRV Actions in Phase I

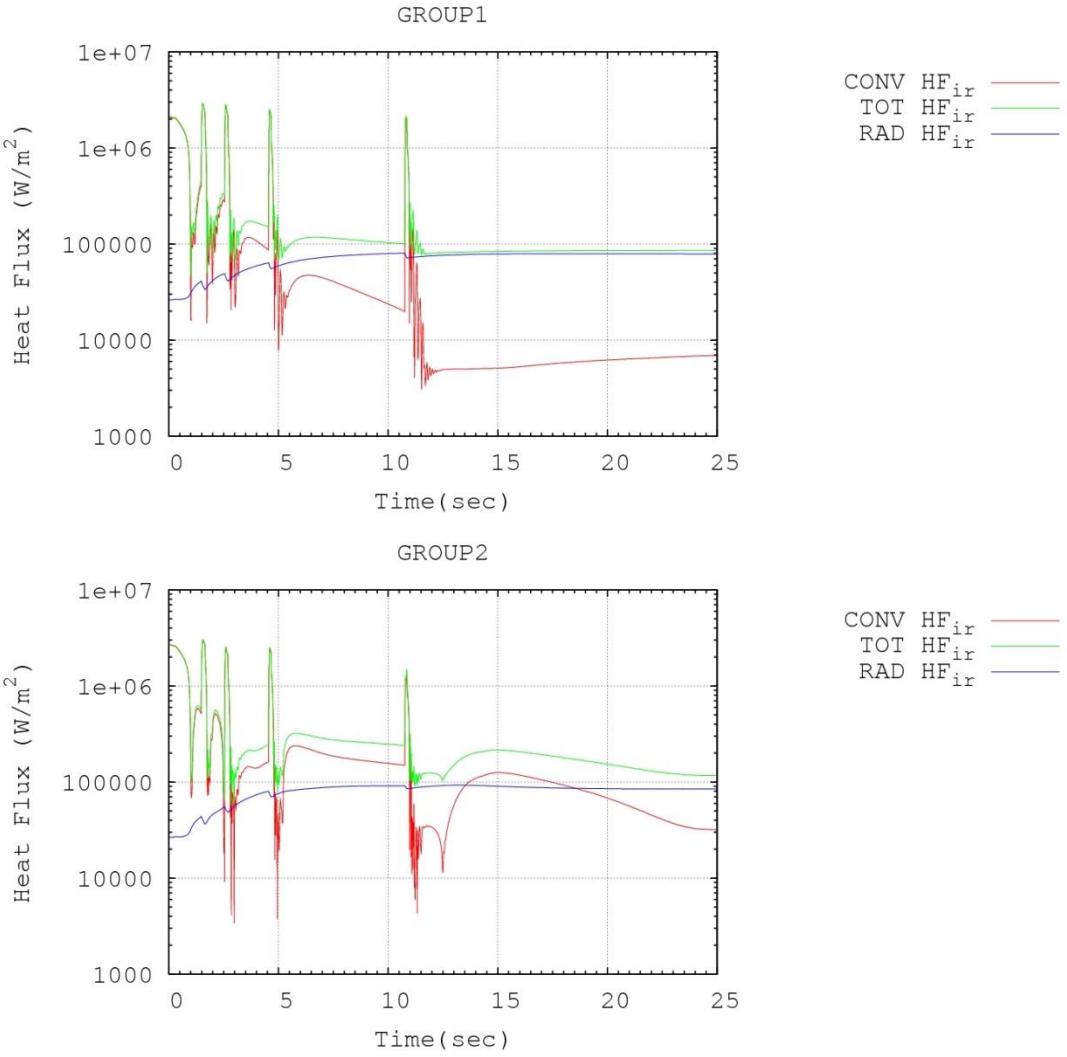

Figure 5.7 Heat Flux at Fuel Cladding of CH2(10) in Phase I

Also note that radiation heat transfer became the dominant heat transfer mechanism at the end of Phase I. Figure 5.7 illustrates the heat flux variation during phase I at node 10 of the Inner Ring fuel rods as a function of time. During steady state, convective heat flux contributes to more than 90% of the total heat flux, and radiation heat transfer only plays a minor role. However, as the transient progresses, and the temperature of the fuel cladding rises rapidly, the outer surface temperature of the center flow tube and inner surface temperature of the pressure tube remain largely unchanged. The increasing temperature differences promoted radiation heat exchange among the fuel sheath and the surrounding surfaces. By the end of phase I, the majority of heat removed from fuel cladding is by radiation heat transfer. This is also confirmed in Figure 5.8

which shows the decay heat generated and the heat removal by convection and radiation in node 10.

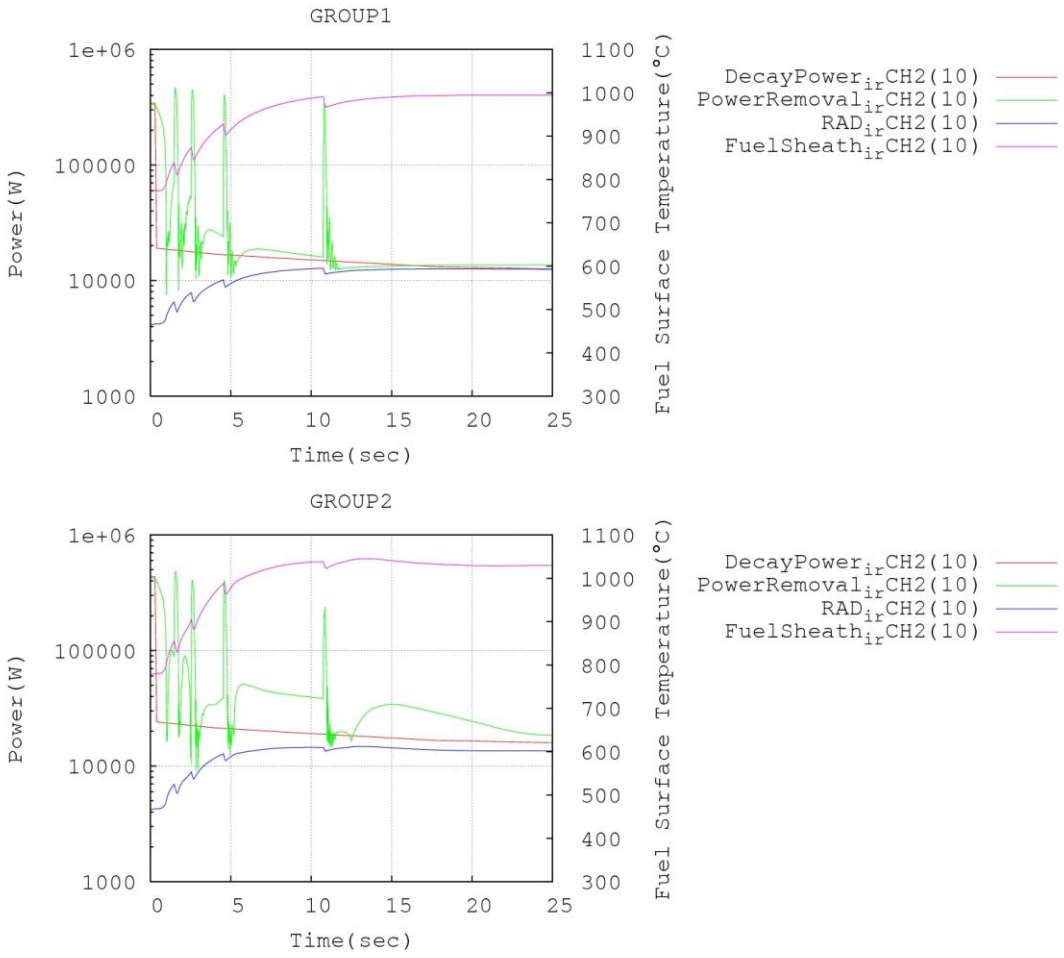

Figure 5.8 Power Generation and Removal at Inner Ring CH2(10) in Phase I

Group2 (0-14s)

Phase I of Group2 is very similar to Group1. However, as the maximum power group which only consists of one maximum power channel, the changes of Phase I in Group2 is accelerated in time relative to Group1. A maximum fuel cladding temperature of 1045 ^{o}C is achieved at 14 s. Figure 5.6 shows the mass flow rate of Group2. Compared to Group1, three major mass flow surges took place at approximately 4s, 7s and 15s respectively. Although low in magnitude, these mass flow surges preserve a certain amount of convective heat transfer. As a result, by the end of phase I,

both radiation and convection contribute to heat transfer among fuel rods and the surrounding components. In comparison to the average channel group (Group1) radiation heat transfer is not the only dominant heat transfer mechanism for Group2. The presence of the mass flow surges early in the transient significantly reduces the maximum sheath temperature found during Phase I. In comparison to Group 1 the power levels are much higher, however the fuel clad temperatures are only significantly larger due to the additional contributions from convection.

The causes of the mass flow surges found in phase I have not been firmly established, although their timing is closely related to the times when nodes in the channel and center flow tube reach their pseudo-critical temperature. One potential cause is that when the coolant volume at the bottom of fuel region expanded due to pseudo critical transition, mass flow pulses are generated and propagated in the channel. However, in Group1, when the nodes at same locations go through pseudo critical transitions, mass flow pulses are barely noticeable. The stronger effect of the pulses in Group2 as compared to Group1 may be a result of the higher power levels which cause the pseudo critical transition to take place over a shorter time, hence producing more pronounced flows. They may also be stronger because the inlet orifice used to match flow to power at the steady state is bigger, thereby giving a lower flow resistance. In comparison the average channel power group produces only modest flows as the transition through the pseudo-critical point takes place over an extended time period and with more restrictive orifices.

For both groups, pressure rises as heat is continually generated in the fuel and heat removal through radiation is insufficient resulting in net energy being deposited in the coolant. When the pressure reaches the opening set point of the safety relief valve, the valve opens to release fluid and depressurizes the core. When the pressure decreases to the closing set point, the valve closes to prevent further pressure drop. As shown in Figure 5.6, the opening and closing motions of safety relief valve lead to high mass flow peaks within short duration which enhance the convective heat transfer in both groups, and subsequently these spikes result in the temperature

profiles in Figure 5.5. Since there is more heat transferred from the high temperature components to the low temperature components during these massflow peaks, temperature decreases are found at the fuel cladding, coolant within the fuel region and center flow tube inside surface while temperature increases are found at the outside surface of center flow tube and pressure tube.

5.2.1.2 Phase II

Group1 (22-125s)

In this phase, as shown in Figure 5.10, heat removed from the fuel rods by radiation and convective heat transfer exceeds the decay heat generated in the fuel, such that the fuel cladding temperature starts to gradually decrease (see Figure 5.9). During this phase, in Group1 channels there is virtually no mass flow so radiation dominates heat transfer.

Goup2 (14-55s)

In Phase II, the thermal-hydraulic behaviors of group2 are similar compared to group1, but again, the time frame for Group2 is shorter than for the average channel group. For Group2, several mass flow pulses are observed, similar to Phase I, of which the timing is roughly overlapping with the pseudo-critical transition time but the causes of the pulse are not fully confirmed .These pulses improve the convective heat transfer at fuel cladding surfaces. As a result, the fuel cladding temperature of the hot channel decreases faster than that of Group1.

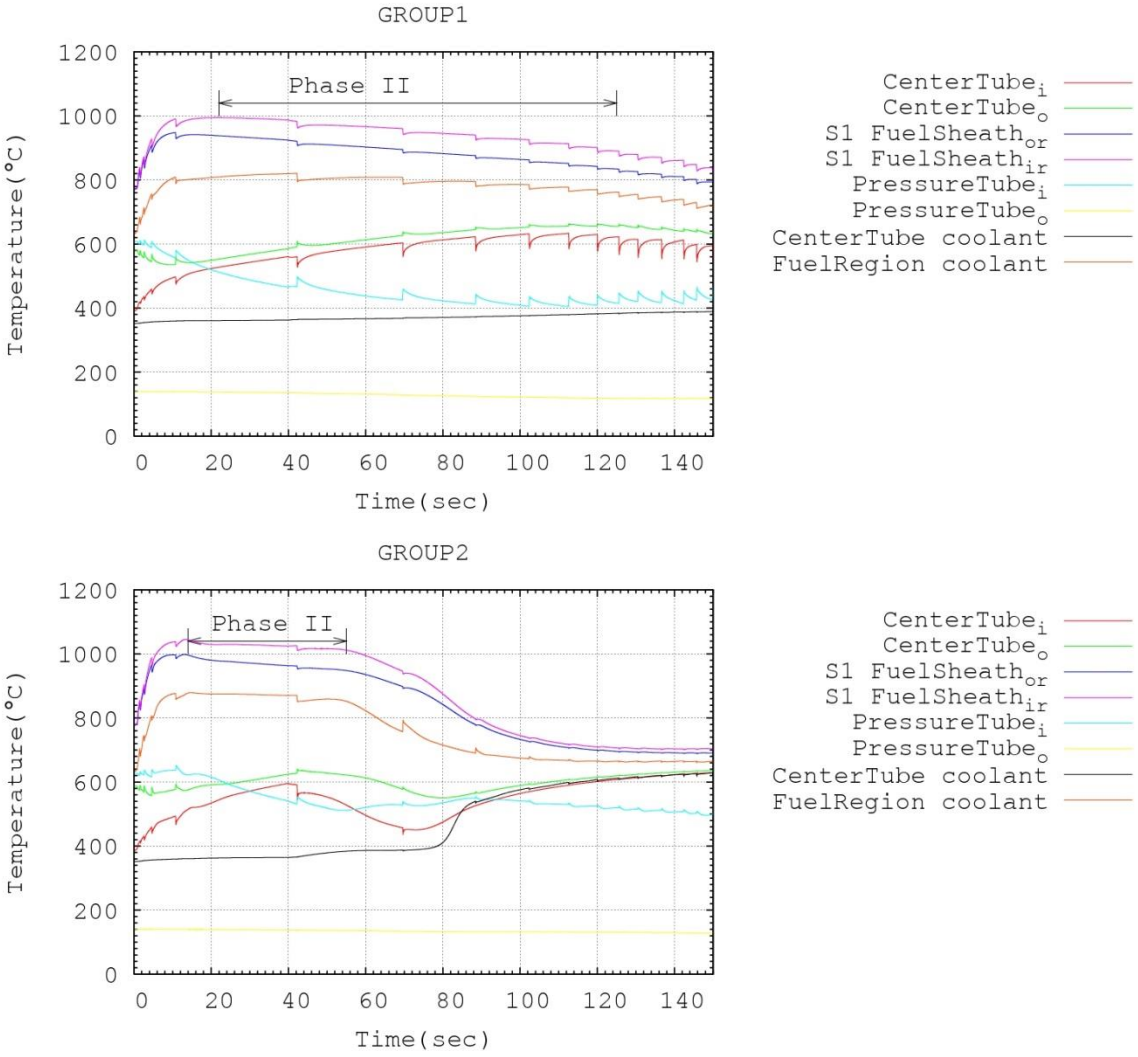

Figure 5.9 Temperature of Various Components at CH2(10) in Phase II

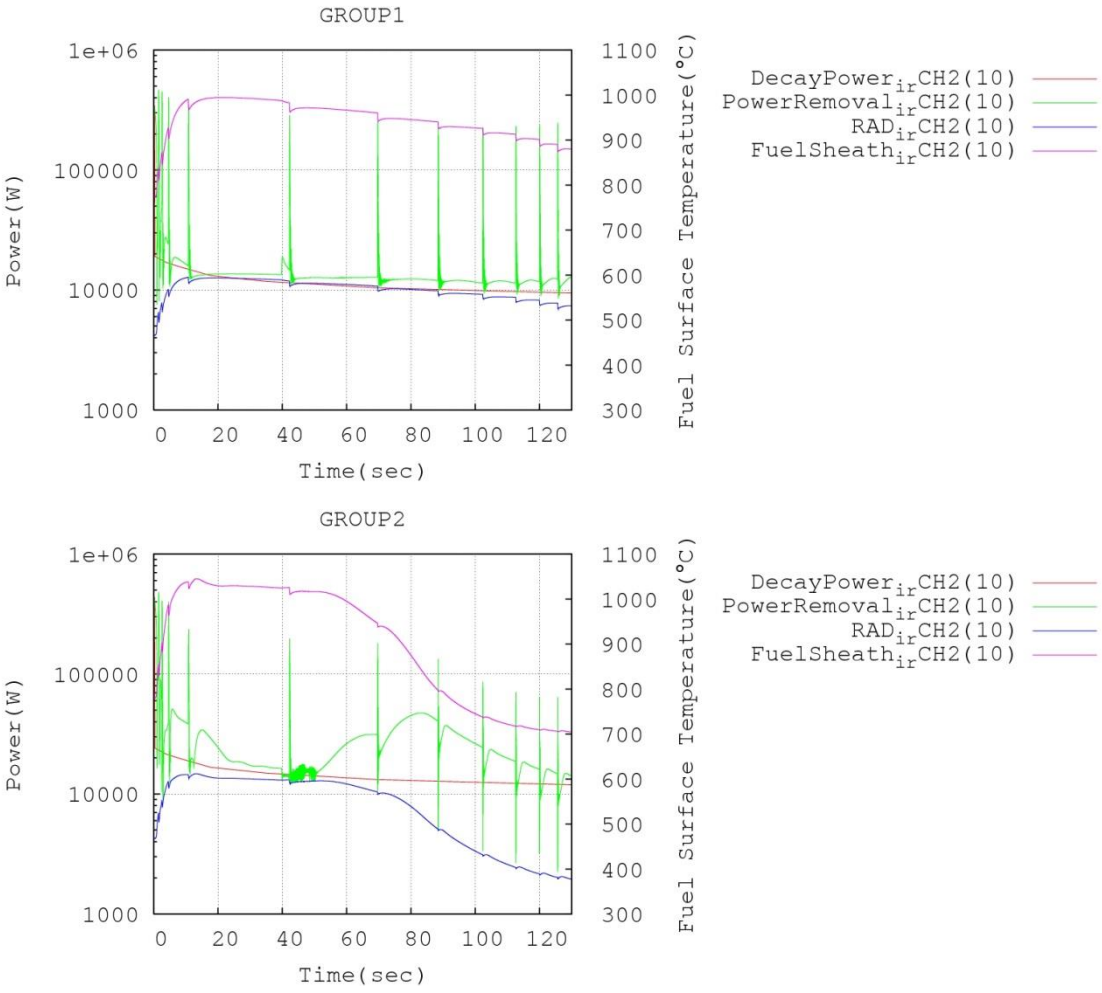

Figure 5.10 Power Generation and Removal at Inner Ring CH2(10) in Phase II

All the results and discussions above are regarding the temperatures and heat transfer behavior at node 10. In this paragraph, fuel cladding temperatures along the axial direction are discussed. Figure 5.11 shows the fuel sheath temperatures along the Inner Ring fuel rod (IR S1) as a function of time. For both groups, node 10 achieves the maximum sheath temperatures at the end of phase I. However, for other nodes located below node 10, the maximum sheath temperatures are not achieved until later time. As a matter of fact, by the end of Phase II, sheath temperatures of nodes located at the bottom of fuel region, such as node 1 and 2, are still increasing. The reason is straightforward. Sheath temperatures at the bottom of the fuel rod are approximately 500 ^{o}C at the beginning of Phase II. Compared to node 10, of which the sheath temperature is around 1000 ^{o}C,

the amount of heat removed from the fuel rods by radiation heat transfer is extremely small. Consequently, radiation and convective heat transfer are insufficient to remove the decay heat generated by the fuel. And the sheath temperature keeps rising until the combination of the two heat transfer mechanisms balance the decay heat power.

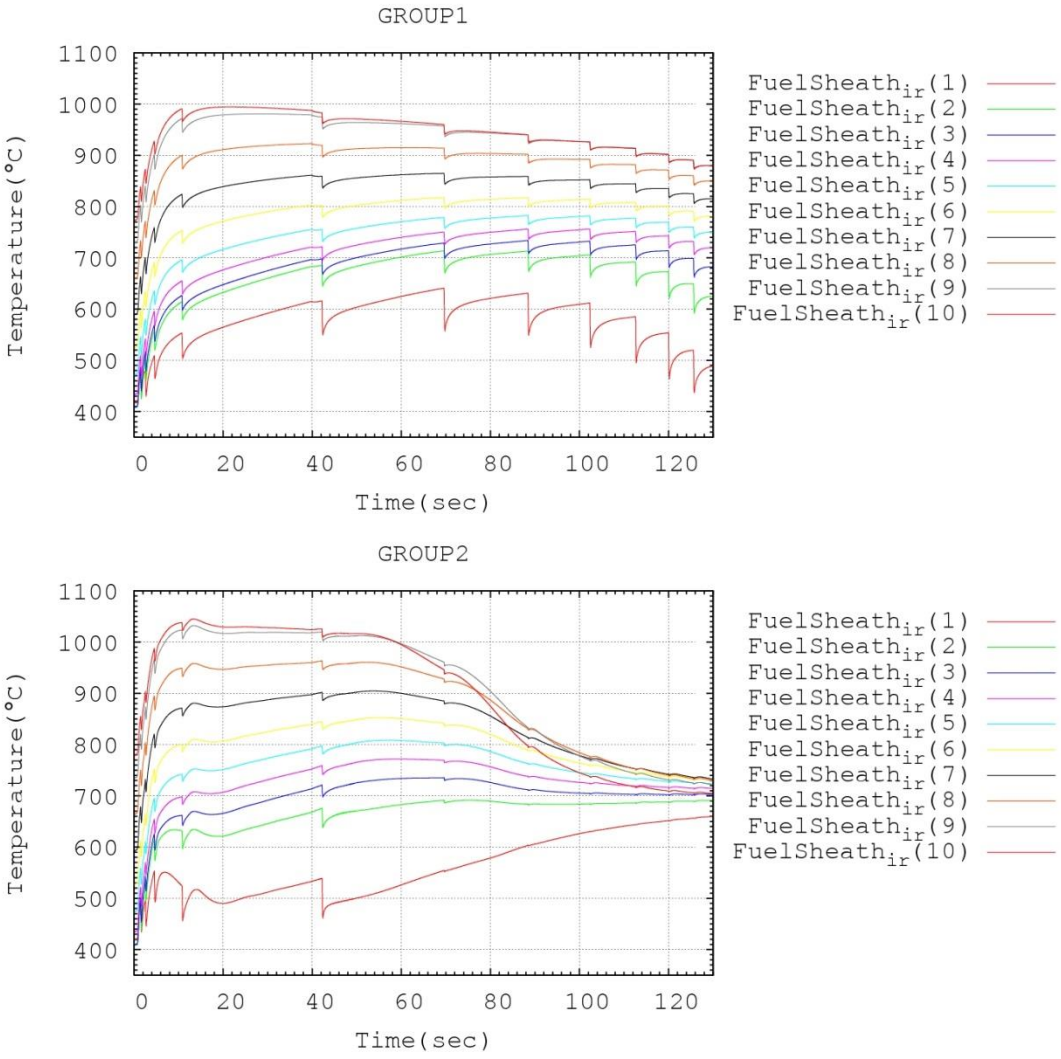

Figure 5.11 Inner Ring Fuel Sheath Temperature at Different Axial Locations in Phase II

5.2.1.3 Phase III

Group1 (125-240s)

In Phase III, enhanced heat transfer among different wall surfaces and the coolant leads to increased cooling of the fuel sheath. As shown in Figure 5.12, the inner surface temperature of the

center flow tube decreases while interior coolant temperature increases. In the fuel region, fuel cladding temperature and coolant temperature decrease while outer surface temperature of the center flow tube and inner surface temperature of the pressure tube increase.

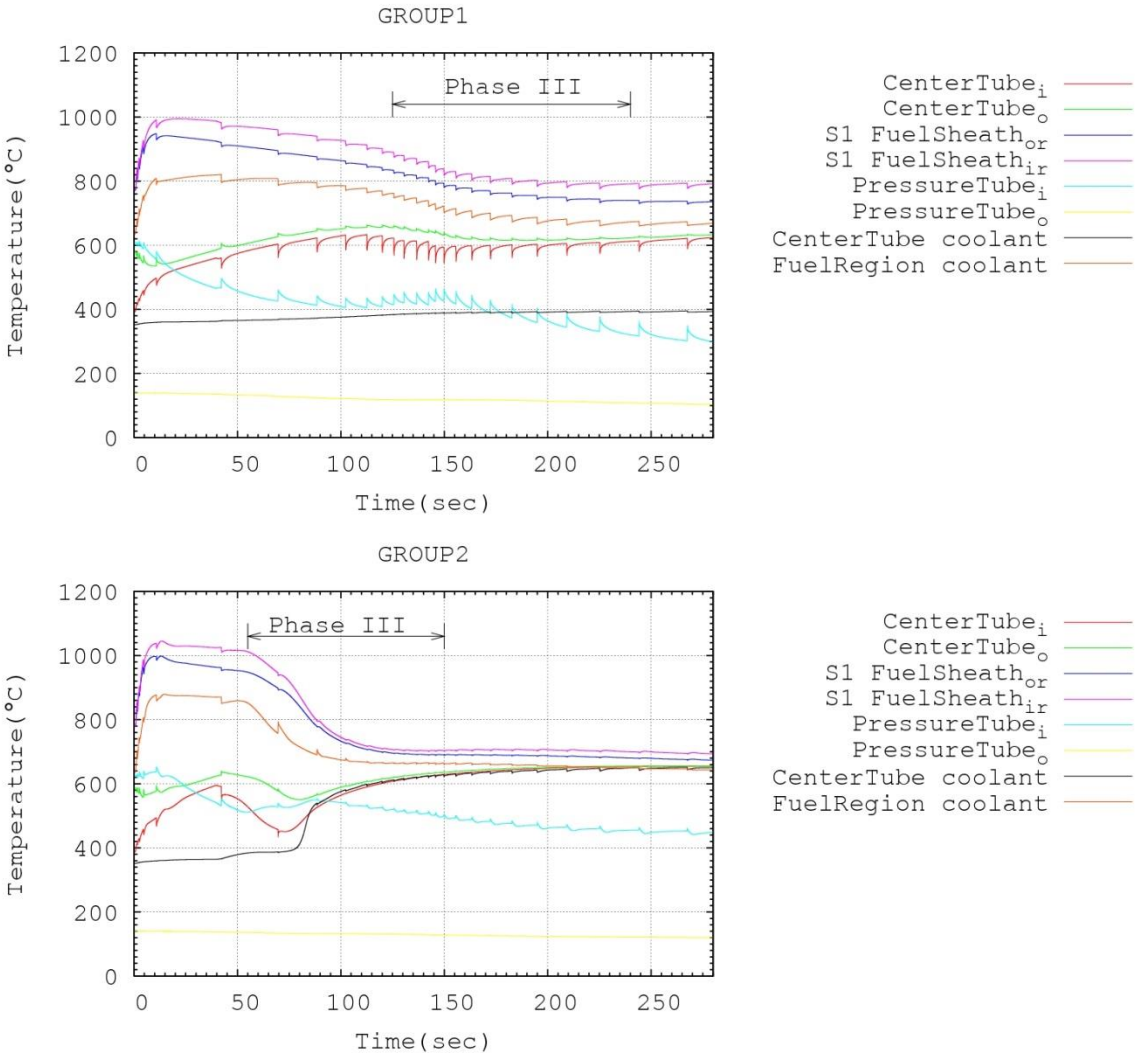

Figure 5.12 Temperature of Various Components at CH2(10) in Phase III

There are three reasons why the simulations show improved heat transfer in Phase III.

1) Accumulated SRV Actions.

During Phase III the opening frequency of the SRV increases. As shown in Figure 5.13, the high massflow peaks caused by SRV opening are concentrated in Phase III, especially from 125s to 160s. As mentioned above, even for a very short period of time, the repeated massflow pulses improve the convective heat transfer between wall surfaces and coolant. SRV actions

increase because the coolant in the center flow tube is going through pseudo-critical temperature during this period of time and the volume expansion of the fluid causes pressurization. As shown in Figure 5.14, 80% of the nodes in the center flow tube go through pseudo-critical transitions in Phase III. As shown in Figure 5.15, the coolant density decreases from approximately 600 kg/m^3 to 150 kg/m^3 which means the volume of the coolant inside center flow tube has expanded 4 times. This would sharply increase the core pressure in addition to that from decay heat accumulation. When the SRVs actuate, the core pressure first dropped to 24.25MPa which is the closing set point of the valve, and then, the decay heat would reinstate the pressure increase. However as the subsequent center flow tube nodes transition through the pseudo critical point the core pressure would rapidly approach the SRV set point of 26MPa. This process repeats until all the coolant in the center flow tube has gone through pseudo-critical temperature, or until the time when decay heat can be effectively removed by radiation heat transfer to the passive moderator system such that further pressure rise is precluded.

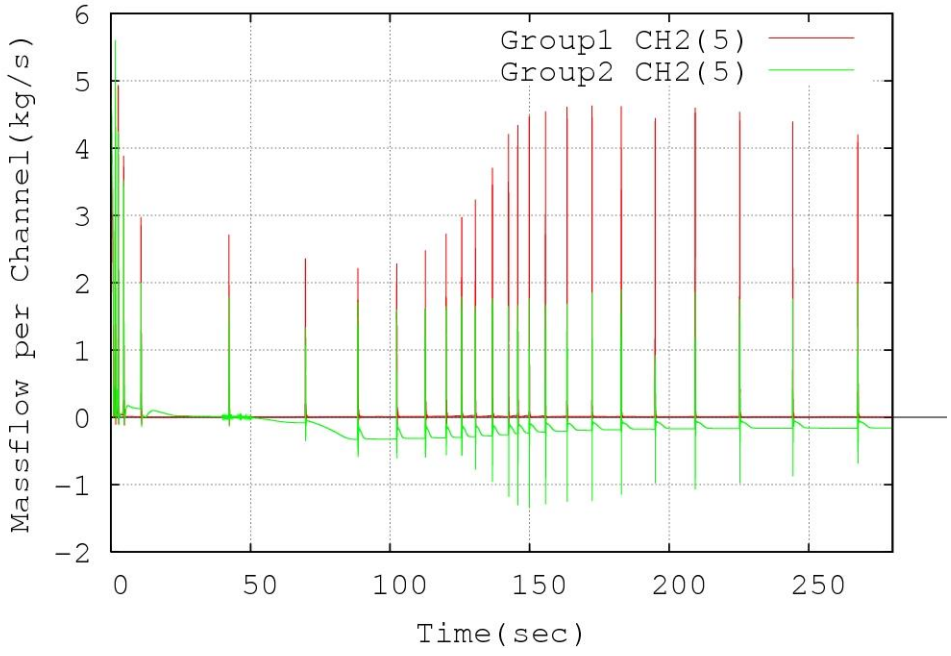

Figure 5.13 Coolant Massflow Rate per Channel

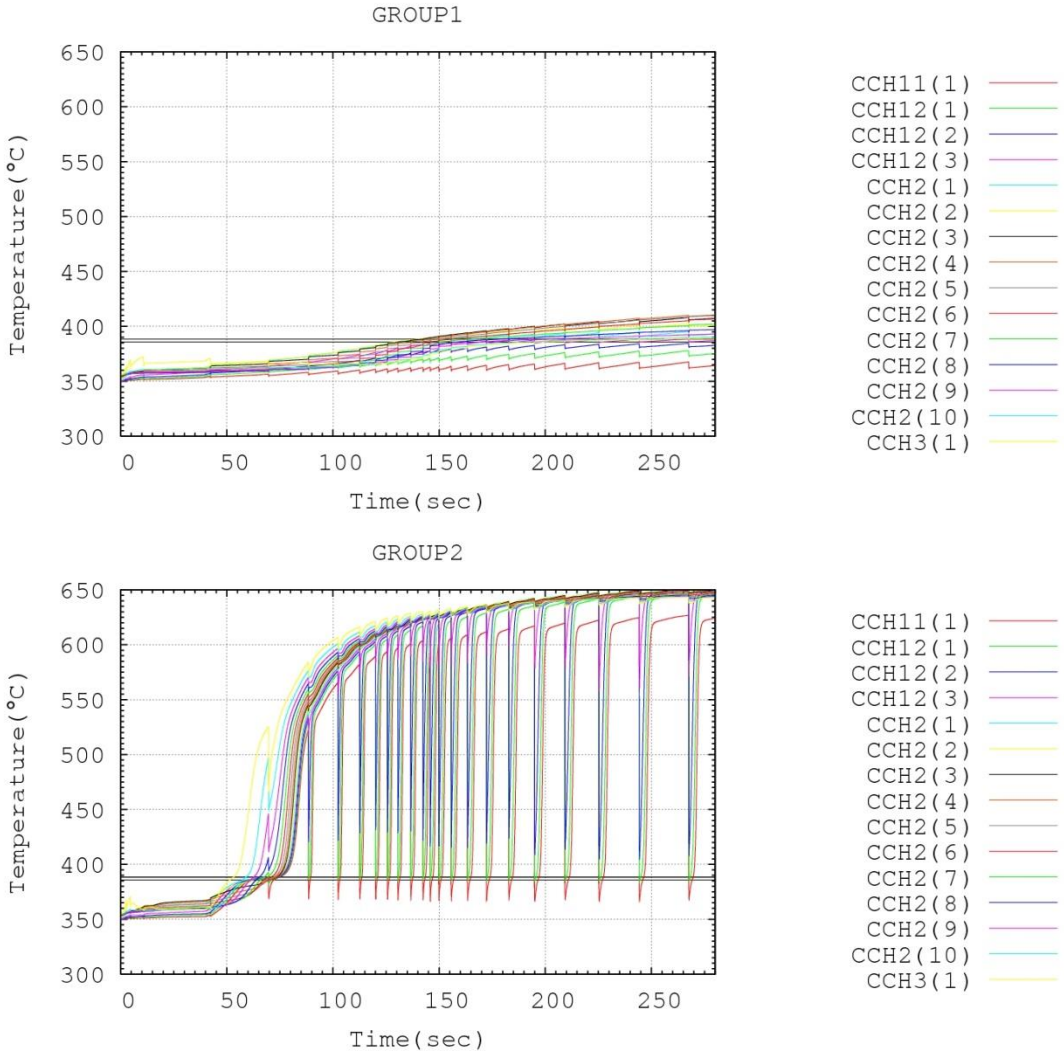

Figure 5.14 Coolant Temperature Inside Center Flow Tube

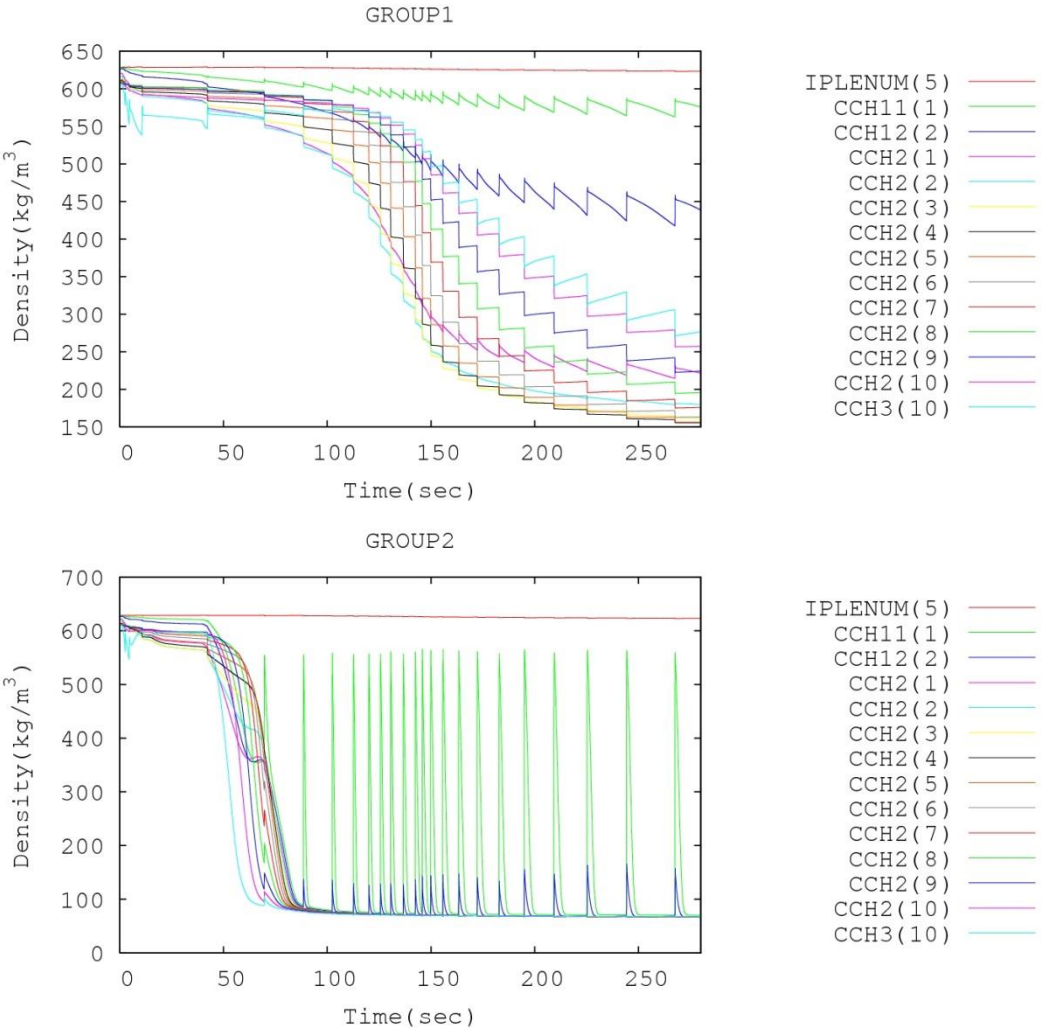

Figure 5.15 Coolant Density Inside Center Flow Tube

2) Improved Convective Cooling.

This mechanism is related to the improved heat transfer resulting from the flow initiated during the transition of the center flow tube cooling channel through the pseudo critical temperature. In bullet 1 above, the transitions initiated pressure increases which cause SRV opening with short duration bursts. A related but different phenomenon is the associated improvement in convection heat transfer caused by the flow initiated as a result of the local expansions within the center flow tube wherein the stored mass in the liquid like nodes is redistributed and causes addition flow in the system. Figure 5.17 illustrates the heat transfer coefficient variations for CH2(10). Not only are there concentrated narrow spikes due to SRV

opening, the value of the heat transfer coefficients at times outside of these spikes also increased. During center flow tube heat up the coolant in these nodes will undergo a transition from liquid-like density to gas-like densities. Thus, a massflow is generated (often bidirectional and centered about the transition node) from the redistribution of mass in the closed system and propagated throughout the fuel channel. During this Phase, almost all the nodes in the center flow tube go through pseudo-critical temperature and the individual nodal expansions combine to form a long-lasting large massflow surge. Compared to the brief massflow pulses generated by the SRV openings, the magnitude of the mass flow slug is fairly small, which is the reason why it is not obvious in the massflow plot for CH2(10) (Figure 5.13). Further magnification of the scale in Figure 10 would indeed show a prolonged and low magnitude mass flow slug during the 90 to 120s period (note this is similar but lower in magnitude than the flow surges seen in Group 2 Phase 1 as discussed above). Furthermore, the fuel cladding heat transfer coefficient plot (Figure 5.17) indirectly shows that the existence of volume expansion induced massflow pulse and it has helped to improve the heat transfer among components in the assembly. This is consistent with the “mass flow effect” noted by Oka in the Japanese SCWR design where the moderator flow boxes provide flow to the fuel regions even with total inlet flow stoppages [5].

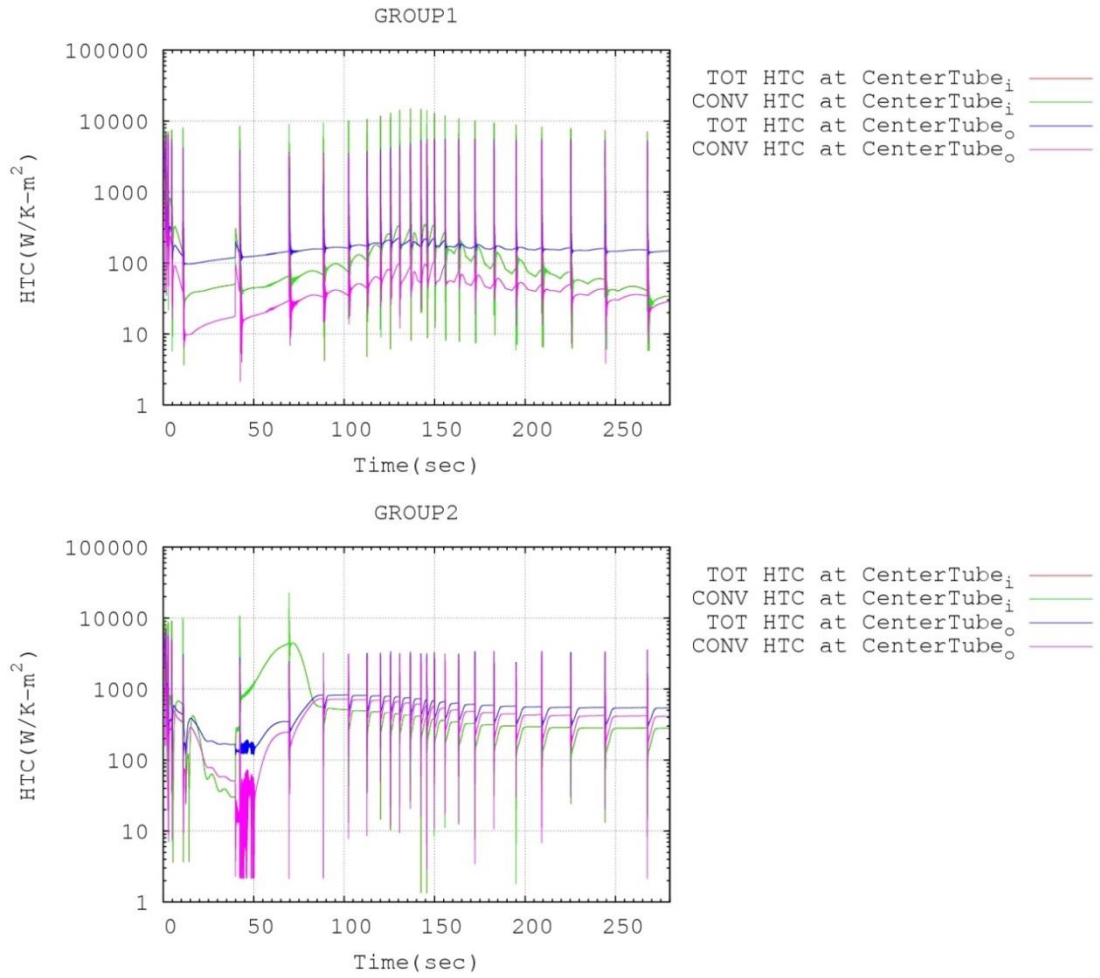

Figure 5.16 Heat Transfer Coefficient at Center Flow Tube Inside and Outside Surfaces

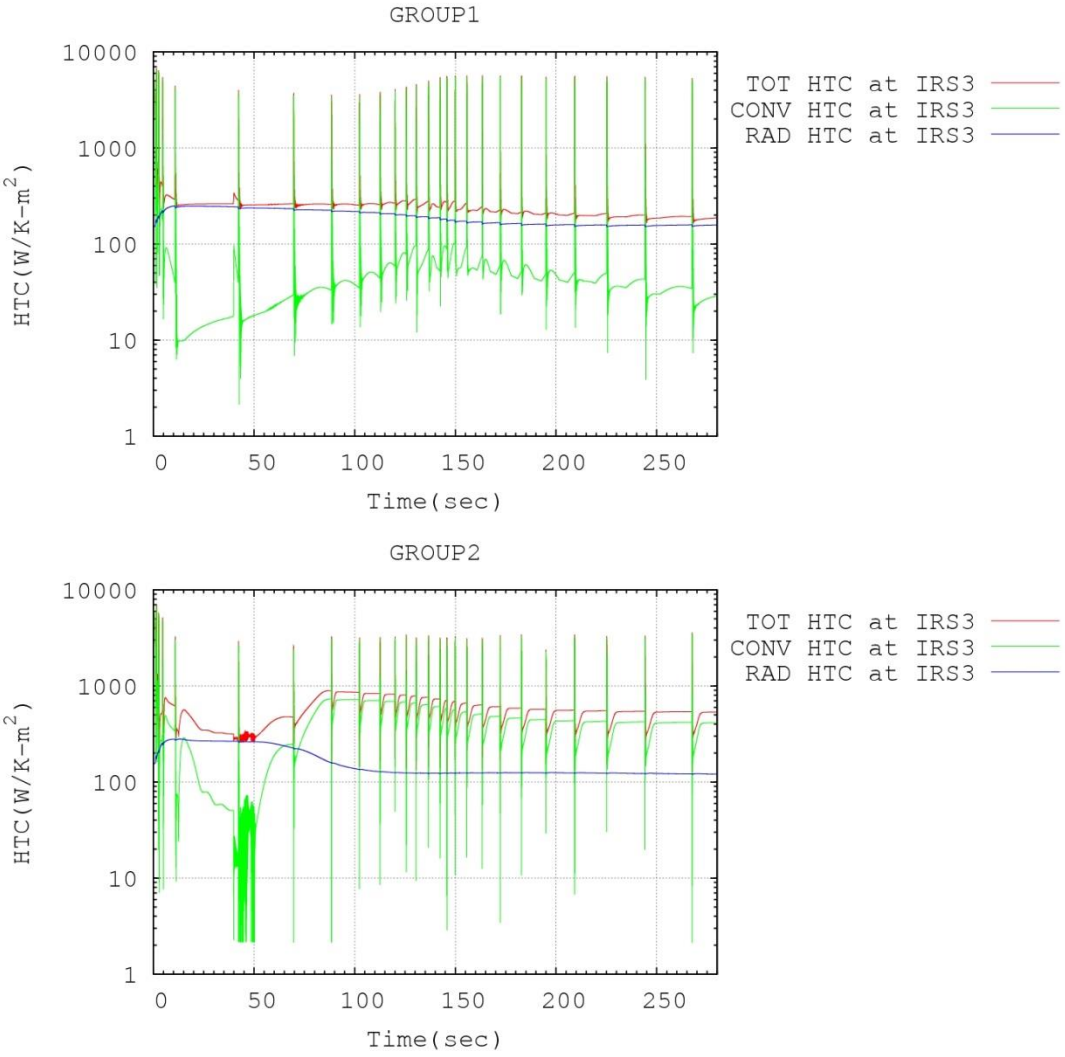

Figure 5.17 Heat Transfer Coefficient at Fuel Cladding Surface of Inner Ring CH2(10)

3) Incorrect Convective Heat Transfer Model.

While the above 2 phenomena represent physical changes to the heat transfer, there is an issue with the existing CATHENA version that results in a bias in the predicted temperature during this Phase of the transient. The CATHENA version used for this simulation is CATHENA MOD-3.5d/Rev 3. In this version, the Dittus-Boelter correlation is automatically selected for convective heat transfer under super-critical pressure. Dittus-Boelter correlation provides fairly accurate heat transfer coefficient under super-critical pressure conditions, but when fluid temperature is close to the pseudo-critical transition, Dittus-Boelter (D-B) correlation can significantly over predict the convective heat transfer component. For fuel temperature

predictions under steady state predictions this is not usually a significant bias, since the nodes that contain the maximum fuel sheath temperature are surrounded by coolant which is well beyond the pseudo critical temperature. However under transient conditions, although the fuel region is above the pseudo-critical temperature, there is still a transition which takes place in the center flow tube which must be examined. For the two phenomena above these transitions initiate mass flow due to SRV opening and mass redistribution, but there is another subtle effect which artificially reduces the fuel temperatures further during this Phase.

At the onset of Phase III the coolant in the center flow tube is below the pseudo-critical temperature, and the center flow tube itself is at a fairly high temperature owing to the radiative heat transfer coming from the inner fuel ring. As heat is gradually conducted to the stagnant fluid in the center flow tube it will transition to the pseudo critical temperature. Also as noted above, small flows will be initiated within the node and also driven by other node transitions as a result of these densities driven expansion. With some finite flow and a temperature difference the convective heat transfer contributions from the center flow tube to the central coolant are expected. However, since the fluid is transitioning through the pseudo critical temperature the D-B correlation used by CATHENA is invoked. As noted in Pioro and Duffey's book [27], depending on the flow conditions heat transfer can either be considered augmented, normal, or deteriorated during the pseudo critical transition. However, irrespective of which occurs, the D-B correlation systematically overestimates the heat transfer, sometimes by orders of magnitude, relative to experimental results. As a result of the D-B bias under these conditions, the heat transfer will be overestimated and hence the transitions within a node from liquid to gas-like will be predicted to occur much faster than would occur in reality. The end result is that the codes over predicts the magnitude of these mass flow surges and hence over estimates heat transfer even in nodes well away from the pseudo-critical transition. At this time there is no way to assess the impact of a delayed or longer duration transitions in the affected nodes. However it is expected that the mass flow rates initiated from the phase

transitions would be of longer duration and lower magnitude in reality, and hence sheath temperatures would be under predicted.

Currently there is nothing can be done to adjust the artificial heat transfer coefficient unless the CATHENA source code could be changed. However, the impacts of the artificially heat transfer coefficients on the systems are examined. As shown in Figure 5.12, from 125s, the temperature of center tube inside surface starts to decrease. This is caused by the volume expanding induced massflow surge as well as the artificial heat transfer coefficient predicted by Dittus-Boelter correlation. The center tube material is zirconium hydride of which the thermal diffusivity is around $6 \times 10^{-6}\ m^2/s$ at 350°C. So, after several-second delay, the center tube outside surface temperature starts to decrease. Since the artificial heat transfer coefficient is higher than the actual value, CATHENA overestimates the heat transfer between the center tube and the coolant within it. And thus the predicted center tube outer surface temperatures are also underestimated. The low center tube outer surface temperature leads to higher predicted radiation heat transfer between the fuel cladding surface and center tube outside surface. The above analysis leads to the conclusion that the actual temperature of the fuel cladding and fuel tube coolant should be higher than those predicted by CATHENA in any transient Phases which undergo pseudo critical transitions in the center flow channel region. I.e., some reductions in the cladding temperatures are expected during Phase III due to SRV flow as well as bulk flow initiated by the pseudo critical density transitions, but the reductions are over predicted due to the over estimation of convective heat transfer coefficient.

Despite the above, the maximum cladding temperature has already passed its maximum value in Phase I, and the transitions noted above occur well beyond the time frames of Phase I. In other words, the artifact in the HTC noted above should have no significant influence on predicting the maximum fuel cladding temperature in these transients.

It is well-known that radiation heat transfer rate is proportional to the 4th power of temperature. As shown in Figure 5.17, during phase III, as the fuel cladding temperature decreases, radiation heat transfer between the fuel and the surrounding surfaces reduces. However, during the whole process, the fuel cladding temperature for node 10 is maintained above 920 °C. As a result, during Phase III, the radiation heat transfer for Group1 remains at high value and it is still the dominant heat transfer mechanism in fuel region.

Group2(55-150s)

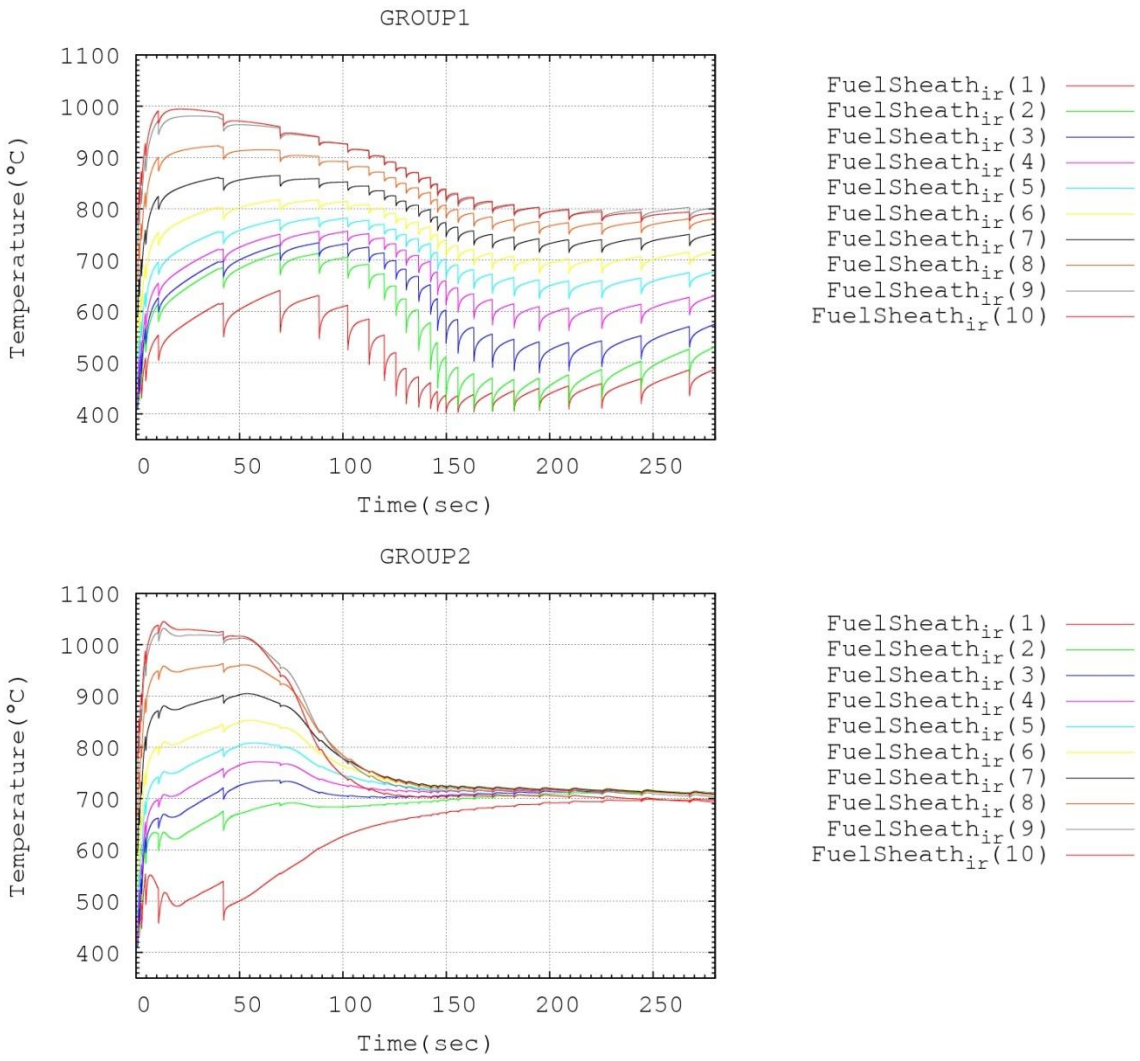

Figure 5.18 Inner Ring Fuel Sheath Temperature at Different Axial Locations in Phase III

Figure 5.18 shows the Inner Ring fuel sheath temperature variation as a function of time. Take the

temperature profile at 100 second as an example. Coolant is flowing from outlet plenum through fuel region, center flow tube to the inlet plenum. The temperature of coolant at outlet plenum is at approximately 650 ^{o}C. As coolant flows through the fuel region, heat is deposited in coolant from fuel rod and at the same time removed from coolant to the center flow tube and the pressure tube. The net energy deposited in the coolant can be either positive or negative depending on the absolute values of heat input from fuel and the heat transferred to the surrounding components. In this case, at 100s, the coolant temperature increases at first there nodes (i.e. CH2(10), CH2(9), CH2(8)) meaning there is net energy deposing in coolant. After coolant passing CH2(8), the coolant temperature starts to decrease which means the amount of heat transferred from coolant to the center flow tube and the pressure tube exceeds the amount of heat transferred from fuel rod to the coolant. Here the temperature of the center flow tube and the pressure tube declines along axial direction from top to bottom. In other words, wall temperatures at the bottom of the center flow tube and the pressure tube are lower than the temperatures at the top. As coolant flows down the fuel channel, an increasing temperature difference between coolant and the surrounding components can be found which directly leads to an enhanced convective heat transfer from coolant to the center flow tube and the pressure tube. In addition, the decay heat power is distribute roughly evenly along the fuel rods. As a result, the heat output exceeds the heat input between node CH2(7) and CH2(8), and coolant temperature starts to decrease afterwards.

Unlike Group1, where coolant temperatures at different altitudes of the fuel region always follow the same trend, coolant temperatures of Group2 have different behaviors along the axial direction. As shown in Figure 5.19, the coolant temperatures at the top fuel region decreases while the coolant temperatures at bottom fuel region increases. This phenomenon is directly linked to the reversed flow in the fuel channel. The reversal originates from the outlet plenum and as a result, the temperature gradient along fuel channel decreases as a function of time. By the end of this phase, a uniform temperature field establishes in the fuel channel at approximately 650 ^{o}C, which is the coolant temperature at outlet plenum. I.e., the heat load is sufficiently low and the induced convection heat removal is sufficient such that the surface temperatures are near that of the

coolant.

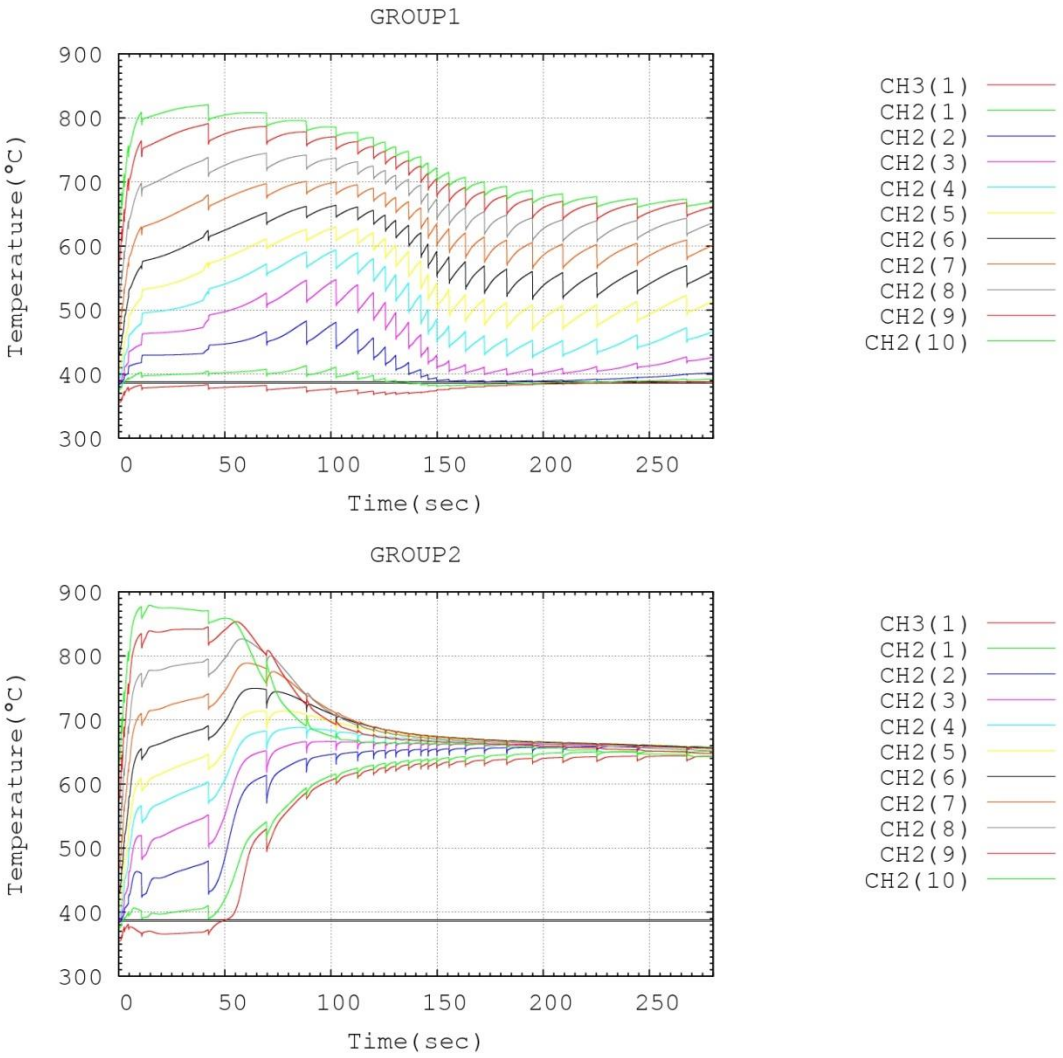

Figure 5.19 Coolant Temperatures at Various Axial Locations in Fuel Region

As stated previously significant natural circulation initiates during Phase III. The flow directions are such that cold coolant from inlet plenum flows through Group1 channels to outlet plenum and warm coolant from outlet plenum flows backwards from Group2 channel to inlet plenum. The reversed flow direction is the major reason why the temperature fields of various components of Group2 are very different from those of Group1. However, since Group2 only consists of one channel, there is virtually no natural circulation taking place in the core since the majority of

channels contained in Group 1 show very small flows. In order to gain insight into how natural circulation works in the system, the study of another grouping scheme is performed below.

Although the reversed flow initiated by natural circulation is the main factor that governs the heat transfer process as well as the temperature behaviors, the other heat transfer phenomena that are discussed in bullet 1, 2 and 3 above for Group1 are also applicable for Group2.

For Group2, the coolant inside the center tube goes through pseudo-critical transition during 55-80s periods which is much earlier than Group1. Part of the reason for the earlier pseudo-critical transition is that the decay heat level of Group2 is higher compared to Group1. Consequently, the center flow tube coolant is heated up at higher rate. However, the major reason for the center flow tube coolant early transition is likely due to the improved convective heat transfer caused by SRV-initiated mass flow oscillations. As shown in Figure 5.13, in Phase II, due to the low mass flow rate, the convective heat transfer is very low despite the high temperature difference between the center flow tube and interior coolant. At 50s, the SRV actions cause mass flow oscillation in Group2 channel. This phenomenon greatly improves the convective heat transfer between center flow tube inside surface and interior coolant, thereby accelerating the heating process of the coolant in the center flow tube and eventually, leading to the early pseudo-critical transitions. Also, since there is only one channel in Group2, the coolant volume expansion owing to pseudo-critical transition does not lead to SRV actions. In other words, the pressure increase in one channel does not sufficiently affect the overall core pressure. SRV actions are still mainly found during the period of time when the majority of channels (i.e, Group1) go through pseudo-critical transition. However, this result is directly linked to the grouping scheme. In reality, the thermal hydraulic properties of all 336 channels change individually as a function of time. Consequently, the pseudo-critical transitions scatter in a longer period of time rather than concentrating in 125-250s periods as the mass flow plot (Figure 5.13) indicated. Moreover, as discussed in bullet 3 above, when coolant goes through pseudo-critical transition, the corresponding convective heat transfer

coefficients are overestimated by CATHENA. As shown in Figure 5.16, in both plots, the heat transfer coefficient at center flow tube inside surface increases during the transitions which eventually causes the underestimated center flow tube outside surfaces and fuel cladding temperatures.

For Group2, the radiation heat transfer levels in fuel region either increase or decrease depending on the local sheath temperatures at the beginning of phase III. However, as shown in figure 13, by the end of this phase, the overall fuel cladding temperatures are at approximately 650 ^{o}C. Compared to the convective heat transfer induced by reversed flow, the level of radiation heat transfer is quite low. As a matter of fact, by the end of Phase III, only one third of the decay heat is removed by radiation heat transfer and the other two thirds by convective heat transfer.

5.2.1.4 Phase IV

Group 1 (240-1500s)

Figure 5.20 shows Group 1 response after the pseudo-critical transitions in the center flow tube. It shows that the total mass flow in Group1 significantly decreases during Phase IV and SRV action becomes less frequent. The final mass flow rate for the entire group is approximately 0.4 kg/s (see Figure 5.20, i.e., 0.0011kg/s per channel).

As a result of the reduced flow and declining convective heat transfer the total heat removal is less than the decay heat generated and thus leading to increasing fuel sheath temperatures. Nevertheless, the feedback effect of growing sheath temperature is that an increasing amount of heat radiates out of fuel rods. And by the end of Phase IV, the combination of radiation and convective heat transfer balances decay heat and the temperatures begin to decrease again due to continuously decreasing decay heat.

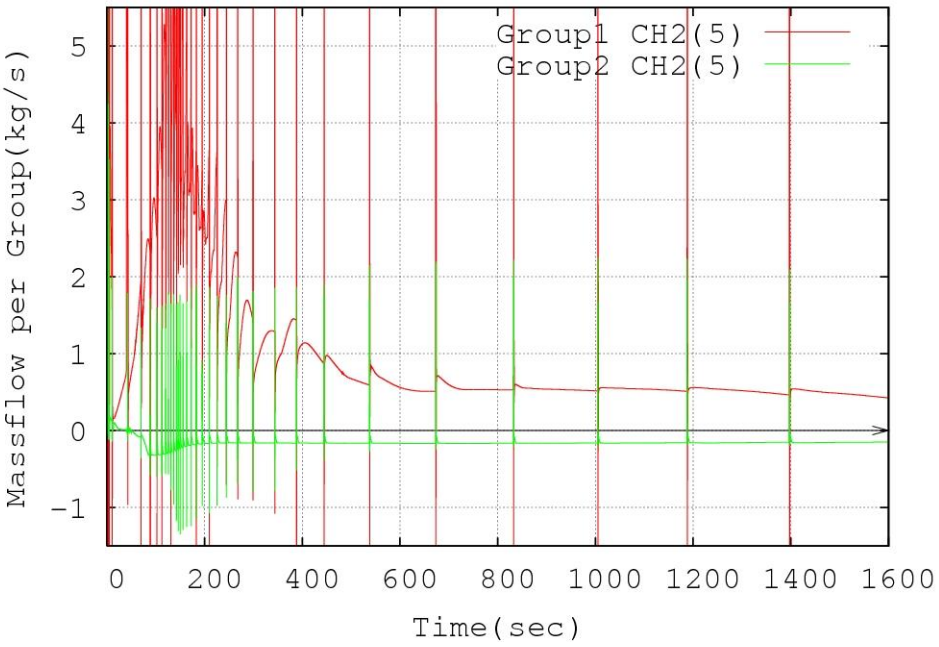

Figure 5.20 Coolant Massflow Rate per Group

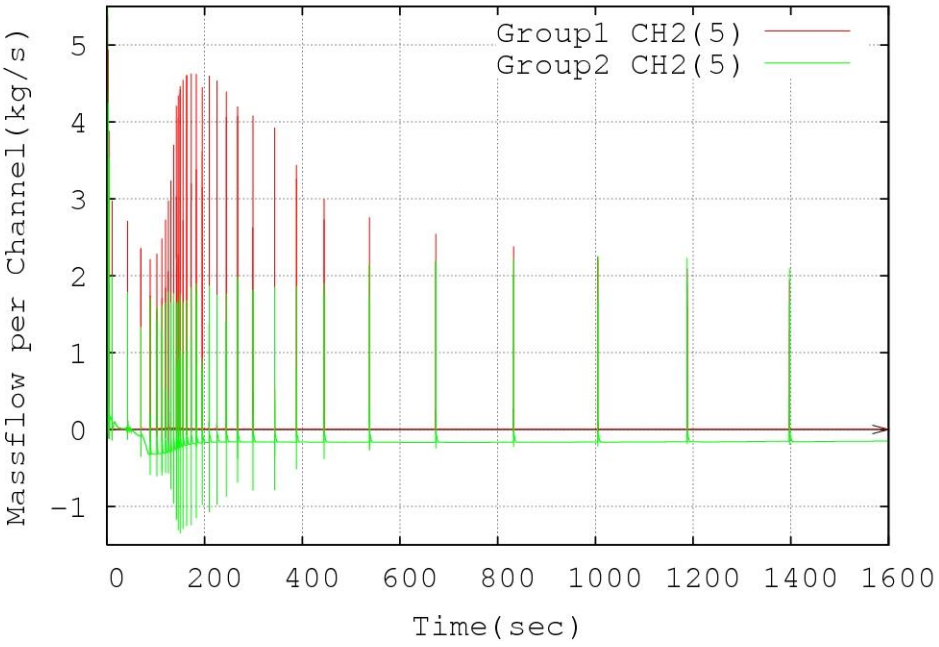

Figure 5.21 Coolant Massflow Rate per Channel

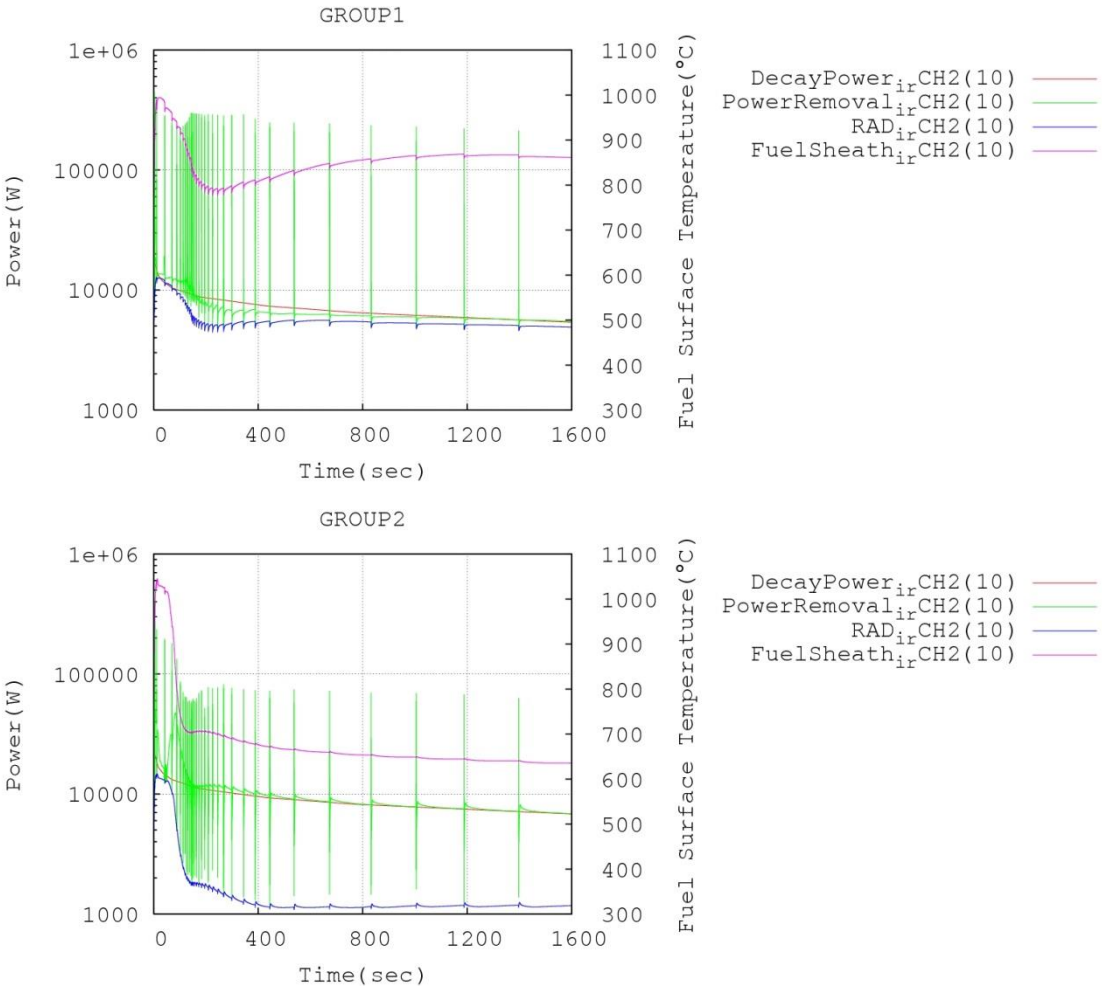

Figure 5.22 Power Generation and Removal at Inner Ring CH2(10) in Phase IV

Group2 (150-210s)

Figure 5.21 shows that the Group2 reversed flow decreases from 0.35 kg/s to 0.1 kg/s and is maintained at approximately 0.1kg/s until the end of transient. This along with the average channel flow in Group1 implies that a net mass flow of approximately 0.3kg/s is flowing from inlet plenum to outlet plenum. The causes and effects of the net mass flow are discussed in the Section 5.2.2.

During this period of time, the fuel cladding temperature decreases as the total heat removal exceeds the decay heat power in Group 2. This directly leads to the reduction in radiation heat

transfer. Figure 5.22 shows the total heat removal and radiation heat transfer level at node 10 as a function of time. As shown in the plot, by the end of Phase IV, the radiation heat transfer level has decreased to approximately 1kW whilst the decay heat is around 10kW. Radiation heat transfer only accounts for 10% of the total heat removal at node 10 and convective heat transfer accounts for the remaining 90%. At this time of the transient, the natural circulation convection dominates heat transfer. The initiation of internal circulation patterns within the core greatly reduces the maximum sheath temperature predicted in these transients.

5.2.1.5 Phase V

Group1(1500- 2000s)

During Phase V, as shown in Figure 5.24, the net massflow continuously flows from inlet plenum to outlet plenum with slightly decreased magnitude as a result of a lower density difference between the plenums. The fuel sheath temperatures gradually decrease reflecting the reduction in decay heat generated within the fuel (see Figure 5.23).

Group2 (210-2000s)

Overall, the thermal-hydraulic behavior of Group 1 and Group2 are very similar. Hence both channel group responses are discussed in the following section.

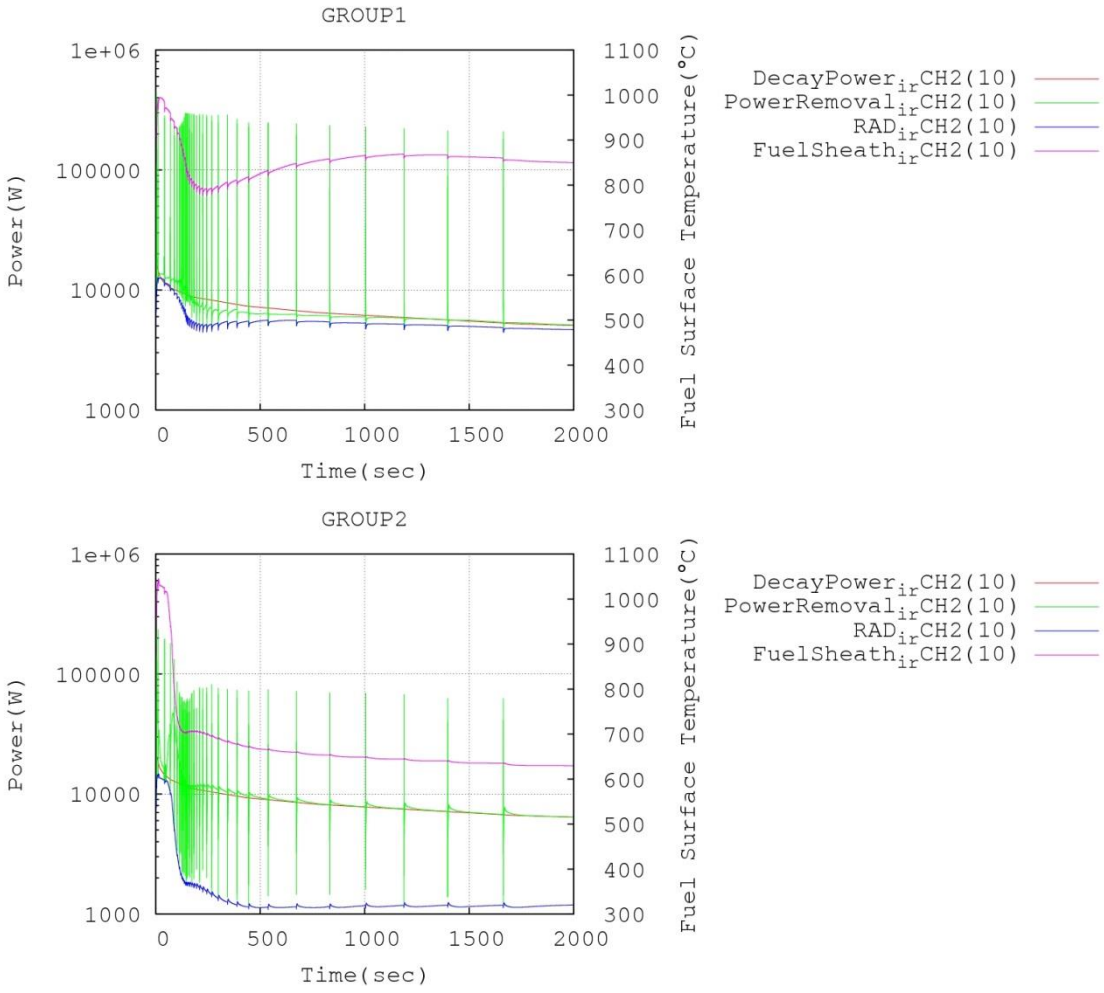

Figure 5.23 Power Generation and Removal at Inner Ring CH2(10) in Phase V

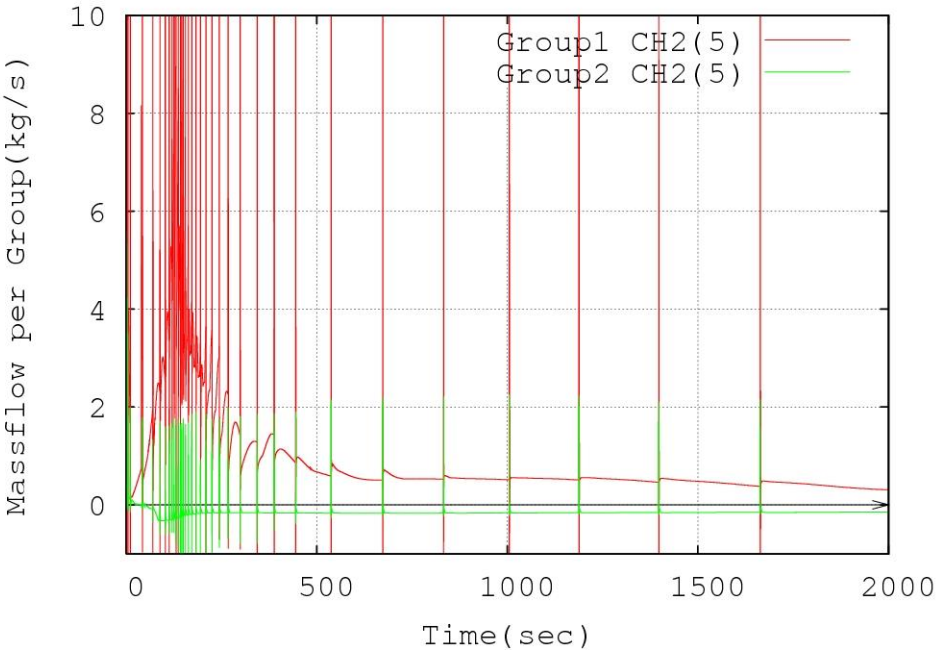

Figure 5.24 Coolant Massflow Rate per Group

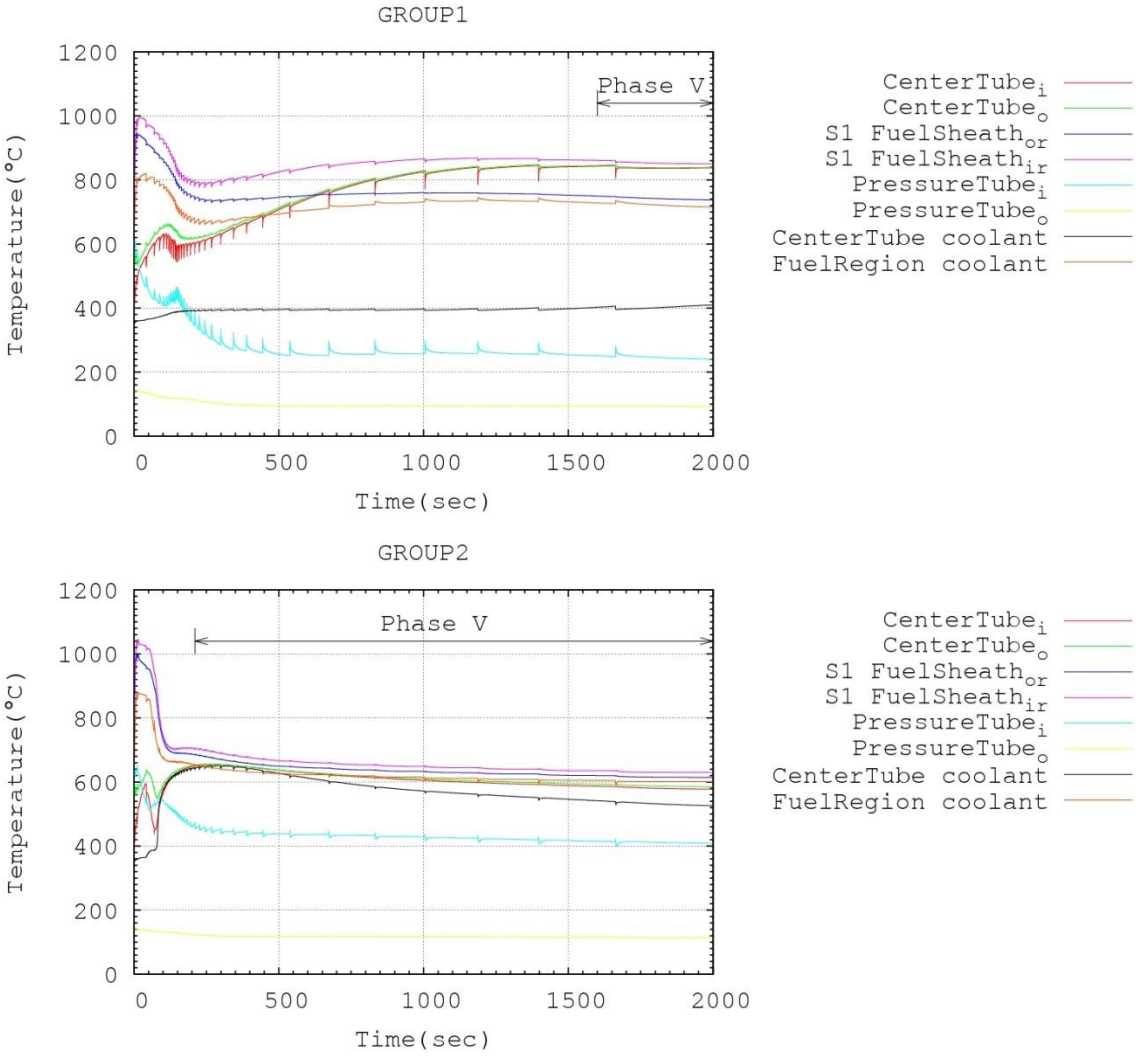

Figure 5.25 Temperature of Various Components in Phase V

At the early stage of transient, for Group1, the fuel cladding temperature of different sectors from highest to lowest was: IR S1>OR S3>IR S2>OR S2>IR S3>OR S1.

As expected, low cladding temperatures are found in OR S1 and IR S3 which are the sectors facing the pressure tube and center flow tube. In general the maximum temperature occurs in the inner ring sector facing the outer ring. In the early stage of transient, the temperature of center flow tube outside surface and pressure tube inside surface are relatively low compared to the fuel cladding temperature. Consequently, the radiation heat transfer among these surfaces is higher than elsewhere so that IR S3 and OR S1 (i.e., sectors facing the cool surfaces) are cooled efficiently. On the other hand, IR S1 and OR S3 are the hottest sectors since they are facing high

temperature fuel surfaces. Surfaces IR S2 and OR S2 have view factors that include both high temperature fuel rods as well as cooler pressure tube and center flow tube surfaces, which explains why their temperatures fall between the two other surfaces. In general, since the inner ring is directly exposed to the 650 ^{o}C center flow tube surface, while outer ring is close to the 500 ^{o}C pressure tube, the inner ring sector temperatures are consistently higher than their respective outer ring sector temperatures during this phase. The fuel cladding temperature of different sectors of group2 are in the same order with group1.

By the end of transient, for Group1, the fuel cladding temperatures of different sectors, from highest to lowest is: IR S3>IR S2>IR S1>OR S3>OR S2>OR S1. The outer ring fuel cladding temperature is consistently lower than the inner ring temperature. This is because the Outer Ring is exposed to the pressure tube that is continuously cooled down by the moderator while the inner ring is facing the center flow tube. Due to the lack of cooling, the center tube temperature increases to almost the same value as the Inner Ring sheath temperature (IR S3). Consequently, the Inner Ring fuel rods are not cooled down as sufficiently as Outer Ring fuel rods since the direct heat sink of the Inner Ring is the Outer Ring that subsequently radiate to the pressure tube. During the later stage of transient(i.e. Phase IV and Phase V), the most effective heat transfer mechanisms for the high temperature sectors such as IR S3 are circumferential conduction within the fuel rods and convective heat transfer by natural circulation. For the fuel cladding temperatures of different sectors in Group2, the temperatures of Inner Ring sectors are lower than Outer Ring's which is consistent with the result of Group1. However, all three sectors of Inner Ring are at similar temperatures, with IR S1 (i.e., sector facing the center tube) being slightly cooler than the other two. For Group2, center flow tube is adequately cooled down by the reversed flow. As shown in Figure 5.25, after 900s the center tube outer surface temperature reduces the coolant temperature in the fuel region as well as OR S3 (i.e., the sectors facing the Inner Ring) which explains why IR S3 has the lowest temperature among the three Inner Ring sectors.

5.2.2 LOFA Simulation Results Using 4 Channel Groups

In this section, a 4-group channel-grouping scheme is selected for the LOFA transient to illustrate the effect of grouping on the transient predictions. The grouping scheme is summarized in Table 5.7.

Table 5.7 4-Group Channel-Group Scheme

	Type of Channel	Number of Channels	Single Channel Power (MW)	Total Channel Power (MW)	Normalized Power Distribution
Group1	Low Power	112	6.35	711.20	0.28008
Group2	Medium Power	112	7.59	850.08	0.33447
Group3	High Power	111	8.74	970.14	0.38169
Group4	Maximum Power	1	9.56	9.56	0.00376
The Total Power of all 336 Channels is 2540MW					

As shown in Table 5.7, the 336 channels are divided into 4 groups. Group1 is the low power group which consists of 112 channels with an average channel power of 6.35MW. Group2 is the medium power group which consists of 112 channels with an average channel power of 7.59MW (and is comparable in magnitude to the average channel, Group1 in the preceding simulations. The high power channels are divided into 2 groups; Group4 has the maximum power channel and Group3 has 111 high power channels. The average channel power of Group3 and Group4 is 8.74MW and 9.56MW respectively.

This grouping scheme is closely related to the type of scenarios that are simulated and the

phenomena under investigation. Generally, for loss of flow scenarios, it is advisable to perform channel-grouping according to the channel power, since a large number of parameters and phenomena are power-related. Moreover, in this specific LOFA scenario, the 2-group simulation indicates that as the transient progressed, natural circulation is initiated and established in the system. In order to simulate the flow directions as well as the mass flow rate, the relative channel numbers of each group are also considered and are selected to be equal. Without convective cooling, as shown in the case above, the fuel cladding temperature at the top region of fuel rods rises by more than 300 ^{o}C within the first 20s. The more decay heat generated in the fuel, the higher temperature of the fuel sheath. Since the decay heat levels are linearly related to the channel power before the reactor trip, the grouping scheme is developed based on the steady-state channel power.

The relative channel number of each group is another factor which has been taken into consideration. In CATHENA, channels that are grouped together share the same mass flow rate, orifice size, power and flow directions. The 2-group simulations show that natural circulation takes place during the transient with very low mass flow rates. Since in the 2-group simulation, reversed flow only takes place in Group2 which consists of a single channel, the total mass flow rate for the reversal is restricted which might lead to an impaired prediction of natural circulation. Through trial and error it was discovered that the direction of flow that occurs after the initial stagnation is very sensitive to the total power and flow in a channel group. If the channel grouping is performed in the manner that equal numbers of channels are assigned to each group, the flow direction was positive in the group with higher total power. However when the relative size of the high power group is decreased relative to a low power group, at some ratio the predictions will show the low power group in forward flow and the high power group in reverse flow. This occurs approximately at the point where the total massflow and power in the low power group exceeds the high power group. The reason for this behavior has not been established, but it appears that once the total power in a low power group exceeds the total power in high power

group, the additional buoyancy force in that group dominates. It was our expectation that the average power in a group would dominate the flow direction. In our discussions with the code experts this issue has not been resolved. In order to avoid this issue, in this case, except for maximum power channel, the rest of channels are approximately equally divided into three groups.

The fuel channels were first divided into 8 groups: a single channel group with maximum channel power plus 7 groups with equal number of channels. However, during the transient for this grouping scheme, some groups produced almost identical results. After combining those groups, the grouping scheme evolved to a 4-group scheme as described at the beginning of this section. The discussion above does not necessarily mean that the 4-group scheme is the best way to simulate LOFA transient. For more detailed safety analysis, all 336 channels could be further divided into 8 or 12 groups. However, in this thesis, the focus is on the major phenomena during the LOFA transient that is why the 4-group scheme is considered appropriate. The effect of grouping on the flow direction is important, however since maximum clad temperatures occur during Phase I where there is little induced flow and where the decay heat is the highest, resolution of the flow direction issue has been flagged for future work. A recommendation from this work is to perform these LOFA simulations with no channel grouping, however currently this is beyond the CATHENA codes capability.

The simulation results for the 4-group transient are summarized in Table 5.8.

Table 5.8 Simulation Results for the 4-Group LOFA Transient

Parameter	Unit	Group1	Group2	Group3	Group4
Maximum Fuel Cladding Temperature	^{o}C	938	990	1021	1059

Time when MCST approached	s	19.5	19.5	12.7	18.2
Total Massflow at 700s	kg/s	-8.77	6.37	13.84	-0.10
Massflow per channel at 800s	kg/s	-0.0783	0.0574	0.1240	-0.10

As shown in the Table 5.8, forward flow is mainly found in the medium power group (Group2) and high power group (Group 3) whilst reversed flow is mainly found in the low power group (Group1) and maximum power group (Group4). And the channel mass flow rate of Group3 is higher than Group2. The potential reasons for natural circulation directions may be higher decay level and larger orifice size. The CATHENA developers have stated that under such low driving force conditions the code may be extremely sensitive to the small differences in orifice size, power level, axial fuel and pressure tube temperature etc…., and even possibly the order in which the matrices are solved within the code.

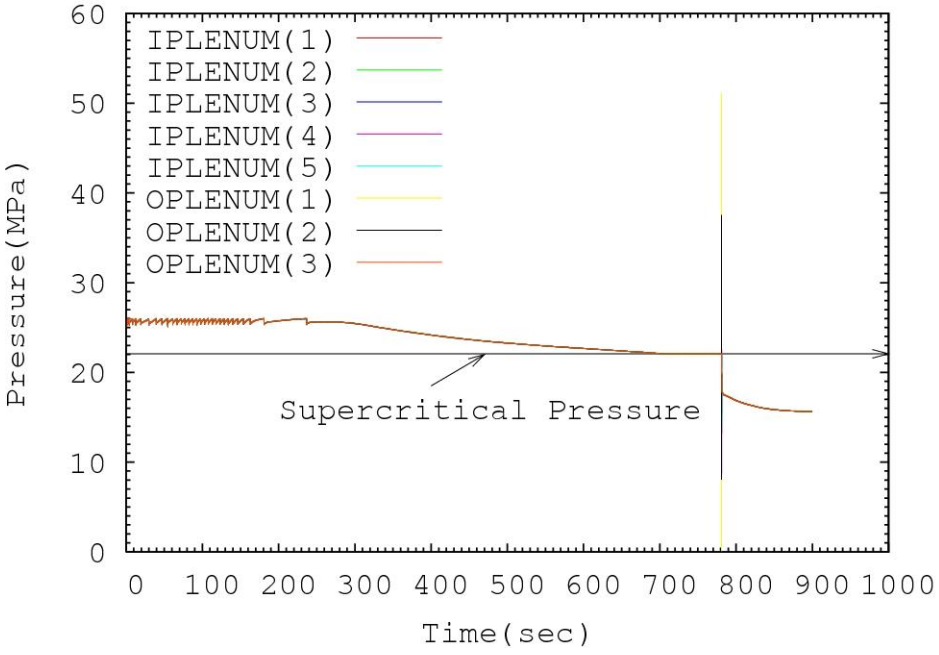

Figure 5.26 Pressure at Inlet and Outlet Plenum

A significant difference is observed in the 4-channel group case as compared to the 2-channel group case discussed previously in that the system cooldown rate proceeds much faster in the 4-group case. This results from the increased internal convection heat transfer to the pressure tube (and ultimately moderator) caused by much larger recirculation flows. Figure 5.26 illustrates the pressure variation of the inlet plenum and outlet plenum as a function of time. As shown in the plot, at approximately 700s, the core pressure is at 22.07MPa, which is the lower limit of the CATHENA supercritical pressure region. As the system transients through the supercritical to subcritical pressure, a significant discontinuity in core pressure is found at 780s. Since CATHENA cannot be applied through trans-critical pressures all the simulation results after 700s (i.e. the time when system pressure drop to supercritical-subcritical transition region) are unreliable and hence are not shown.

The simulation results of the 4-group scheme share many similarities with those of 2-group's. Accordingly, most of the analyses made for the 2-group simulation are also valid here. To avoid repetition, the transient procedures as well as the heat transfer mechanisms will not be discussed in detail. Instead, the natural circulation phenomenon which has not been fully investigated in the previous case is examined here. In addition, primary conclusions about the effects of natural circulation on system cooling are drawn based on the 4-group simulation results.

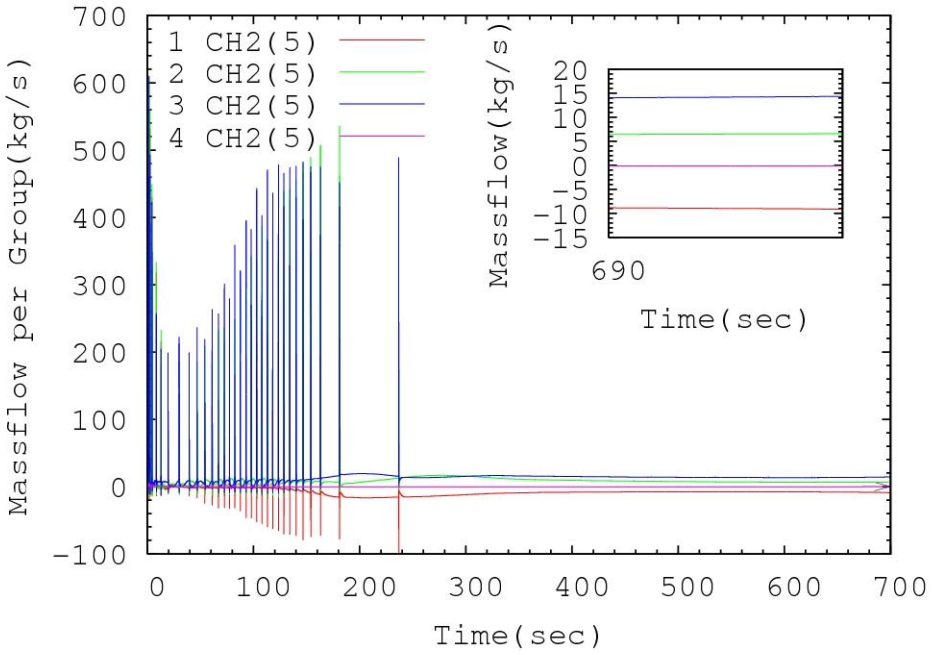

Figure 5.27 Coolant Massflow per Group

Figure 5.27 shows the total mass flow rate of each group during the LOFA transient at the core centerline. As shown in the plot, at 700s the total mass flow rate for Group1 to 4 are -8.77 kg/s, 6.37kg/s, 13.84 kg/s and -0.10kg/s respectively which yields a net mass flow of 11.34 kg/s flowing from inlet plenum to outlet plenum. The results indicate much higher magnitude flows in Groups 1, 2 and 3 and lower total flow in the Group 4 since it only consisted of 1 channel. However on a per channel basis the relatively large flow is achieved in Group 4, and it forms a significant contribution to fuel cooling in the latter Phases of the transient. Compared to the net mass flow rate of 0.3 kg/s which is given by 2-group simulation, the net mass flow of the 4-groups simulation is 35 times higher. Thus, we can draw the conclusion that the mass flow rate of natural circulation calculated by CATHENA is highly sensitive to channel-grouping. This is especially true for the grouping scheme with a few groups.

Although the net massflow induced by natural circulation for the 4-group model is approximately one order larger than the 2-group model, the predictions on the maximum fuel temperatures are

similar (see Figure 5.28), mainly because the maximum fuel cladding temperature occurs in Phase 1 of the transient and before natural circulation can be established. Therefore while the increased natural circulation flows affect later system response, in the early transient near the point of maximum fuel sheath temperature prediction, the coolant massflow rates are similar. Thus, both simplified and detailed grouping scheme can provide acceptable predictions of maximum fuel sheath temperature.

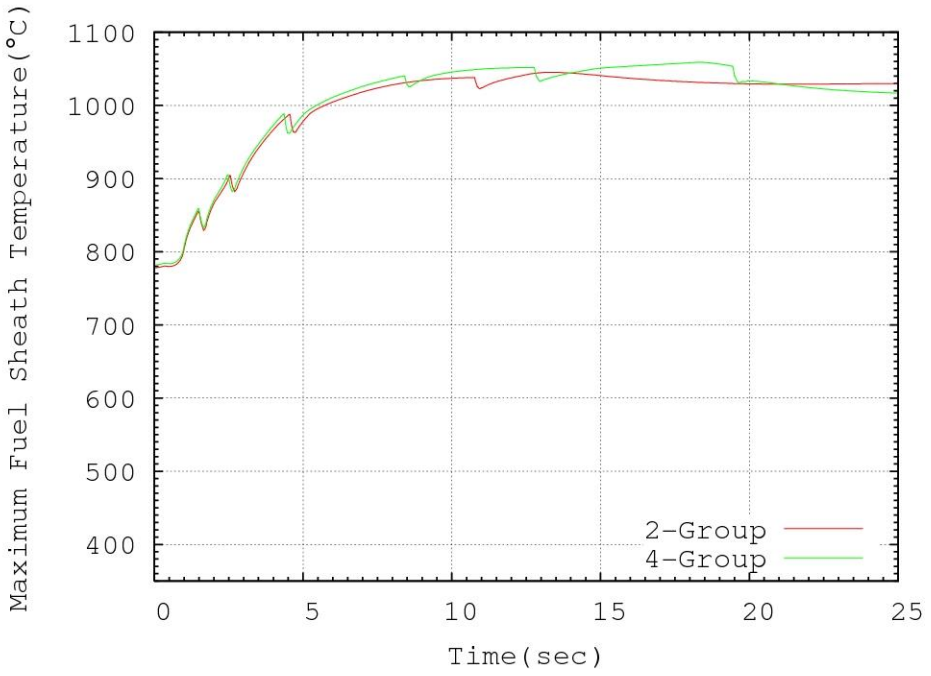

Figure 5.28 Predicted Maximum Fuel Sheath Temperatures For 4-Group and 2-Group Model

The primary impact of natural circulation on the system is to provide extra convective cooling within the fuel assemblies which acts to transport more heat to the moderator system. As is shown in Figure 5.29, in the 4-group simulation, the fuel sheath temperatures of the group with forward flow (Group2 and Group3) and the group with reversed flow (Group1 and Group 4) have dropped to below 400 ^{o}C at approximately 300s and 600s respectively. In comparison, the sheath temperatures at the bottom of fuel region are still increasing at 2000s in the 2-group simulation indicating that the fuel assemblies in the 4-group case cool down at a much higher rate. Since the system shows significantly high flows and cooling during these later Phases, the system started to naturally depressurize at 250s without SRVs. However, in the 2-group case, pressure is oscillating

between 25.25MPa and 26.00MPa for more than 2000s. Figure 5.29 illustrates the heat generation and removal at node 10 as a function of time. As is shown in the plot, after natural circulation is established at approximately 200s, convective heat transfer becomes the dominant heat transfer mechanism (approximately 10 times higher than radiation heat transfer). Convective heat transfer is promoted by natural circulation, which effectively reduces the fuel sheath temperatures. As a result of these decreases, the radiation heat transfer also decreases accordingly. In conclusion, the natural circulation established at approximately 200s greatly improves the convective heat transfer inside the core, thus allowing natural depressurization at an earlier time.

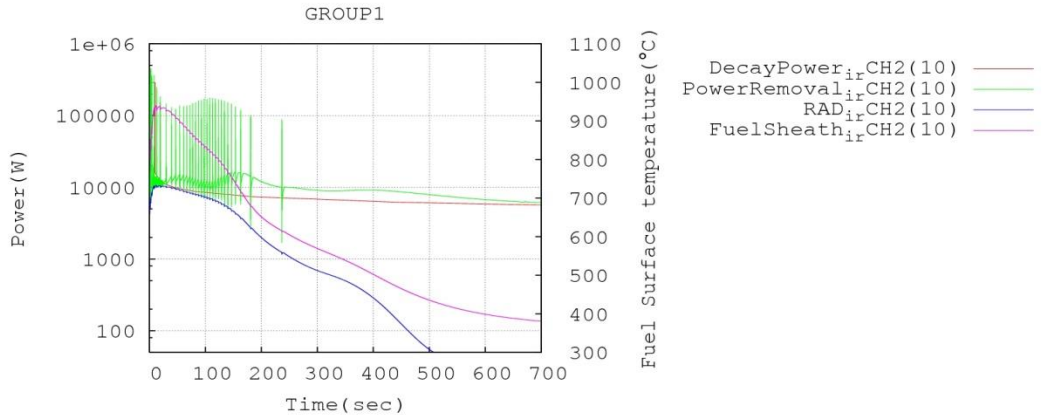
GROUP1
Power(W)
Fuel Surface temperature(°C)
Time(sec)
DecayPower_irCH2(10)
PowerRemoval_irCH2(10)
RAD_irCH2(10)
FuelSheath_irCH2(10)

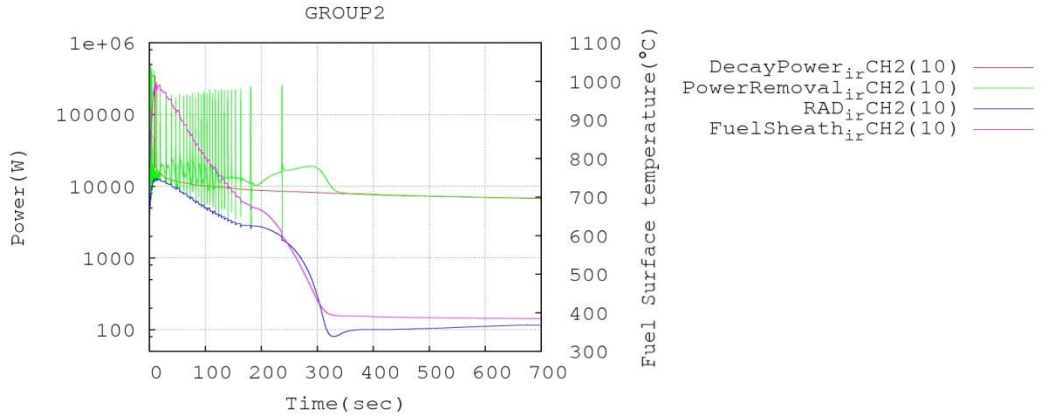
GROUP2
Power(W)
Fuel Surface temperature(°C)
Time(sec)
DecayPower_irCH2(10)
PowerRemoval_irCH2(10)
RAD_irCH2(10)
FuelSheath_irCH2(10)

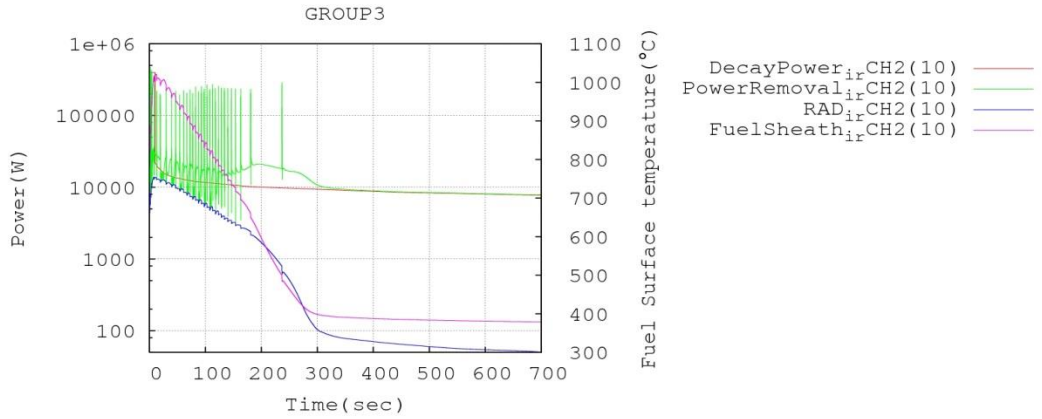
GROUP3
Power(W)
Fuel Surface temperature(°C)
Time(sec)
DecayPower_irCH2(10)
PowerRemoval_irCH2(10)
RAD_irCH2(10)
FuelSheath_irCH2(10)

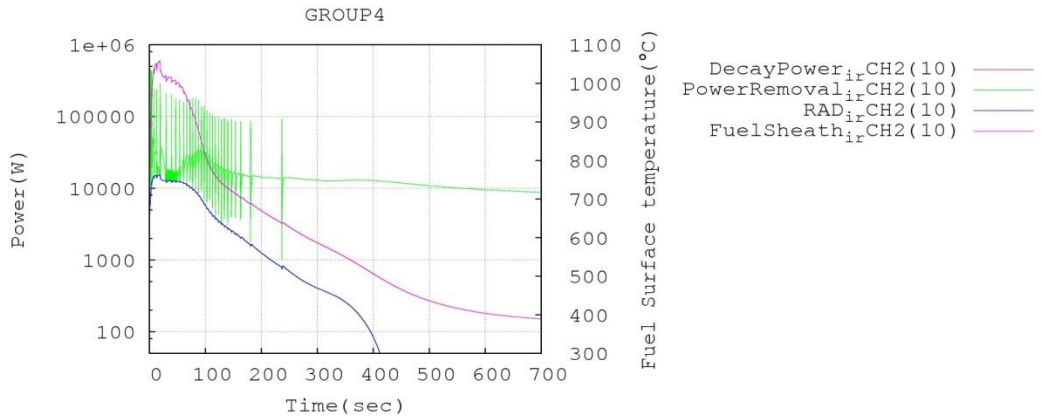
GROUP4
Power(W)
Fuel Surface temperature(°C)
Time(sec)
DecayPower_irCH2(10)
PowerRemoval_irCH2(10)
RAD_irCH2(10)
FuelSheath_irCH2(10)

Figure 5.29 Power Generation and Removal at Inner Ring CH2(10) for 4-Group transient

Another phenomenon associated with natural circulation is mass redistribution in the system. As is mentioned earlier, net mass flow is found flowing from the inlet plenum to the outlet plenum of which the magnitude related to the mass flow rate of natural circulation. This is also verified by the coolant inventory plot (Figure 5.30). The plot shows that as the transient precedes the coolant inventory in the inlet plenum decreases whilst the coolant inventory in the outlet plenum increases. During 200-400s periods, the coolant inventories at both the inlet plenum and outlet plenum change at a higher rate compared to other times of transient due to the high mass flow rate at 200s (Figure 5.27).

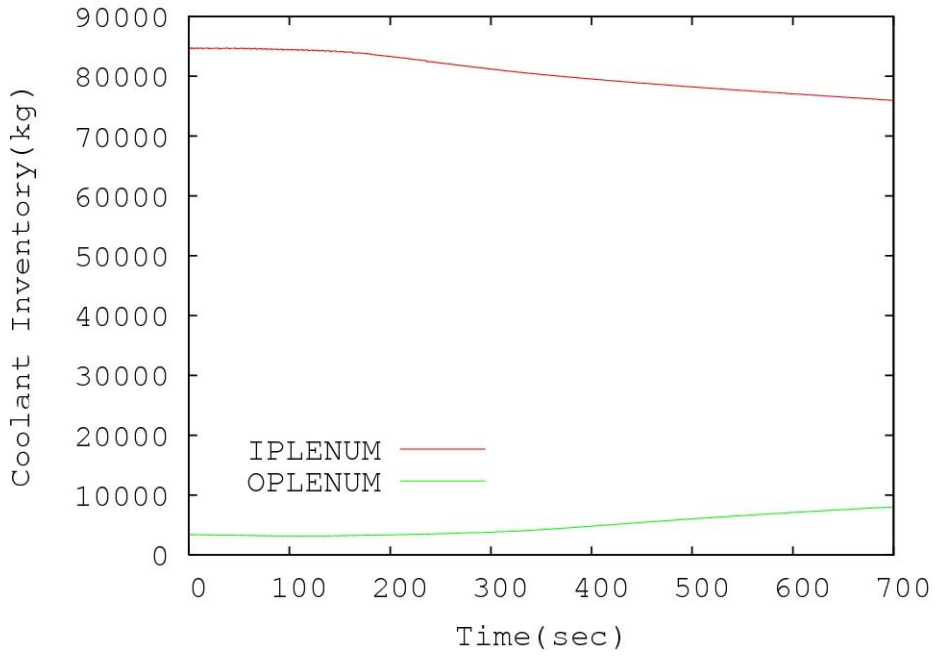

Figure 5.30 Coolant Inventory at Inlet and Outlet Plenum

5.3 Sensitivity Analysis

The previous sections have shown that the steep decrease in massflow rate leads to significant increase in fuel sheath temperature in the early phases of the transient. As the fuel cladding

temperature increases the radiation heat exchange between fuel sheath and surrounding wall surfaces becomes stronger which prevents excessive increases in sheath temperature. Generally, the prediction of maximum fuel sheath temperature is largely governed by the massflow rate, the power level and the efficiency of radiation heat transfer. Sensitivity analysis of these key parameters and one additional analytical model are performed to demonstrate how the predicted temperature is affected by reactor trip time, power ramping time, emissivity and the convective heat transfer at fuel surfaces during the early stage of transient.

Note that all the sensitivity analyses are applied to the 2-group CATHENA idealization, as the 2-group model and 4-group model provide similar predictions on the fuel cladding temperatures before natural circulation initiates.

5.3.1 Reactor Trip Time

Isolation valves located at either side of the reactor core are closed from 0-1s. The reactor trip time specified in the CATHENA input table is 0.29s which is the time when the massflow rate at the inlet plenum drops to 90% of its original value. To demonstrate how the trip time affects the simulation results, 5 additional runs are performed with trip time corresponding to 70%, 50%, 30%, 10%, 0% of the steady state main feed water flow (In the 0% case, the trip time is delayed until the maximum fuel sheath temperature excess the melting point of the cladding material.). The simulation results are summarized in Table 5.9. The results show that the perditions of maximum fuel sheath temperature are dependent on the time required for the core to reach decay heat. By delaying the trip time from 0.15s to 4.40s, the predicted maximum sheath temperatures are increased by approximately 355 ^{o}C. The upper bound trip time that ensures the acceptance criteria are met is 4.4s. Since this is well within the trip times typical of GEN II and GEN III designs, it can be concluded that the no core melt option can be achieved so long as safety systems actuate and reduce power within this period.

Table 5.9 Sensitivity Analysis of Reactor Trip Time on the Prediction of Maximum Fuel Sheath Temperature

Trip time (s)	Flow Ratio ($\frac{\dot{m}_{tr}}{\dot{m}_{ss}}$)	Maximum Sheath Temperature for Inner Ring (^{o}C)	Maximum Sheath Temperature for Outer Ring(^{o}C)
0.29	**90%**	**1045**	**1043**
0.57	70%	1063	1061
0.73	50%	1077	1075
0.84	30%	1087	1084
0.93	10%	1093	1091
4.40	-	1400	1398

5.3.2 Power Ramping Time

In addition to the above analysis, power ramp time (I.e., the duration of time it takes for power to be reduced from 100% full power to decay heat after the trip signal is received) is another factor determining the reactor power at the early stage of transient. In the current study, a ramping time of 0.1s is employed by the CATHENA transient model. However, depending on the design of the reactor, the power ramping time could be up to several seconds. To this end, various ramping time from 0.1s to 3s are selected for the sensitivity study. The simulation results are listed in Table 5.10.

As shown in Table 5.10, the ramping time does not have as large impact on the fuel cladding temperature prediction as the reactor trip time. For instance, if the power ramps down in 1s which is a typical value for CANDU reactor, the maximum sheath temperature would be 1077 which is 32 ^{o}C than the reference case. If the power ramps down in 2s which is a typical value for pressurized water reactor, the maximum sheath temperature would reach 1121 ^{o}C which is 76 ^{o}C higher than the current prediction.

Table 5.10 Sensitivity Analysis of Power Ramping Time on the Prediction of Maximum Fuel Sheath Temperature

Ramping Time (s)	Maximum Sheath Temperature for Inner Ring (^{o}C)	Maximum Sheath Temperature for Outer Ring(^{o}C)
0.1	**1045**	**1043**
0.2	1046	1041
0.5	1059	1057
1.0	1077	1074
1.5	1100	1097
2.0	1121	1119
3.0	1164	1161

5.3.3 Emissivity

Radiation heat exchange largely depends on the emissivity properties of the surfaces. In the current analysis, an emissivity of 0.8 is assumed for the fuel cladding, center flow tube outer surfaces, and liner tubes inner surfaces. A wide range of emissivity values are covered by this sensitivity analysis (from $\varepsilon = 0$ to $\varepsilon = 1$) to determine how emissivity affects the predictions of maximum fuel sheath temperature . The predicted maximum fuel cladding temperature by using different emissivity is plotted in Figure 5.31and summarized in Table 5.11.

In this specific LOFA transient, the emissivity of the wall surfaces affects the prediction of maximum sheath temperature modestly. As is shown in Table 5.11 (see line 1 and 6), by reducing the emissivity value from 1 to 0, the maximum fuel sheath temperatures for the inner and outer rings are increased by 118 ^{o}C and 112 ^{o}C respectively. Also note that in the case where $\varepsilon = 0$ (i.e. radiation heat exchange between fuel cladding and surroundings is not simulated), the maximum fuel cladding temperature is 1151 ^{o}C, which is still lower than the melting point of the cladding material. Figure 5.31 shows that during the early stage of transient, radiation heat transfer

eliminates the fuel sheath temperature from rising further. Subsequently, for those cases with higher emissivity (i.e. $\varepsilon = 0.8$ and 1.0), the fuel temperature decrease takes place earlier and the predictions of the maximum fuel sheath temperature are lower as compared to the cases with low emissivity (i.e. $\varepsilon = 0.2, 0.4$ and 0.6). As indicated earlier, the massflow surges observed in the early stage of transient greatly affect both the prediction of the maximum fuel sheath temperature and the time it happens. Further work is needed to examine the causes of these surges. (One possible explanation for these surges is the pseudo-critical transition of the coolant at the bottom of the fuel region. However, no concrete conclusion can be made before further simulations are performed since the convection cooling taking place at the early stage of the transient is highly sensitive to many parameters and it is difficult to conclude the effect of emissivity in isolation from the effect of flow surges and natural circulation.

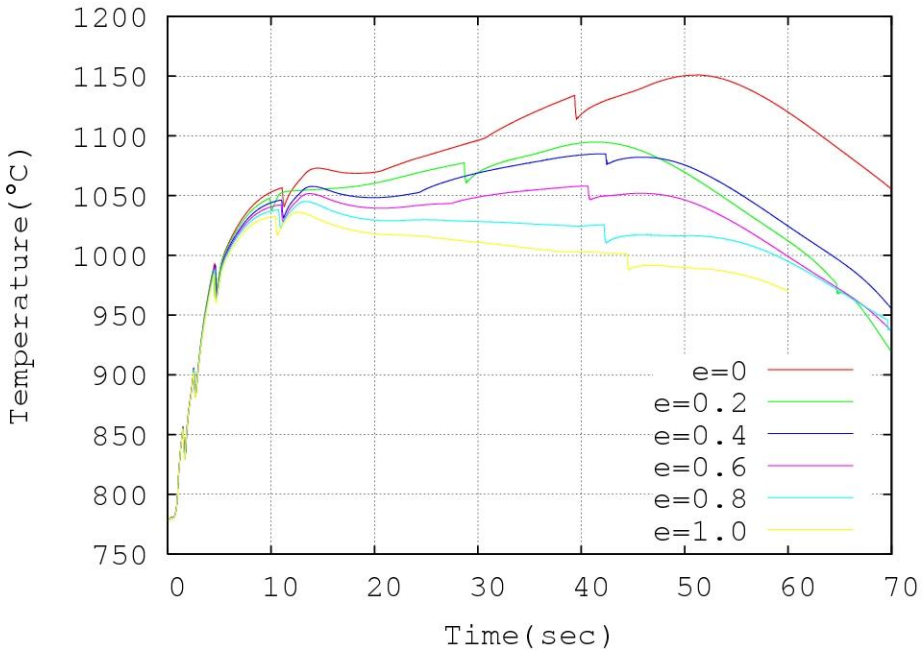

Figure 5.31 The Prediction of Maximum Fuel Sheath Temperature Using Different Emissivity

Table 5.11 Sensitivity Analysis of Emissivity on the Prediction of Maximum Fuel Sheath Temperatures

Emissivity	Maximum Sheath	Maximum Sheath	Time

	Temperature for Inner Ring (^{o}C)	Temperature for Outer Ring(^{o}C)	(s)
1.0	1033	1032	10.45
0.8	**1045**	**1043**	**14.0**
0.6	1065	1060	36.7
0.4	1082	1079	46.1
0.2	1095	1090	41.6
0.0	1151	1144	51.2

5.3.4 Convection

As mentioned above, massflow surges have been found at 10-20s which roughly matches with the time when the maximum fuel sheath temperature is predicted. Although small in magnitude, this massflow preserves a certain amount of convective cooling that prevents the fuel temperature from rising further. During the time when the maximum fuel sheath temperature is predicted, not only radiation heat transfer, but also convection plays an important in cooling of the maximum channel power groups. To examine how convective heat transfer affects the temperature prediction, a LOFA transient is performed with the convective heat transfer coefficient set to zero.

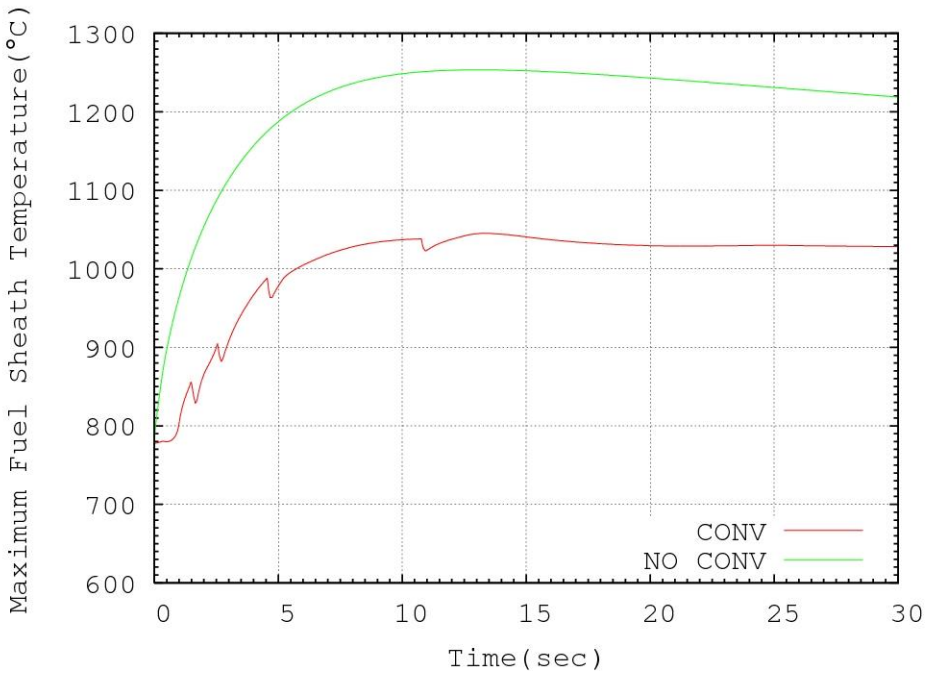

Figure 5.32 Maximum Fuel Sheath Temperature of Inner Ring With or Without Convection

Figure 5.32 shows the variation of the Inner and Outer Ring temperatures as a function of time. Even though the convective heat transfer is not the dominant heat transfer mechanism during the early phase of transient, it still plays a very important role on the prediction of fuel cladding temperature. By eliminating the convective heat transfer coefficient, the maximum fuel sheath temperature is increased by 200 ^{o}C for the reference case. Therefore it is important that CATHENA resolve it correlation issues near the pseudo critical point since this is closely tied with the mass flow surges that occur early in the transient and which also act to reduce the predicted fuel temperatures.

Given the strong sensitivity to flow during the early portions of the transient a more thorough analysis would include the effects of flow rundown, which would provide a large amount of convective cooling during the first Phase of the transient and hence would greatly reduce the predicted sheath temperatures.

6 Conclusion and Future Work

6.1 General Conclusions

The objective of this study was to assess the Canadian pre-conceptual SCWR design for Loss of Flow events leading to degraded cooling conditions. A CATHENA idealization based on the Canadian SCWR has been developed. The 336 channels are implemented through various channel grouping schemes and detailed heat transfer models (including radiation heat transfer mode) are included in the idealization. The open fraction of orifices located at fuel channel inlets are calculated based on the MOC power and are applied for all the simulations.

The simulations are performed using various channel grouping schemes. The grouping methods for thermal-hydraulic simulation are adopted according to the scenarios being modeled. In general, the maximum power channel is placed in a separate group and the remaining channels are divided according to channel power. The steady state simulations are performed with a seven branch (I.e., group) CATHENA model. The LOFA transients are simulated using a two branch model and a four branch model separately (a 4 branch model was considered through trial and error which showed little difference between a 4 channel group and 7 channel power group).

6.1.1 Steady State Normal Operation

Three steady-state thermal-hydraulic conditions (i.e. BOC, MOC and EOC) are simulated by employing the CATHENA idealization. The 336 fuel channels are divided into seven groups according to not only the channel power but also the channel power history. For BOC simulation, the lowest-power channel has the channel power equivalent to 79% of the average channel power while the highest-power channel has 136% of the average channel power. The total primary pump flow is 1253.0kg/s and the individual channel mass flow rates ranges from 3.07kg/s to 4.70 kg/s. The maximum sheath temperature and maximum centerline temperature in the BOC are found to

be 829.2 ^{o}C and 2809.6^{o}C respectively. The steady state simulation results at MOC and EOC are quite similar and the branch power ranges from 82% to 126% of the average channel power. The primary pump flows at MOC and EOC are 1256.3kg/s and 1256.6kg/s respectively. The channel massflow rate varied from 3.07kg/s for the lowest power channel to 4.78kg/s for the highest channel group. The maximum fuel sheath temperatures at MOC and EOC are 778.0 ^{o}C and 795.6^{o}C respectively. The maximum fuel centerline temperatures at MOC and EOC are 2459.0 ^{o}C and 2398.0 ^{o}C respectively.

Much higher fuel sheath and centerline temperature are found at BOC. The potential causes are firstly, the maximum channel power is higher at BOC when comparing to the later fuel cycle and secondly, at the maximum power channel, the MOC orifice size is too small for BOC power. This work focuses on MOC channel powers since the irregularities at BOC will be managed through an active reactor power control system (using some combination of burnable absorbers, moderator poisons and control blades).

6.1.2 LOFA Transient

The transient simulation is performed using two channel grouping schemes. In the first grouping scheme the 336 channels is divided into two groups, with the highest power channel in Group 2 and the remaining 335 channels in Group 1. By studying the LOFA transient in this way, an understanding of the behavior of heat transfer inside the high efficiency channel is obtained. In addition, the maximum fuel cladding temperature of 1045 ^{o}C is predicted based on the simulation results of the highest power channel. In the second grouping scheme, the core is divided into 4 groups. Again, the highest power channel is placed in a separate group and the rest 335 channels are divided into three groups with approximately equal number of channel in each group. By applying this grouping scheme, the natural circulation established among various channels groups is examined. The maximum fuel cladding temperature predicted for this grouping scheme is 1059 ^{o}C.

The simulation results show that the transient developed very fast during the first 20s. For the 2-Group scheme, the maximum cladding temperature reaches 1045 ^{o}C at 14.0s for the reference case and 1400 ^{o}C for the case where a reactor trip is delayed by 4.4s. Radiation heat transfer dominants the cooling process during this period of time, however there is a significant contribution from convection in the maximum power channel. This early phase convection was driven by pseudo-critical transitions of components in the fuel channel (primarily in the inner flow tube). In the later transient, natural circulation has been observed in all cases, however, the direction and magnitudes of this recirculation are sensitive to many parameters. The level of recirculation dictates the rate of system cooldown and the cores eventual passively driven transition to subcritical pressures.

The study also discovered that the current CATHENA code produces incorrect predictions on system behaviors under two conditions.

Firstly, the current CATHENA code overestimates the heat transfer coefficient when the coolant temperature approaches the pseudo-critical line. In the supercritical pressure regime, the Dittus-Boelter correlation is the only method currently implemented in CATHENA for calculating the convective heat transfer. When the coolant temperature (bulk temperature) is far from the pseudo-critical line this method works well [5]. However, during pseudo-critical transient simulations, CATHENA significantly overestimates the convection cooling which leads to erroneously high heat transfer in the affected components. This may have significant impact on the cooling during the early phases of the transient where the maximum fuel cladding temperature is reached since the flow induced by such transitions may not be accurately predicted.

Secondly, significant discontinuities are found in mass flow, coolant pressure, coolant temperature, etc. during the transition between subcritical pressure and supercritical pressure. This

characteristic of CATHENA forces the simulation of LOFA transients to be terminated when the core pressure drops to 22.07MPa.

6.2 Recommendations for Future Work

6.2.1 Determination of the Impacts of Orifice Sizes

As described previously, the channel power evolution through the burnup cycle makes it impossible to determine a fixed orifice size that matches the channel power variation at all times during the full fuel cycle. However, in LOFA transients, the orifice sizes in some channels have significant influence on the predicted maximum channel temperature and on the flow direction post-stagnation. This work assumed matched flow-power characteristics at MOC conditions; an expanded study of the effect of channel power evolution during burnup is needed once the designs for reactivity and channel power control have been completed.

6.2.2 Channel Decay Heat Modelling

In addition to the above, the channel powers at BOC tend to be higher than other times in the fueling cycle for the limiting fuel sheath temperature channels. Hence some analysis at BOC channel powers is needed. However fuel burnup calculations also indicate that the time evolution of channel powers is highest at BOC but only for the first several days of operation. After this initial high period, many of the limiting channels approach their respective MOC values [19]. Another complexity at BOC is that the limiting channels tend to be in fresh fuel assemblies, and hence the decay heat fraction may be considerably less than that assumed in the analyses in this thesis. Some best estimate representation of the specific local decay heat as a function of burnup would improve the fidelity of these calculations.

6.2.3 Modification to the CATHENA code

The Dittus-Boelter correlation produces unrealistic results for conditions in LOFA transient when coolant temperatures are close to pseudo-critical points. Heat transfer correlations that provide better predictions of the convective heat transfer behavior near the pseudo-critical temperatures are available [14]. Those correlations should be added to the GENHTP models.

For accident scenarios such as loss of flow accident with significant internal natural circulation or for large-break LOCA, the core could depressurize to subcritical pressure during the transients. Furthermore, immediately below the critical pressure some fuel assemblies may transition from supercritical heat transfer to film boiling. Since the heat transfer under film boiling may be significantly lower than the supercritical case, it is possible that the peak cladding temperatures for these transients may occur at the transition to film boiling. If the code cannot simulate the pressure transition smoothly, any simulation results preformed after the transition point are potentially unreliable. Thus improving the code to obtain a smooth pressure transition is a priority.

6.2.4 Sensitivity Studies on Channel grouping

The magnitude and timing of both the flow surges caused by pseudo critical transition and the bulk recirculation in the later phases of the accident appears to be highly sensitive to channel grouping. Accurate simulation of the internal circulation flows is needed to predict the maximum fuel cladding temperature and hence additional work to resolve the channel grouping phenomena during the transient is needed. As a recommendation there should be no channel grouping employed so the best possible picture of recirculation flows can be determined. From this it may be possible to determine a better grouping scheme.

References

[1] L. K. Leung, "Thermalhydraulics and Safety-Related Experiments in support of the Canadian SCWR Concept Development," in *Canada-China Conference on Advanced Reactor Development*, Niagara Falls, Canada, 2014.

[2] Stainless Steels[M]. ASM international, 1994.

[3] Yetisir M, Gaudet M, Rhodes D. "Development and Integration of Canadian SCWR Concept with Counter-flow Fuel Assembly". ISSCWR-6, March, 2013.

[4] Hanna B N, " CATHENA: A Thermalhydraulic code for CANDU analysis". Nuclear Engineering and Design, 1998, 180(2): 113-131.

[5] Oka Y, Koshizuka S, Ishiwatari Y, et al," Super light water reactors and super fast reactors", Springer, New York/Dordrecht/Heidelberg/London, 2010.

[6] Status report 71 - Japanese Supercritical Water-Cooled Reactor (JSCWR) [Online]. Available: https://aris.iaea.org/sites/..%5CPDF%5CJSCWR.pdf [Accessed September 2014].

[7] Status report 109 - High Performance Light Water Reactor (HP-LWR) [Online]. Available: https://aris.iaea.org/sites/..%5CPDF%5CHP-LWR.pdf [Accessed September 2014].

[8] J.Starflinger, T.Schulenberg, D.Bittermann, M.Andreani and C. Maraczy, "Assessment of High Performance Light Water Reactor concept," *Proceedings of the 5th International Symposium on Supercritical-Water-cooled Reactors*, Vancouver, Canada, March 2011.

[9] Vasic A., Khartabil H.F., (2005), "Passive Cooling of the CANDU SCWR Fuel at LOCA / LOECC Conditions", *Proceedings of GLOBAL*. Atomic Energy Society of Japan, Tsukuba, Japan.

[10] Shan J., Jiang Y., Leung L.K.H., (2011), "Subchannel and Radiation Heat Transfer Analysis of 54-Element CANDU-SCWR Bundle", *ISSCWR-5*, Vancouver, British Columbia, Canada.

[11] Licht J., Xu R., "Preliminary No-core Melt Assessment for the High Efficiency Channel Preconceptual Design", *The 3rd China-Canada Joint Workshop on*

Supercritical-Water-Cooled Reactors, CCSC-2012, Xi'an, China

[12] Pioro I, Mokry S, "Thermophysical properties at critical and supercritical conditions". Heat Transfer Theoretical Analysis, Experimental Investigations and Industrial Systems. InTech, Rijeka, 2011.

[13] J. D. Jackson and W. B. Hall, "Forced convection heat transfer to fluids at supercritical pressureTurbulent Forced Convection in Channels and Bundles," *Hemisphere Publishing Corporation*, p. 563–611, 1979.

[14] Mokry S, Pioro I, Farah A, et al. "Development of supercritical water heat-transfer correlation for vertical bare tubes". Nuclear Engineering and Design, 2011, 241(4): 1126-1136.

[15] Bishop, A.A., Sandberg, R.O., and Tong, L.S., "Forced convection heat transfer to water at near-critical temperatures and supercritical pressures", A.I.Ch.E.-I.Chem.E Symposium Series No. 2, pp. 77–85, 1965.

[16] Swenson, H.S., Carver, J.R., Kakarala, C.R., "Heat transfer to supercritical water in smooth-bore tubes", Journal of Heat Transfer: Transactions of the ASME Series C 87 (4), 477–484,1965.

[17] Pioro, R. Duffey," Heat Transfer and Hydraulic Resistance at Supercritical Pressures in Power Engineering Applications" ,ASME Press, New York, NY, USA ,2007, 334 pp.

[18]John Wiley & Sons, Incropera F P. Fundamentals of heat and mass transfer[M], 2011.

[19] Hummel D., Novog D, "Optimized Channel Inlet Orifice Sizing for the Pressure Tube Type Supercritical Water-cooled Reactor", *The 19th Pacific Basin Nuclear Conference*, PBNC-2014, Vancouver, Canada.

[20] Crane handbook[M]. Construction Safety Association of Ontario, 1975.

[21] Wang D F, Wang, "A Preliminary CATHENA Thermalhydraulic Model of the Canadian SCWR for safety analysis", AECL Nuclear Review, 2014, 3(01): 9-16.

[22] Data was sent to David Novog by Wang, David Fangyou (AECL) on October 24st by email

[23] AECL Report, Canadian SCWR Core and Lattice Physics Concept Descriptions, 217-123700-REPT-010, Revision 0.

[24]Data was sent to David Novog by Wang, David Fangyou (AECL) on October 21st by email

[25] Yamanaka S, Yamada K, Kurosaki K, et al," Thermal properties of zirconium hydride", Journal of nuclear materials, 2001, 294(1): 94-98.

[26] Raghavan S, Wang H, Porter W D, et al," Thermal properties of zirconia co-doped with trivalent and pentavalent oxides". Acta materialia, 2001, 49(1): 169-179.

[27] Pioro I," Heat-Transfer at Supercritical Pressures", *14th International Heat Transfer Conference,* American Society of Mechanical Engineers, 2010: 369-382.